MATERIAL CHARACTERIZATION OF GRAPHENE ENHANCED CLASS-H CEMENT UNDER THERMAL CYCLIC CONDITIONS

By

HAVILA JUPUDI

Bachelor's in Technology, Chemical Engineering
Andhra University College of Engineering
Visakhapatnam, AP, India
2011
Master's in Technology, Chemical Engineering
Andhra University College of Engineering
Visakhapatnam, AP, India
2014

Submitted to the Faculty of the
Graduate College of the
Oklahoma State University
in partial fulfillment of
the requirements for
the Degree of
MASTER OF SCIENCE
December, 2022

MATERIAL CHARACTERIZATION OF GRAPHENE ENHANCED CLASS-H CEMENT UNDER THERMAL CYCLIC CONDITIONS

Thesis Approved:

Dr. Mileva Radonjic

Chair and Thesis Adviser

Dr. Shohreh Hemmati

Dr. Camelia Knapp

ACKNOWLEDGEMENTS

The Creator of this universe who never gave up on me, I always acknowledge His constant presence. No person can do everything by themselves and man being a social soul would depend on somebody to finish a task. With these thoughts in mind, I heartfully thank my advisor, Dr. Mileva Radonjic for her constant guidance, inspirational motivation and support throughout my research work and writing. Also, my sincere thanks to my committee members Dr. Camelia Knapp and Dr. Shohreh Hemmati for their encouragement and timely motivation. Deepest thanks to the Associate Dean, Dr. Jean Van Delinder who gave me strength to move forward during my most difficult times. I recognize the assistance from graduate college, Richard Shephard, who helped me with all the formalities required. This research would not have been completed successfully without the evergreen support of the research lab manager, Cody Massion who taught me on using every equipment in the lab and spent many hours in helping me be where I am. I thank the immense support of Lisa Whitworth and Brent Johnson at the Oklahoma State University Microscopy Laboratory. I am grateful to Dr. Simon Iremonger, Sanjel Energy Services for his expertise in cement chemistry and his thoughtful discussions every now and then which helped me think from an industry perspective. My gratitude to Amelia Letvin, President of Women in Geothermal who supported me in presenting my work at the Geothermal Rising Conference, 2022. Thanks to my Hydraulic Barriers lab team, postdoctoral scholar, and graduate students: Dr. Fengyang Xiong, Allan Katende, Gabriel Awejori. I would especially thank my parents, Ruth and Samprasad Jupudi, other family members and friends, for their constant emotional support and strength. Gena Hellman, thank you for your help with editing the document. Lastly, but a significant one who made a huge difference in my life, my dearest son Jeremy who has been there for me throughout this journey and gave me unending courage to come this far.

Name: HAVILA JUPUDI

Date of Degree: DECEMBER 2022

Title of Study: MICROSTRUCTURAL AND MICROMECHANICAL EVALUATION OF WELLBORE CEMENT WITH GRAPHENE NANOPLATELETS UNDERGONE THERMAL CYCLIC LOADING FOR GEOTHERMAL WELLBORE APPLICATIONS

Major Field: CHEMICAL AND PETROLEUM ENGINEERING

Abstract: Geothermal heat harvesting is the process of extracting heat from the earth's subsurface where it is trapped below the diverse rock formations to be converted into usable energy. Cementing of the drilled wells requires the use of materials that are stable at high cyclic temperatures as production ranges between 160°C and +300°C. Ordinary Portland Cement a brittle material (OPC) when mixed with additives can provide improvement to the mechanical stability and enhance fracture resistance at these conditions. One such additive that has gained interest in other fields and applications, but not much explored in cementing field due to its unreactive and hydrophobic nature, is graphene nanoplatelets (GNPs). This study focuses on mixing GNPs with Class-H cement in very low concentrations of 0.1% or less by weight of cement (bwoc) and evaluating the performance and effectiveness in fracture prevention when undergone thermal cycling between 20 ^{o}C and 110 ^{o}C, 95% relative humidity when hydrated for 7 and 28 days in pH 13 $Ca(OH)_2$ solution. GNPs in the form of powder (PG) prepared from the environmental waste and a 99.5% carbon purity lab grade liquid dispersion GNPs (LG) were used. 0% GNPs (neat) control, 0.008%, 0.1% of PG and LG mix design cement samples were prepared following API 10B specifications. Results show that 0.1%LG samples hydrated for 28 days had greater dispersion of GNPs with a notable increase in the ductile behavior out of all the designs tested. There is a 13.21% decrease in permeability, 27.77% decrease in hardness and 50.71% decrease in elasticity when compared to neat sample hydrated for 28 days thus proving its effectiveness for wellbore integrity with increase in hydration time.

TABLE OF CONTENTS

Chapter Page

LIST OF TABLES

Table Page

LIST OF FIGURES

Figure Page

Figure Page

CHAPTER I

INTRODUCTION

As we progress in transitioning from fossil fuels to renewable sources of energy, extracting heat from the earth's subsurface needs a new approach as geothermal reservoirs are made up of diverse rock formations (U.S. Energy Information Administration, 2022). This thermal energy harvesting from the geothermal resources is expected to contribute towards mitigation of climate change as it provides near net zero emissions. Cementing the wellbore for geothermal heat harvesting is demanding because of the rock formations and the never ending dynamic thermal cycles that constitute geothermal reservoirs. Ordinary Portland Cement (OPC) is used for cementing these drilled wellbores for wellbore integrity towards effective zonal isolation. Therefore, wellbore cementing needs tested barrier materials that require stability at high cyclic temperatures resisting possible thermal shocks. These materials should also be chemically resistant to geofluids that come in contact with Ordinary Portland Cement (OPC) causing loss in mechanical strength that could lead to fracturing and wellbore integrity failures. Mixing appropriate additives with OPC cement will lead to wellbore stability and integrity. With the progressing technological advancements in cementing, nanoadditives are being used in building materials due to their outstanding properties such as large surface area, high conductivity, improved mechanical strength (Bittnar et al., 2016). When considering mixing nano additives with OPC cement for hot geothermal wells, microstructural changes in cement involves a prominent role as strength retrogression exists where the CSH phase increases in porosity and permeability as

temperature increases above 110 ^{o}C (Bergen et al., 2022). Silica stabilized cement slurries have shown to be effective at temperatures above 110 ^{o}C (Guerrero, 1998; Mahmoud & Elkatatny, 2019; Costa et al., 2017). Studies have also shown that adding graphene nanoparticles (GNP) to cement can improve porosity, permeability, elasticity and hardness thereby reducing risks from mechanical failures (Zheng et al., 2017 ; Jupudi et al.,2022 ; Massion et al., 2021). Class-H cement mixed with GNP and other additives suitable for subsurface conditions is used in this study. The cement slurry is prepared with and without GNP, a lab grade 99.5% pure liquid form and powdered form prepared from environmental waste, and then hydrated under dynamic thermal loading conditions between 20 ^{o}C and 110 ^{o}C for 7 and 28 days. The potential problem with GNP application is their hydrophobic nature, leading to dispersion issues when mixed in cement slurries. Thus, the first objective is to compare effectiveness and performance of wellbore cement reinforced with liquid GNP vs dry powdered GNP and address current concerns regarding dispersion of GNP at field conditions. The second objective is to examine if graphene nanoplatelets (GNP) can prevent deterioration of Portland cement-based slurries hydrated at different levels and subjected to cyclic thermal changes at 95% RH.

Geothermal wells are yet to be utilized to their complete potential; thus, the ultimate objective of this work is to prepare a better design of the barrier material that withstands cyclic temperature loads, is environmentally safe for energy production and storage, is cost efficient and implementable by field operators. Finally, these materials have to pass testing at reservoir like conditions, and verified for safe implementation, in order to be used on a large scale in the upcoming geothermal projects with numerous new wellbores.

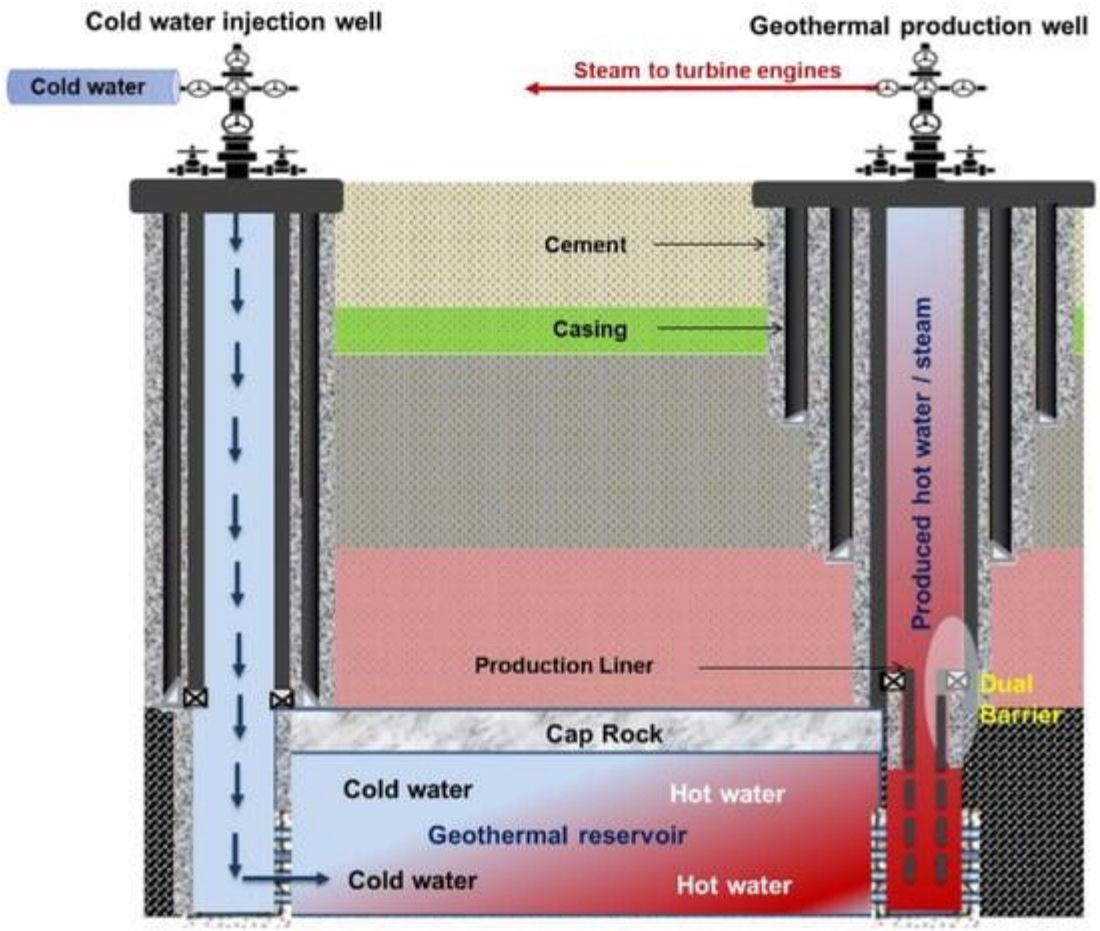

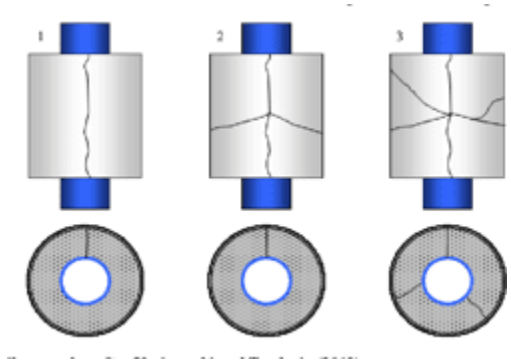

Figure 1: Schematic of geothermal well for production of heat energy from the earth's subsurface (Applications, 2022) Below is the cement failure modes beginning with a radial crack (Teodoriu, 2013)

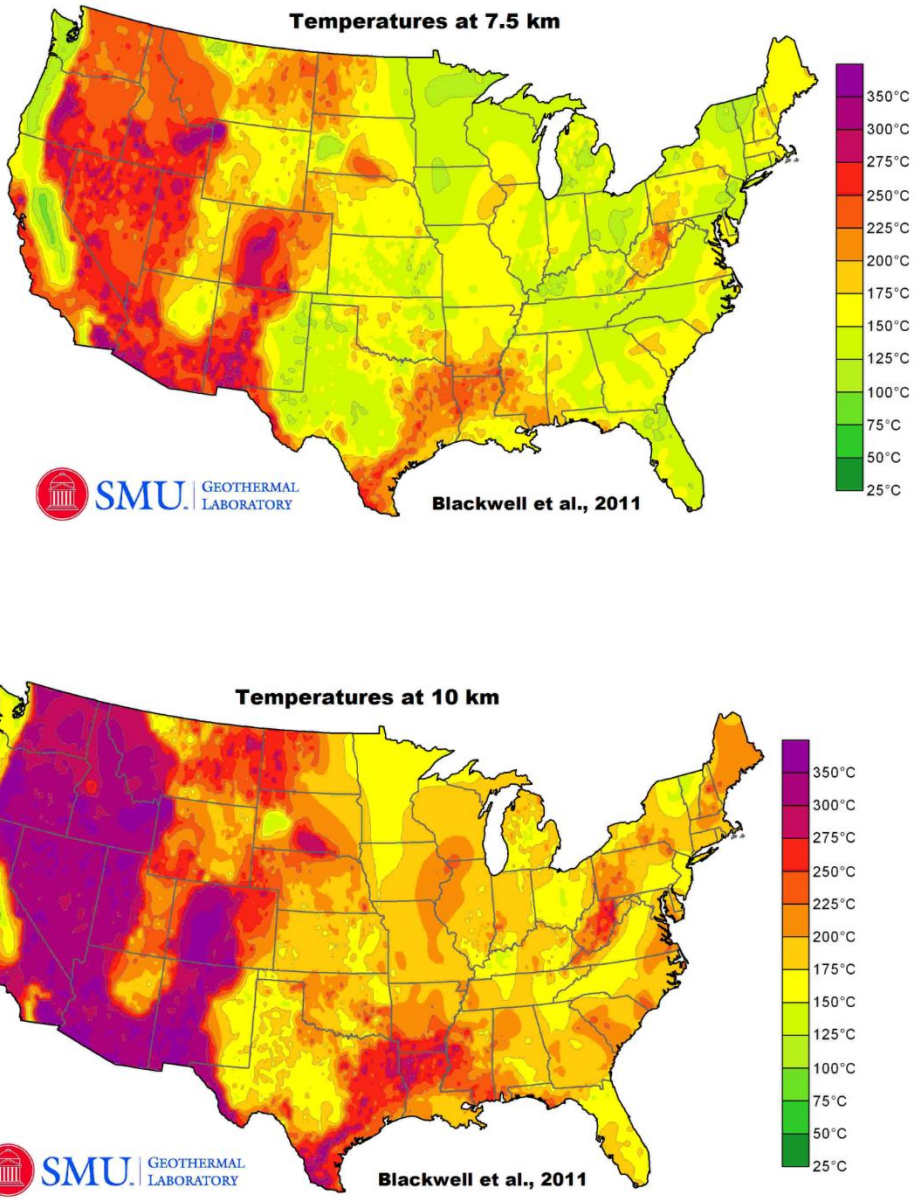

Figure 2: The temperature-at-depth maps for geothermal resources at 7.5 km and 10 km in the US from the surface of the earth. The west region has higher temperatures for the same depth when compared to the other regions making it a highly potential zone for extracting thermal energy. Source of maps: (Blackwell et al., 2011).

CHAPTER II

LITERARTURE REVIEW

In the long run, energy supply security is a necessity given the growth and demand, based on the population rise worldwide. As shown in Figure 3, November 2022 is when we will reach eight billion people, with one billion added in the last 12 years. Most of the current contribution is from the non-renewable U.S. base-load capacity that comes from thermal (coal based), nuclear and gas-combustion turbines. To meet the inflated demand, importing huge amounts of oil is beyond environmental security concerns. Climate change, environmental justice and social equities of underprivileged communities are all part of the energy transition agenda, towards a net carbon zero emissions and implementation of the United Nations sustainability goals.

The impact of implementing new technologies to extract the renewable thermal energy source used as base-load power without storage costs and very low carbon footprint from the depth of the earth's subsurface is a possible way to enhance the energy transition globally (Systems, 2006). Looking back at the history of geothermal energy across the world, the first few successfully drilled geothermal wells for heat were drilled in Luttelgeest, Netherlands by the Daldrup & Söhne AG group (Geothermal Energy News, 2020). In 1807, John Colter located the hot springs at Yellowstone Park, listing it as the first documented geothermal energy resource in the US (DOE, n.d.). Since then, the use of geothermal energy has increased and the current production

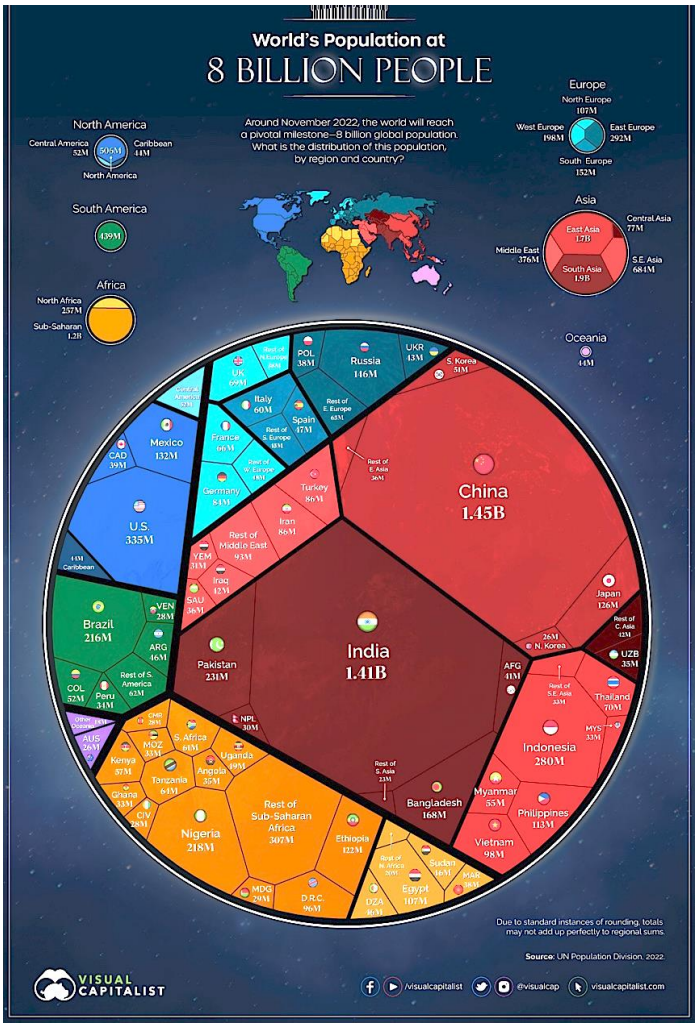

Figure 3: The numbers of world population in November 2022 according to the United Nations, Department of Economic and Social Affairs, Population Division via Worldometer's live tracker as of September 27, 2022 (Routley, 2022).

is approximately 15 GW of power on a global scale and is limited to only volcanic regions (Energy, 2021).In 2021, according to (Richter, 2022), the US was listed as the topmost country in the world with the highest installed capacity of geothermal resources in use, with California having the largest and highest production (California Energy Commission, 2019). Higher amounts are promised in the next 50 years from stats in or about 2006 by R&D. This led to potential EGS areas being identified in the US that could supply around 100 GW with current generation at

3.7 GW (Clean, 2022). In addition, geothermal energy would support economic stability given that there would be less disruptions in supply and cost (Systems, 2006). For this young technology to become a powerhouse, revolutionary methods are required to lower the drilling costs and improve the approaches to hot and deep regions while considering the rock and fluid interactions. As a part of the drilling process, wellbore cementing techniques also need to be researched and developed.

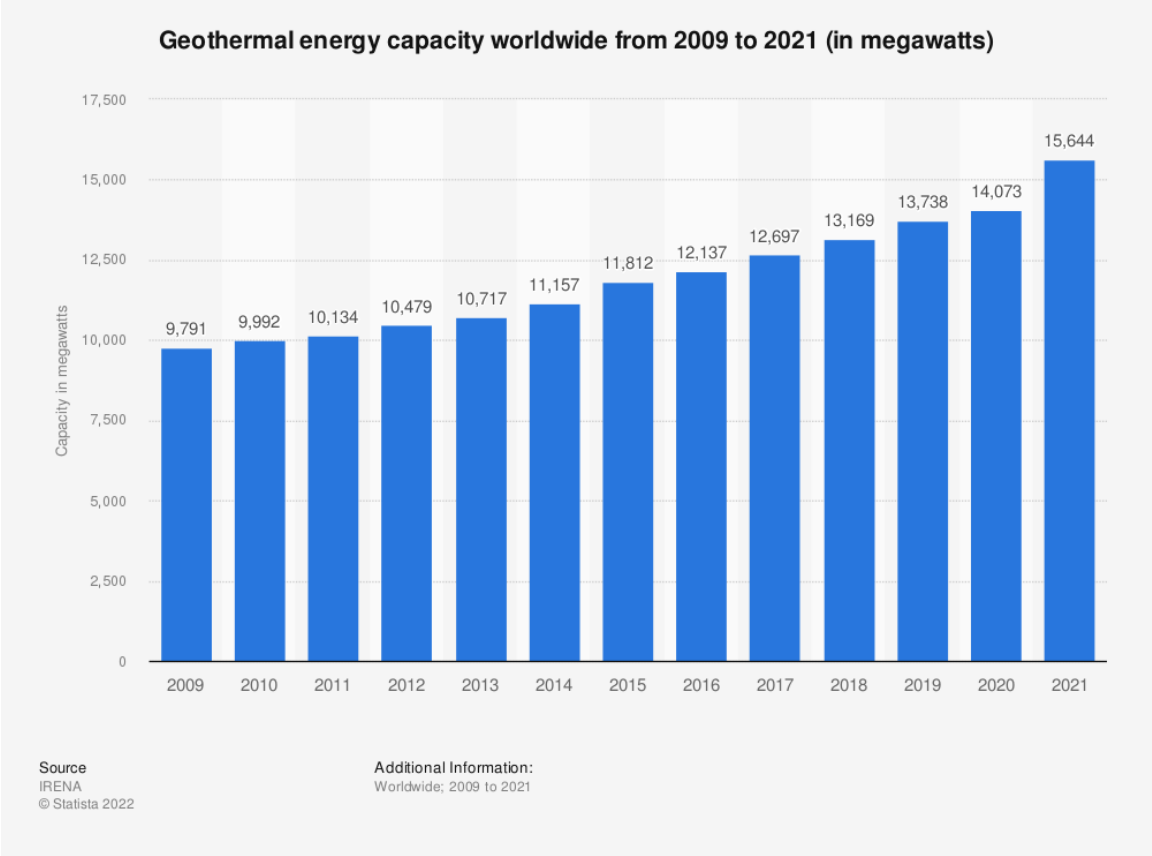

Figure 4: Geothermal installed capacity worldwide from the years 2009 to 2021 showing the production of thermal energy in megawatts (Jaganmohan, 2022). It constitutes 8.3% of the total energy consumed across the globe with the US being the largest producer.

The US is the highest thermal energy producer (Richter, 2022), and efforts are being made in lowering drilling and completion costs in order to have geothermal energy competitive with other renewable energy technologies such as solar and wind. About 50% of the $20 million sanctioned

for geothermal projects by the Department of Energy towards net-zero emissions goes towards drilling and well completion which includes cementing of the wellbores. The chart below explains the prominence of cost and risk associated with cementing geothermal wellbores.

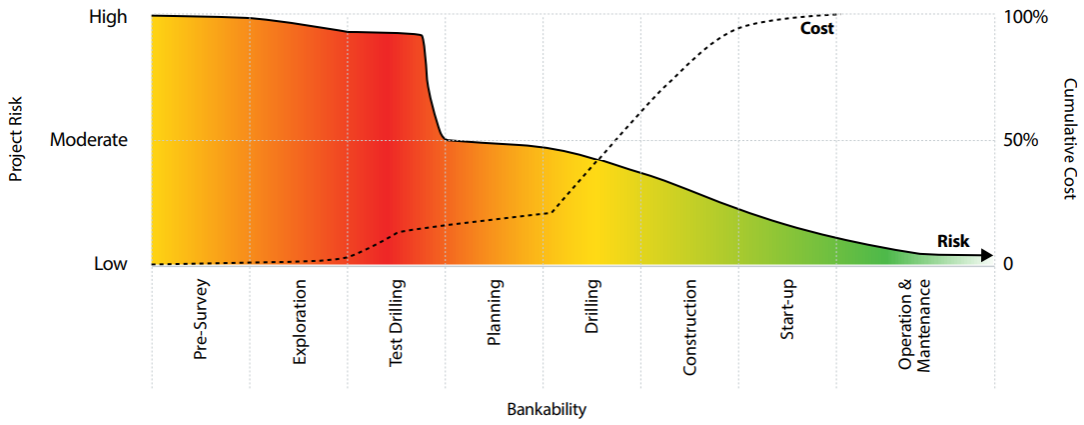

Figure 5: Geothermal project cost precent estimate at each stage along with the projection of risk (Robins et al., 2021). Unlike oil and gas, the long-term returns are consistent and constant as there is unlimited thermal energy below the earth's surface.

2.1 CEMENTING GEOTHERMAL WELLBORES

The location of geothermal resource correlates with the tectonic plates, thermal settings, rock column and rock type with respect to depth (Energy, 2021). Temperatures at depth of these resources are determined based on the thermal conductance of the rock that changes with rock minerology, area of heat flow and rock density (Boden, 2022). The reservoirs with high unlocked potential of thermal energy reserves are made up of different rock formations (U.S. Energy Information Administration, 2022). These rocks are broken to create pathways for fluid flow, the downside it potentially results in earthquakes when cold water comes in contact with hot water leading to induced seismicity. Reestablishing the rock formation properties after drilling to access the heat energy is necessary for non-leaky production and later for plugging and abandonment.

All these geo systems produce heat by the process of convection that depends on area, temperature, and heat transfer rate. These parameters i.e., temperature and permeability (depends on area and rate) do not change much with rocks thus not allowing heat to escape. Also, rocks are poor conductors of heat. Therefore, cementing these wellbores exposed to varying high temperatures up to about 400+^{o}C needs engineering advancements and additive materials that are similar to rocks.

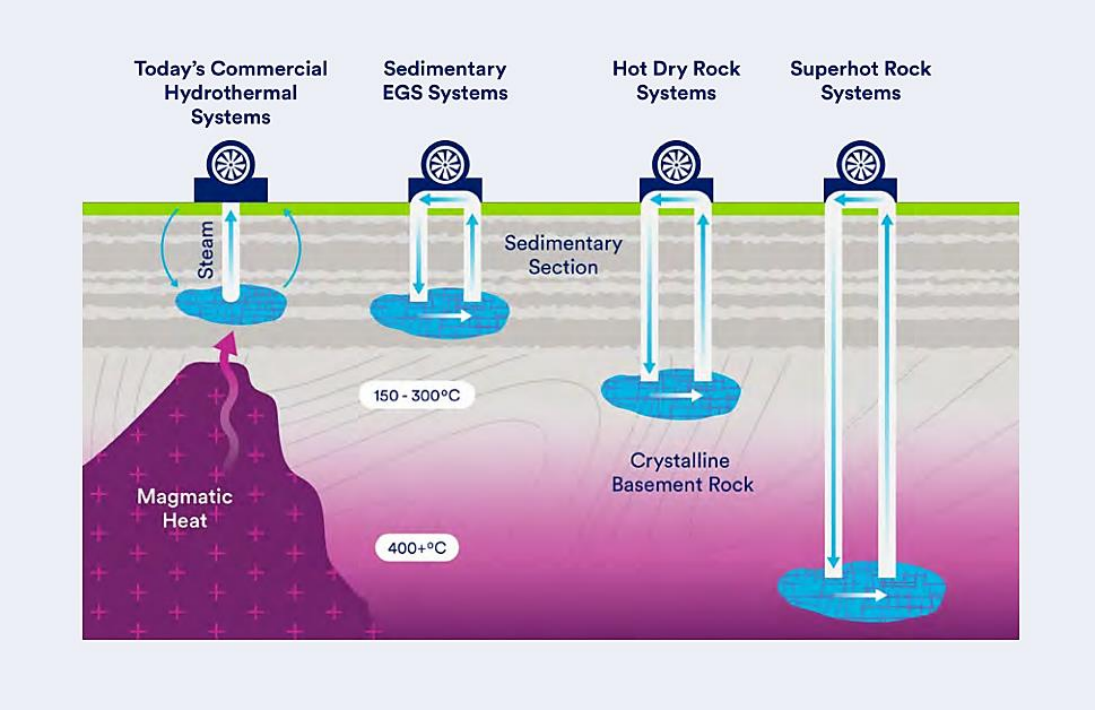

Figure 6: The four kinds of geothermal systems explained diagrammatically (Energy, 2021). There are these conventional hydrothermal systems, from where most of today's heat energy is taken and advanced methods for extracting heat from the other systems is being researched upon.

As geothermal wells are drilled in formation with high temperatures and often within an acidic environment, there is a need for self-healing and strength recovery cements (Pyatina & Sugama, 2020). Furthermore, since geothermal fluids are often rich in CO_2, the research available on cement durability studies for carbon storage technologies is applicable and published

literature suggests that chemical deterioration is a definitive problem due to calcium leaching (Yalcinkaya et al., 2011 ; Kutchko et al., 2008). Significant amounts of CO_2 leaks are reported which could be through fractures in cemented wells. In addition to cement slurry design, cement placement and its interaction with rock formation is also critical, especially if there are issues with formation damage and contamination of slurry at the interface with rocks (Radonjic & Oyibo, 2014 ; Katende et al., 2020 ; Agbasimalo & Radonjic, 2014).

The injected cement slurry pumped into the wellbore would start hydration soon after circulation is finished, and it later hardens in the interface between the steel casing and the rock formation providing a hydraulic barrier to support the structural integrity of the wellbore. Due to pressure, temperature and inadequate cement slurry designs due to loss of water for example, hydrated cement can develop microfractures, channels, which would provide pathway for corrosive fluids and the casing corrosion and finally collapse with variety of wellbore integrity issues as shown on Figure 1. This could be connected to the cement phase changes that primarily depend on temperature, pressure, and hydration time causing changes in microstructure of the cement that is not completely evaluated according to (Aili & Maruyama, 2020). This study is focused on the impact of dynamic thermal cycles that could affect the structure and stability of the cement. Deep down the wellbore, the bottom hole static temperature is primarily taken as the temperature for cement hydration (Liska et al., 2019) and this falsifies the wellbore environment paving a path for substandard performance where thermal fracturing could possibly happen due to dynamic downhole temperatures. The hot and cold water thermal cycles between production and shut-in lead to expansion and contraction of the wellbore cement thereby creating stress and forming microcracks (Feng et al., 2020). When freshly prepared cement samples were cured for below 21 days between 20 ^{o}C and 85 ^{o}C thermal cycles, the mechanical strength was found to increase (Ichim & Teodoriu, 2017).

In relevance to geothermal energy systems, high temperatures, confining and pore pressures were used to study the behavior of Thermal Shock-Resistant Cement (TSRC) in comparison to that of Ordinary Portland Cement (OPC) which showed better results but had cracks that were non-continuous resulting in corrosion (Bauer et al., 2020).

Thus, wellbore cementing could encounter issues due to formation and drilling fluids that contaminate and affect the stability of the structure, impact of thermal changes occurring at the subsurface conditions, elastic deformation due to forces from the rock formations, cement hydration reactions due to the presence of moisture. Considering all the issues, preparing cement slurries for geothermal wellbores with Ordinary Portland Cement (OPC) at subsurface conditions (especially the dynamic temperatures for essential zonal isolation and wellbore integrity) is absolutely challenging. The necessary depth to be kept in mind with respect to geothermal gradient when preparing the slurries is about 600 ft from the earth's surface (Finger & Blankenship, 2010).

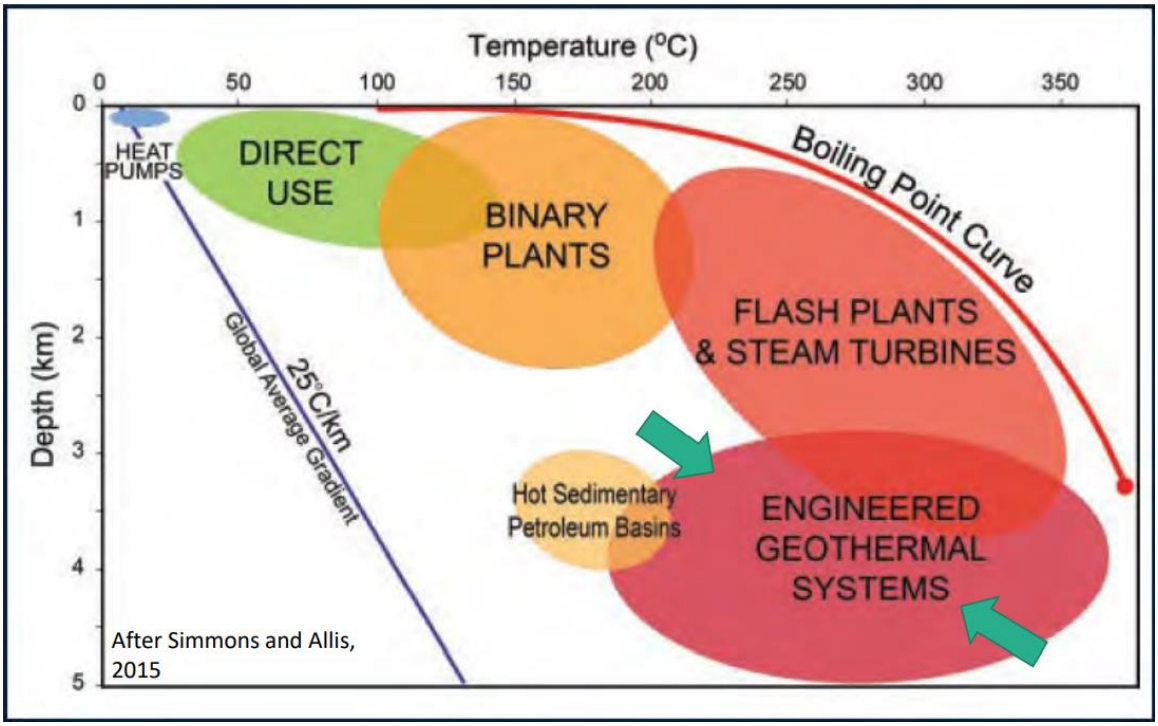

Figure 7: Uses of geothermal including EGS shown on temperature vs depth graph (Boden,

2022). With the increase in temperature-at-depth the extraction of heat energy gets challenging.

2.2. CEMENT CHEMISTRY

In order to design and examine the cement slurries, understanding the cement hydration and formation of phases is essential. Cement is a complex mix of compounds and the addition of water to anhydrous cement undergoes chemical reactions and produces hardened cement paste with calcium silicate hydrate (C-S-H) gel and C-H as the by-products obtained based on the degree of hydration. The initial rapid reactions of cement upon contact with water constitute the interstitial phases and calcium sulphates, responsible for setting and hardening of cement.

Table 1: Average mineralogical composition of Ordinary Portland Cement that reacts with water to form compounds that give mechanical strength to the structure (*CHEMISTRY AND QUALITY CONTROL FORMULAS IN CHEMISTRY AND QUALITY CONTROL*, n.d.).

Compound and Chemical Formula	Short form	By weight%
Alite or tricalcium silicate (Ca_3SiO_4)	C_3S	55
Belite or dicalcium silicate (Ca_2SiO_5)	C_2S	20
Tricalcium aluminate (Ca_3Al_2O)	C_3A	10
Tetracalcium Aluminoferrite ($Ca_4Al_2Fe_2O_{10}$)	C_4AF	8
Gypsum ($CaSO_4.2H_20$)	CSH_2	5
Oxides (K_2O, Na_2O)	N, K	2

The early hydration reactions under ambient conditions and the overall kinetic behavior is as below (Herbert et al., n.d.):

Hydration of tricalcium silicate is a very rapid exothermic reaction as it has an estimated negative enthalpy value.

$$C_3S + (3-x+n)H \rightarrow C_xSH_n + (3-x)CH \quad (1)$$

The hydration reaction of dicalcium silicate is similar to that of C_3S except that the hydration and microstructure development takes place at a slower rate compared to C_3S. The enthalpy of this reaction is lower than that of the C_3S.

$$C_2S + 4.3H \rightarrow C_{1.7}SH_4 + 0.3CH \quad (2)$$

The metastable hexagonal hydrates form stable cubic hydrates during the hydration of tricalcium aluminate.

$$2C_3A + 27H \rightarrow C_4AH_{19} \text{ (or } C_4AH_{13}) + C_2AH_8 \text{ (hexagonal hydrates)} \quad (3)$$

$$C_4AH_{19} + C_2AH_8 \rightarrow 2C_3AH_6 \text{ (cubic hydrates)} \quad (4)$$

The hydration of ferrite phase where $C_3(A,F)H_6$ at high temperatures is unstable decomposing into C_3AH_6 and Fe_2O_3.

$$3C_4AF + 60H \rightarrow 2C_4(A,F)H_{19} + 2C(A,F)H_8 + 4(F,A)H_3 \rightarrow 4C_3(A,F)H_6 + 2(F,A)H_3 + 24H \quad (5)$$

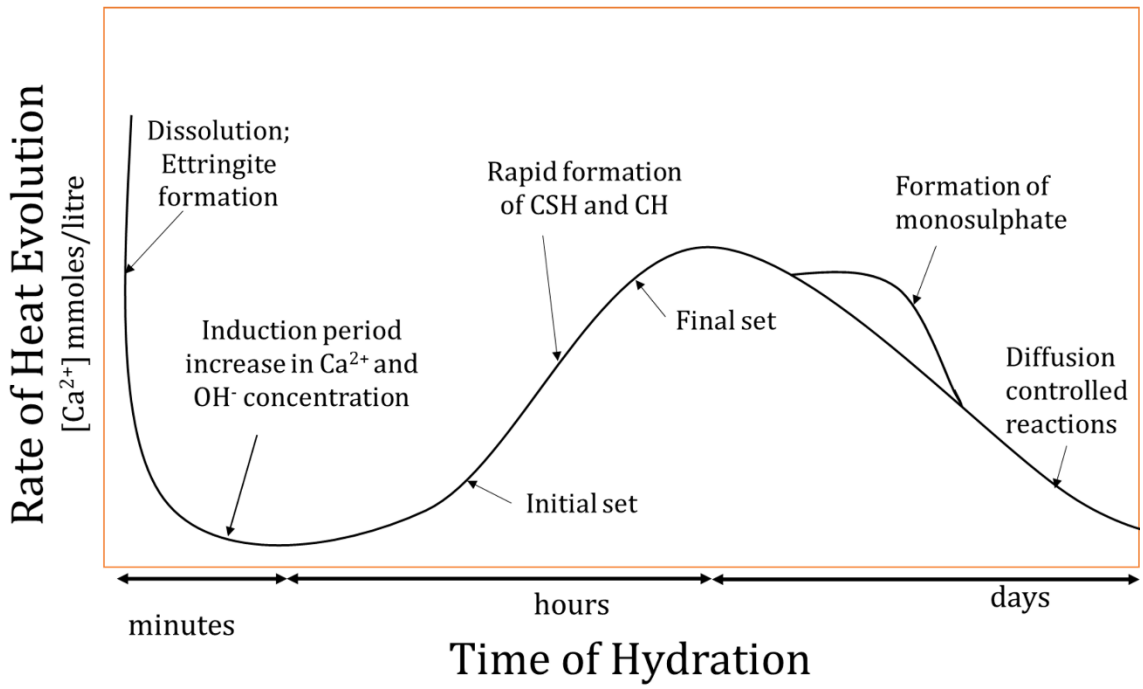

Figure 8: Image modified from (Herbert et al., n.d.) showing the changes in the rate of heat evolution during hydration of the mineral phases in the clinker. C_3S and C_3A react rapidly and exothermically.

The compressive strength development in cement at initial stages is due to alite (C_3S) and then as hydration progresses belite (C_2S) phase becomes important. As hydration of OPC is an exothermic process evolving around 100 cal/g for 28 days of hydration, careful consideration is required when using it for large constructions. According to theory, most of the heat is from C_3S and C_3A reactions. We need to reduce the heat evolved but maintain the compressive strength. This could be done by decreasing C_3S and increasing C_2S which would affect only the initial strength and also partly by decreasing the content of C_3A and increasing C_4AF (Taylor, 1997; Cadix & James, 2022).

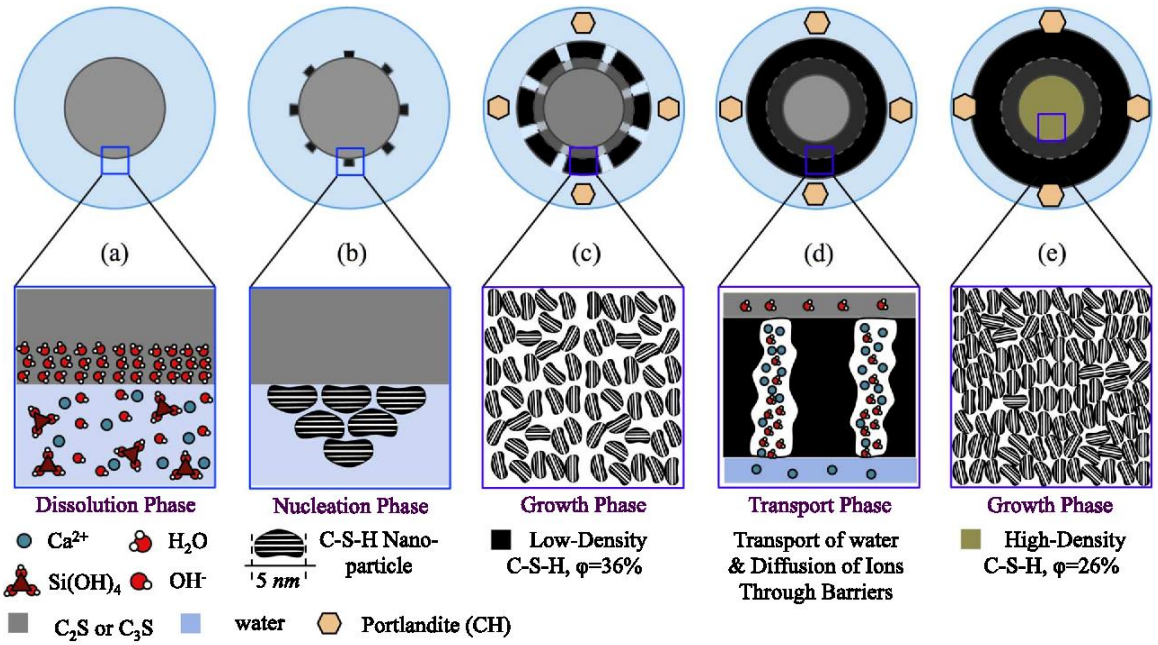

Figure 9: Image is taken from computationally developed five-step cement hydration model to explain diffusion through a spherical CSH shell (Rahimi-Aghdam et al., 2017) a) the semi-impermeable layer is formed around the cement particles. b) the CSH particles are symmetrically nucleated on the surface. c) CSH nuclei continue to grow with time at varying rate but are equally spaced. d) CSH nuclei overlap and cover the entire surface thus stopping the nucleation growth. e) CSH particles grow uniformly by the inward transport of water.

The active components in OPC vary in proportion for each class of cement. Class-H cement, the type used in this work has a maximum particle size of 120 µm with 50% of the particles at an average of 24.5 µm. When mixed with additives the best suitable design is proposed for subsurface conditions for geothermal wellbore cementing according to the API cement classification and communications with cement R&D teams in industry, to replicate field application conditions in this laboratory study to the highest possible level. That is a critical component for new materials to be accepted and implemented by industry and the highest impact of this research.

2.3 CEMENT SLURRY WITH GRAPHENE NANOPLATELETS AS NANOADDITIVES

Carbon based nanomaterials is one of the group of additives that have recently been sought after to improve performance in cementitious materials. Researchers have studied the effect on structural, petrophysical, and mechanical properties of only additives such as single walled carbon nanotubes (SWCNTs), multi walled carbon nanotubes (MWCNTs), graphene, graphene oxide (GO), carbon fiber, and polymeric fiber (polypropylene and nylon). Graphene has the highest surface area, 2600 m^2/g and lowest particle size, 0.1 nm (Lee et al., 2008; Stankovich et al., 2006; Zhu et al., 2010; Yu et al., 2000; Aili & Maruyama, 2020; Peigney et al., 2001). Structural modification of carbon nanotubes (CNTs) to add functional groups by covalent bonding to improve tensile and compressive strength was studied by (Chuah et al., 2014; G. Y. Li et al., 2005). Graphene nanoplatelets, micronized ferrierite and olivine were added to the cement separately and studied for their impact on wellbore integrity and zonal isolation (Massion, Vissa, et al., 2022). Based on current literature graphene is unreactive when mixed with cement and is found to have increased the strength and durability (Chuah et al., 2014). Graphene nanoplatelets (GNPs) were found to influence the effectiveness and performance of the Ordinary Portland Cement (OPC) (Jupudi et al., n.d. ; Massion et al., 2021).

GNPs are produced by liquid phase exfoliation of graphite into monolayered graphene, few layers (~2 to 10) and multi layered (above 10) nanostructured graphite (Achee et al., 2018; Cataldi et al., 2018; Chung, 2002; D. Li et al., 2008).

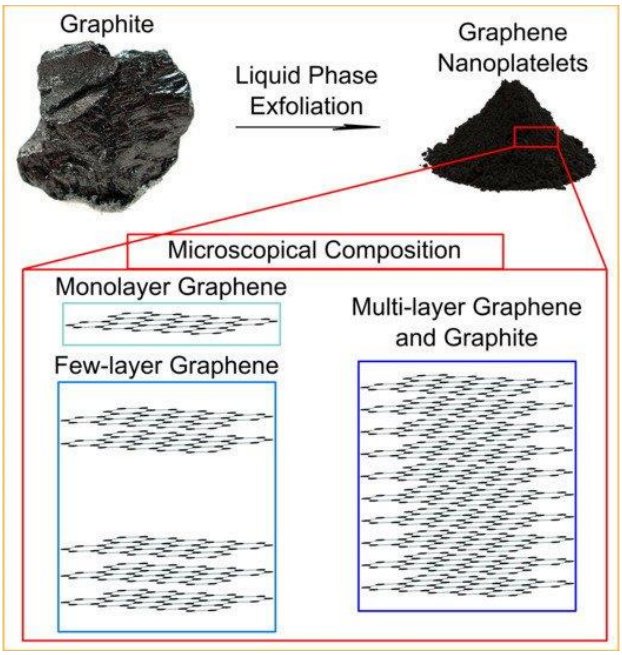

Figure 10: The schematic of the layers of graphene nanoplatelets (GNP) produced by liquid phase exfoliation of graphite as stated by (Cataldi et al., 2018). Few layers (<11) graphene is mixed with Class-H cement in this research.

There is an electronic structural difference which makes a single layer graphene as a semiconductor with zero-gap and multi layered graphite as a semimetal with band overlap of 41 meV. There is a difference of less than 10% band overlap between graphite and for 11 or more graphene layers thus stating the 3D structure starts from 10 layers of AB stacked layers of graphene (Geim & Novoselov, 2007; Partoens & Peeters, 2006). (Terrones et al., 2010) clearly stated and showed the difference between 2D graphene layer and 3D graphite crystal structure. For a single layer graphene as there is no edge modification, it would not interact with cement and lower the overall energy. Only when there is an edge modification that takes place in multi-layers does it interact with cement. This could probably happen with few-layer GNP as well. Also, disruptions in graphite take place at high temperatures. At high static temperature conditions GNP added in low quantities have shown to increase strength and decrease brittleness (Zheng et al., 2017;

Massion et al., 2021; Massion et al., 2020; Rhee et al., 2016; Cao et al., 2016) but the involvement of GNP in the hydration reactions is unknown.

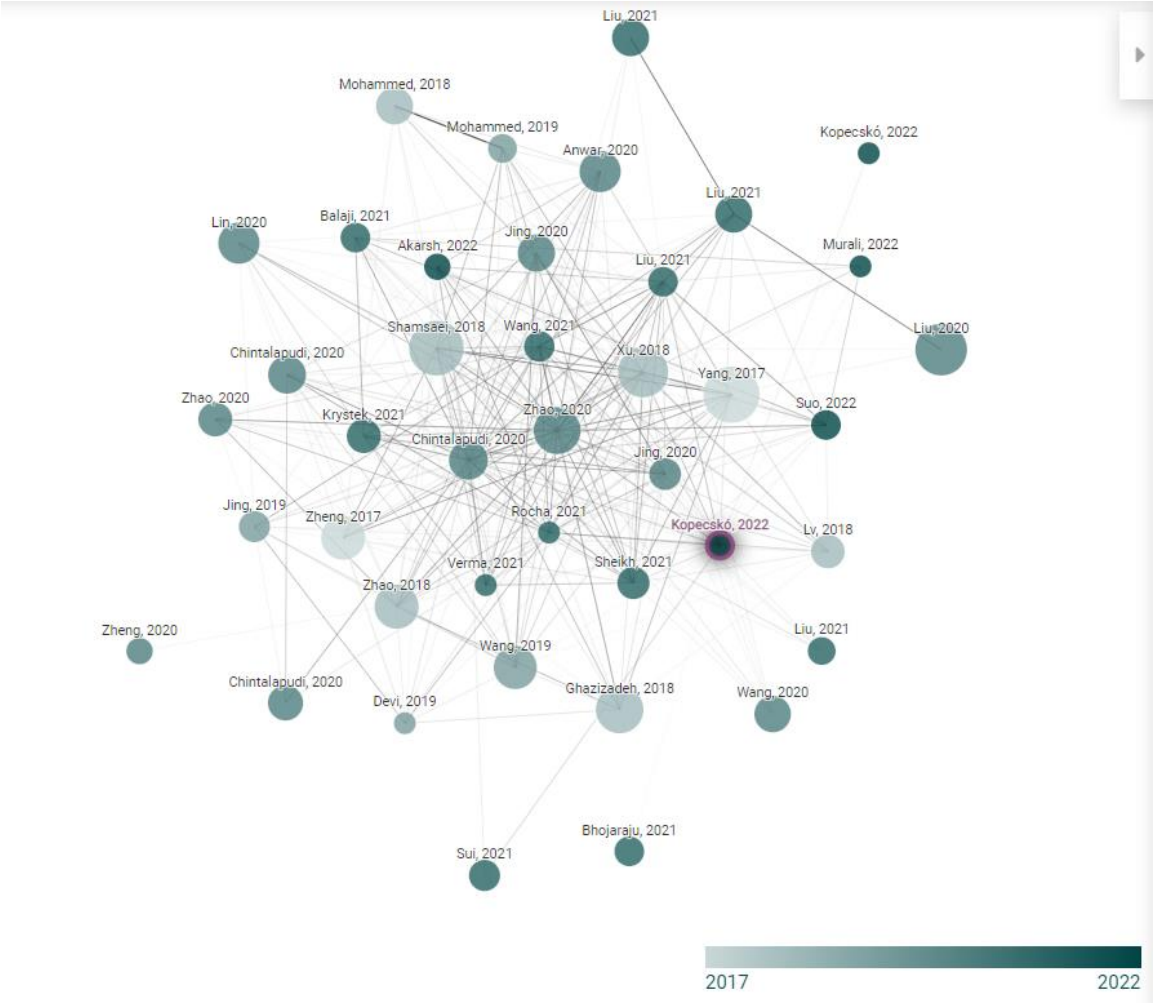

Figure 11: An overview of the work done using graphene oxide in cementing of wells from the years 2017 – 2022 using connected papers.com.

Significant amount of research has been done on graphene oxide (GO) as a nanoadditive to Portland cement-based materials in comparison to graphene nanoplatelets added to Portland cement composites. Influence of GOs on the enhancement of hydration mechanism and functionalizing behavior of it in cement has been reviewed by (Katalin Kopecskó & Zaid Ali Abdulhussein Khaiqani, 2021) while (Murali et al., 2022) focused on the overview of cementitious

composites using GO. This study focuses on GNP enhanced cement as the unexplored gaps are higher in comparison to GO and in continuation of previous works that have focused only on powdered graphene prepared from environmental waste.

A laboratory grade 99.5% pure graphene nanoplatelets dispersed in liquid (LG) and powdered (PG) graphene prepared from biochar were used as nanoadditives in this work. The objective is to evaluate the compositionally modified wellbore cement performance hydrated under dynamic temperature cyclic conditions and to measure and evaluate structural, mechanical properties at 7 and 28 days of hydration. All the samples are subjected to cyclic temperatures loading from 20 ºC to 110 ºC following an 8-hour cycle for 7 and 28 days in ESPEC environmental chamber. These temperature cycles help evaluate close to the realistic conditions where enhanced geothermal systems undergo temperature changes over tens of thousands of times during injection of cold water for rock fracturing and heat harvesting. The cement paste samples are characterized for micromechanical and microstructural properties to investigate GNP effectiveness in fracture prevention and evaluate the level of particle dispersion once hydration of cement is complete.

CHAPTER III

MATERIALS AND METHODOLOGY

In the process of achieving a near to perfect cement slurry for cementing geothermal wellbores, following suitable materials and additives were used in preparing the mix designs as elaborated below. The samples were characterized for micromechanical properties by micro-indentation, scanning electron microscopy (SEM) and energy dispersive x-ray spectroscopy (EDS) for the microstructure of the cement and Raman spectroscopy for chemical analysis and phase identification, permeability (Nano-Permeameter) and porosity (Helium-Porosimeter) measurements for petrophysical analysis.

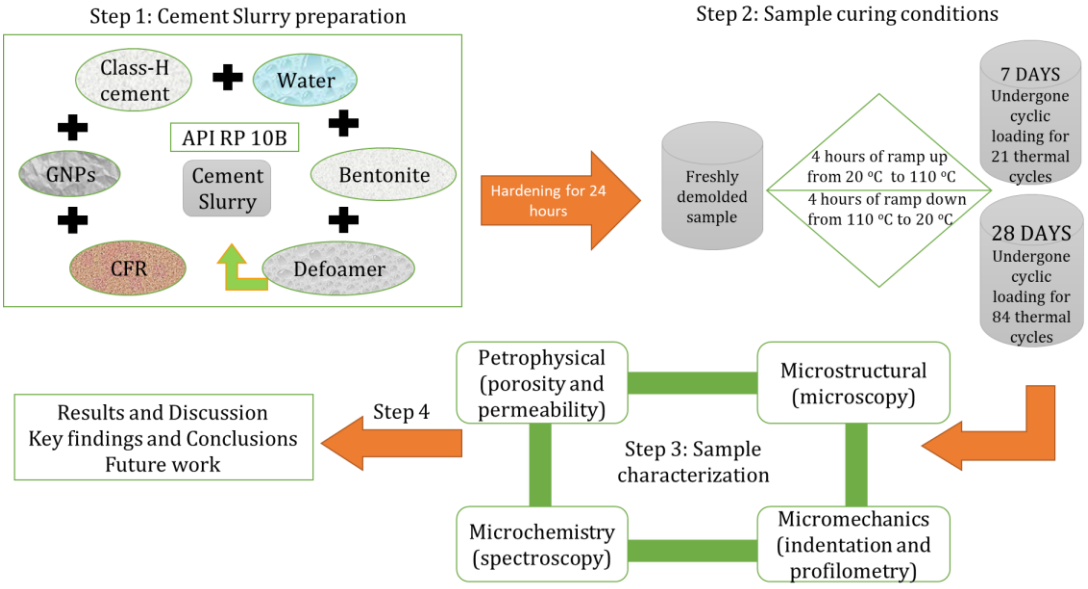

Figure 12: Flowchart showing the approach of activities undertaken during this study. Firstly, the cement slurry is prepared with GNP and other additives. These samples are cured for 7 and 28 days under thermal cyclic conditions, then cut and polished for characterization. Finally, the data is analyzed, and results are discussed.

Table 2: The cement samples mixed with GNP is studied and evaluated for properties as shown in the experimental matrix below.

Sample Name	Hydration time	Petrophysical (Porosity & Permeability)	Micromechanical (microindentation & surface profilometry)	Microstructural (SEM)	Microchemistry (EDS & Raman Spectroscopy)
0% GNPs (Neat)	7 days (21 thermal cycles)	3	1	1	1
0.008% PG		3	1	1	1
0.008% LG		3	1	1	1
0.1% PG		3	1	1	1
0.1% LG		3	1	1	1
0% GNPs (Neat)	28 days (84 thermal cycles)	3	1	1	1
0.008% PG		3	1	1	1
0.008% LG		3	1	1	1
0.1% PG		3	1	1	1
0.1% LG		3	1	1	1
Total number of samples	10	30	10	10	10

3.1 Graphene Nanoplatelets

Powdered graphene and graphene nanoplatelets (GNP) dispersed in liquid as obtained without any modification were examined for microstructure by transmission electron microscope (TEM) and scanning electron microscope (SEM). Powdered graphene (PG), the type used in this study is refined from the biochar having multiple layers of nanoplatelets and amorphous carbon. Powdered graphene from Novagraphene was examined for the elemental composition and showed 88.28% carbon, 10.39% oxygen, and less than 0.3% of calcium, silicon, iron, aluminum, sodium, magnesium, and potassium (Massion et al., 2021). Graphene dispersed in 6wt% water is 99.5% pure having an average of 4-6 layers obtained from US Research Nanomaterials, shortly referred to as liquid graphene (LG) were used in this study. These GNP at 0.008% and 0.1% by weight of cement (bwoc) along with other additives were added to Class-H cement to obtain a 1965.15 kg/m^3 (16.4) ppg cement slurry.

3.2 Portland Cement

3.2.1 Cement slurry preparation and hydration

Class-H cement was used in this study to evaluate the cement properties due to heating and cooling cycles. This is mixed with water, bentonite, dispersant (Halliburton CFR-3), and defoamer (Halliburton D-air 5000) in proportions to prepare the cement slurry. The components were measured and mixed dry before putting them into the blender. A Waring lab variable speed mixer jar initially filled with the measured water was used to mix the components at a low speed for 15s, and then at a higher speed for 35 s to achieve a 1965.15 kg/m^3 (16.4 ppg) slurry based on the API 10B specifications. This was immediately poured into the brass molds that were prepared using a spray to avoid sticking cement to the surface of the mold during hardening. These molds filled with cement are covered with cling wrap to contain the moisture and left for about 24 hours at room temperature. Cement samples are demolded after about 24 hours, and are instantly put into $Ca(OH)_2$

solution to prevent calcium leaching of the cement, sealing it air-tight with aluminum foil and plastic wrap.

For 0.008% and 0.1% of powdered graphene and graphene nanoplatelets dispersed in liquid, we first add GNP to the water in the blender to reduce non-uniform dispersity. Then run at a low speed for 15 seconds later adding the dry mix like that in the neat sample. Powdered graphene has about 88% carbon and about 10.5% oxygen is used. Both powdered and dispersed in liquid graphene nanoplatelets were used without any modification.

Table 3: Materials used to prepare cement core samples at ambient temperature and atmospheric pressure in proportions for the four mix designs and neat sample following API 10B specifications. Water to cement ratio is 0.384, density of the slurry is 16.4 ppg, water to solid ratio is 0.374.

Material	Neat	0.008% LG	0.008% PG	0.1% LG	0.1% PG
Class H (g)	836.71	836.71	836.71	697.26	697.26
Water (ml)	321.05	320.01	321.06	256.71	267.64
Graphene (ml, g)	0.00	1.12	0.07	11.62	0.70
D-Air 5000 (g)	2.09	2.09	2.09	1.74	1.74
Dispersant CFR-3 (g)	2.51	2.51	2.51	2.09	2.09
Bentonite (g)	16.73	16.73	16.73	13.95	13.95
Mix (g)	1179.09	1179.17	1179.17	983.37	983.37
Volume (ml)	600.01	600.05	600.05	500.41	500.41

3.2.2 Thermal Cyclic loading

Cement core samples completely soaked in pH 13 $Ca(OH)_2$ solution are placed in the ESPEC environmental chamber. This chamber was running cyclic temperature loads between 20 ^oC and 110 ^oC, 95% relative humidity (RH) which closely resemble the realistic conditions below the earth's surface on an 8-hour per cycle time. The samples are cured at these conditions for 21 cycles and 84 cycles.

Table 4: Parameters for hydration of cement samples in the ESPEC environmental chamber at atmospheric pressure.

Parameters	Working conditions
Temperature	20 ^oC – 110 ^oC
Relative Humidity	95%
Total cycle time	8 hours (4 hours to ramp up and 4 hours down)
Total number of cycles in 24 hours	3
Total number of cycles at 7 and 28 days	21 and 84

3.2.3 Cement sample preparation: cutting and polishing

The cement cores are cut using a slab saw to remove the uneven edges and to obtain the desired size of the samples. These are then polished using a developed procedure of filing, grinding and polishing using lubes on an Allied AD-5 ™ MultiPrep ™ instrument. Sample cut into 7 mm height is placed on a fixture that goes into the instrument and is initially grinded using an 8" 600 (P-1200) grit silicon carbide magnetic disc to remove distortions. In the next step, a 6 μm diamond suspension and purple-lube was used on a Gold Label cloth followed by 1μm diamond suspension and purple-lube on a White Label cloth. After this, a black cloth was used with colloidal silica for finishing. This polished sample is sonicated with IPA using a bath sonicator for about a minute to

ensure that there are no suspensions of cement particles, or polishing lubes. These are dried for two hours at 50 ^{o}C in a drying oven.

3.2.4 Cement Sample Characterization

3.2.4.1 Petrophysical Analysis

3.2.4.1.1 Porosity

After removing the samples from the environmental chamber, the cores were cut in order to have even edges. Cores sized about 2.5×5.5 cm (1×2.5 in) were individually placed in the matrix cup of the unit to measure porosity. The individual dimensions of each core sample were noted and used as inputs for calculating the grain volume of the sample using the Win pore software connected to the porosimeter. Firstly, the system is calibrated with disks of known volume. Helium gas is flown into the tank chamber at 1.38 MPa (200 psi) and once it stabilizes, the valve opens and the gas flows into the matrix cup. The pressure in the cup stabilizes with time and the difference in the pressure is used to calculate the grain volume, porosity, and density. Measurements are done on three sets of core samples for each mix design, 0% GNP (neat), 0.008% liquid graphene (LG), 0.008% powdered graphene (PG), 0.1% liquid graphene (LG) and 0.1% powdered graphene (PG). The values obtained are averaged for porosity. This system runs based on ideal gas law and Boyle's law.

$$p_1 v_1 = p_2 v_2 \quad (6)$$

p_1 is the pressure flowing from the Helium gas in psi, v_1 volume of the tank chamber in cc, v_2 volume of the grains present in the core sample in the matrix cup in cc and p_2 the corresponding pressure in psi.

From here, pore volume (vp) is obtained by subtracting the grain volume (vg) from the total volume (vt) calculated by the measured dimensions using calipers. Porosity is calculated by,

$$\emptyset = \frac{\mathrm{vp}}{\mathrm{vt}} = (\mathrm{v}t - \mathrm{vg})/\mathrm{vt} \quad (7)$$

3.2.4.1.2 Permeability

Core samples that were measured for porosity were placed in the core sample holder of the permeameter using a rubber sleeve to measure the fluid flowing through the interconnected pores in the sample. These were tested at a confining pressure of 13.8 MPa (2000 psi) and an upstream pressure of 0.0138 MPa (2 psi) uisng Helium gas. Nano-perm software was used to input the specific core sample dimensions measured using calipers, viscosity of Helium gas in cP to obtain the permeabiltity coefficent based on Darcy's law when the outlet pressure reads 4.5 in of H_2O. The average permeability was calculated for 6 hours, beginning at one hour after starting the experiment avoiding any stability errors. The following Darcy's equation was used to measure the permeability.

$$q = \frac{k}{\mu} \mathrm{A} \left(\frac{\Delta p}{L}\right) \quad (8)$$

where q is the volumetric flow rate in cc/s, k is absolute permeability in mD, μ the fluid viscosity in cP, A is the cross-sectional area in cm^2, L the length of the core sample in cm and Δp, the differential pressure over the sample.

3.2.4.2 Micromechanical Analysis

3.2.4.2.1 Micro indentation

Nanovea micro indenter with micro Nanovea software was used to make indents on polished samples. The polished cement sample was physically marked into four quadrants where the first and third quadrants were marked with 10×5 matrix indents on each quadrant totaling up to 100 indents on each sample. The sample is fixed on the cleaned surface of the holder and an area on the first and third quadrants is selected after viewing under the microscope for pores and

artifacts. Then the auto contact is measured using a force of 20 mN and a loading rate of 250 µm/min and the tip force of the indenter is normalized. At z = 0.016 mm, the depth sensor is adjusted between 20 and 40 mm, with an intensity between 40 and 75%. Then dark signal is measured keeping the sensor away from the copper block. Vickers diamond tip that made indents raging between 110-140 µm diameter was used with a load of 5N and loading/unloading rate at 10 N/min. A steel block was used for calibration purposes before indentation on each core sample. The following formula is used to calculate the hardness using a Vickers diamond tip.

$$HV = 0.1891 \times \frac{F}{d2} \tag{9}$$

where HV is the hardness value in GPa, F is the force in N, d is the diameter in mm.

3.2.4.3 Microstructural and Microchemistry Analysis

3.2.4.3.1 Scanning Electron Microscopy (SEM)

Scanning Electron Microscopy (SEM) was done on cured and polished samples. Backscatter electron imaging was performed for low, medium, and high magnifications and fine focus at 10 kV, 1.6 nA, low vacuum mode on Thermofisher Scios 2. The images are captured at multiple locations to examine the microstructure of the cement. Energy dispersive X-ray spectroscopy (EDS) line profile was done at different locations on a sample where various elements such as calcium, carbon, oxygen, silica, aluminum, iron and more were detected using the Pathfinder software. This software allows us to get secondary electron (SE) or backscatter electron (BSE) image from the Scios 2 and set parameters for acquisition under microanalysis.

3.2.4.3.2 Energy dispersive X-ray spectroscopy (EDS)

Energy dispersive X-ray spectroscopy (EDS) line scan mode was used for elemental composition. The EDS detector was inserted into the chamber on Thermofisher Scios2. The settings for image capturing were similar to that of SEM where the Backscatter electron imaging was used

on low vacuum mode i.e., at 0.07 torr (9.33 Pa) chamber pressure. Path finder software was used to create a project file and capture the image. After obtaining the desired image, a line with a specific number of points selected is drawn on where the elemental analysis needs to be done. The line scan parameters such as dwell time, resolution is set to obtain a graph with atomic percentage composition of identified elements on that location with respect to the length of the line.

3.2.4.3.3 Transmission Electron Microscopy (TEM)

TEM images were captured for graphene nanoplatelets as obtained to study the microstructure of the platelets using JEM-2100 TEM microscope. About 0.1mL of liquid GNP and 0.1g of powdered GNP are dispersed in isopropanol solution and sonicated for a minute for uniformity. About 5 µL of the mixed solution is suspended on the holey-carbon 200 µm mesh using a micropipette. This grid is then placed in between the electron source and the lens using the specimen holder for imaging at 200 kV and 40000x magnification.

3.2.4.3.4 Surface profilometry

Polished and mircoindented cement samples were analyzed to obtain surface profilometry and phase identification using green laser of 532 nm wavelength. Control FIVE software was used to get the topography using the true surface option with the configuration setting in Raman mode. The image of the indents is video stitched on a 10×5 matrix at 20x magnification. A large area scan for surface profilometry was performed on the sample on a surface area of 4600 × 4600 μm^2. The sample was tested with a laser energy at 10 kV and an integration time of 1 second.

CHAPTER IV

RESULTS

The cement samples hydrated for 7 days (21 thermal cycles) and 28 days (84 thermal cycles) under dynamic temperatures, after cutting and polishing have been tested for microstructural, micromechanical properties and microchemistry analysis. The core samples were only cut for uneven edges to remove distortions for petrophysical testing. Results showing the porosity and permeability variations with respect to hydration time and the microstructural differences based on the degree of hydration and mechanical stability when a force load is applied for different hydration times can be seen in this chapter.

4.1 Graphene nanoplatelets enhanced cement

4.1.1 Porosity

Three cement core samples from each set of mix designs hydrated for 21 thermal cycles (7days) and 84 thermal cylces (28 days) were measured for porosity (%) and an average was taken. For neat and mix designs 0.008% and 0.1% LG and PG cement cores, the values for porosity is between 27.5% and 29.78%. Hence there is not much variation observed in porosity after 7 days of hydration. Looking into 28 days of hydration, the range of values are between 21.60% and 27.93%. Neat sample measures 21.6% and 0.008%LG as 27.93%. Comparing data for each mix design between 7 and 28 days of hydration, 0% GNP (neat) sample has 21.5% decrease in porosity, that

being the highest percentage decrease. The lowest percentage decrease is 5.5% which is seen in 0.008%LG. The percentage decrease in porosity for each set of designs can be design in Table 4. Porosity is measured in percentage (%).

Porosity comparison on cement samples hydrated for 7 and 28 days

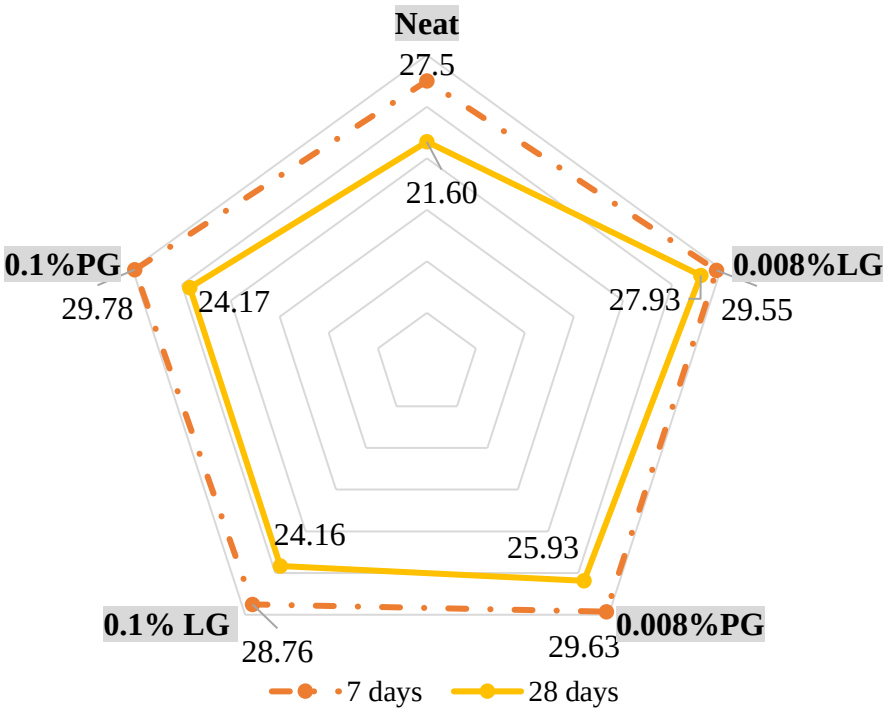

LG: liquid graphene nanoplatelets, PG: powdered graphene nanoplatelets

Figure 13: A radar plot showing the comparison of porosity when hydrated for 7 and 28 days. Three samples for each design hydrated for 7 and 28 days were measured for porosity (%). A decrease was clearly observed for 84 thermal cycles (28 days) compared to 21 thermal cycles (7 days).

4.1.2 Permeability

For this experiment also, three cement cores cut and polished to have parallel edges, were taken and measured for permeability (μD). As described in methodology, the 6-hour data is averaged for each sample and an overall average is calculated for each design. For all the cement samples

hydrated for 7 days or 21 thermal cycles the data was between 78.52 µD and 90.37 µD. The lowest value is seen in 0.008%LG and the highest in 0.1%PG cement samples. For 28 days of hydration, the numbers are between 49.48 µD and 76.64 µD. The lowest values are seen in 0.1%PG and 0.1%LG after 28 days of hydration as seen in Figure 11. The highest percent decrease in permeability between 7 and 28 days of hydration is 45.25 ± 0.02% which is seen in 0.1%PG. There is a 41.9 ± 0.03% decrease in 0.1%LG and 30.48 ± 0.02% decrease in neat sample. A decrease in permeability was observed for all the samples hydrated for 28 days when compared to 7 days hydration just as in porosity. Permeability is measured in µD (SI units: dimensions of length^2).

Permeability comparison on cement samples hydrated for 7 and 28 days

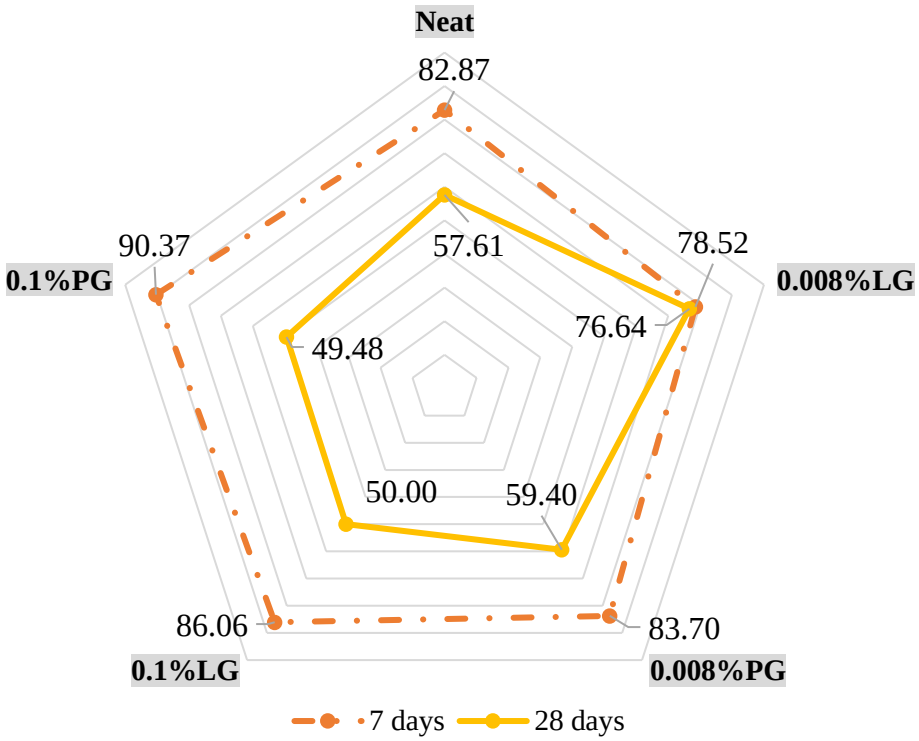

LG: liquid graphene nanoplatelets, PG: powdered graphene nanoplatelets

Figure 14: A radar plot showing the comparison of permeability when hydrated for 7 and 28 days. As effective porosity decreases, permeability also decreases for 84 thermal cycles (28 days) compared to 21 thermal cycles (7 days). Lower values are observed on 0.1% LG and 0.1%PG samples hydrated for 28 days.

Table 5: Percent decrease for 3 porosity samples and 3 permeability samples obtained using Helium porosimeter and permeameter after 7 and 28 days of hydration. Highest decrease in values are observed on 0.1% LG and 0.1%PG samples.

Sample Name	Porosity decrease (%) between 7 and 28 days of hydration	Permeability decrease (%) ± Standard Deviation between 7 and 28 days of hydration
0%GNP control	21.5	30.48 ± 0.02
0.008%LG	5.5	2.39 ± 0.07
0.008%PG	12.5	29.03 ± 0.02
0.1%LG	15.99	41.9 ± 0.03
0.1%PG	18.83	45.25 ± 0.02

4.1.3 Microstructure

Cement samples that were prepared with a mix of 0.008%, 0.1% graphene nanoplatelets (GNP) and neat samples after hydration for 7 and 28 days under thermal cyclic loading were scanned using backscatter electron imaging at low vacuum (low chamber pressure) to avoid charging effect. To identify the presence of GNP in the cement samples, powdered graphene and GNP dispersed in liquid with no modification as obtained were observed under scanning electron microscope (SEM) and transmission electron microscope (TEM). Under SEM, graphene dispersed in 6 wt% water as base has approximately 4 layers and powdered GNP have multilayers and rounded structures on them. Under TEM, some round and thin rod like structures were observed in both powdered and liquid form that closely resembles graphene nanodots as reported in (Yoon et al., 2018). However, the presence of GNP was observed, clearly differentiating between few layers typical for liquid graphene and multiple platelets more common when powdered graphene was used.

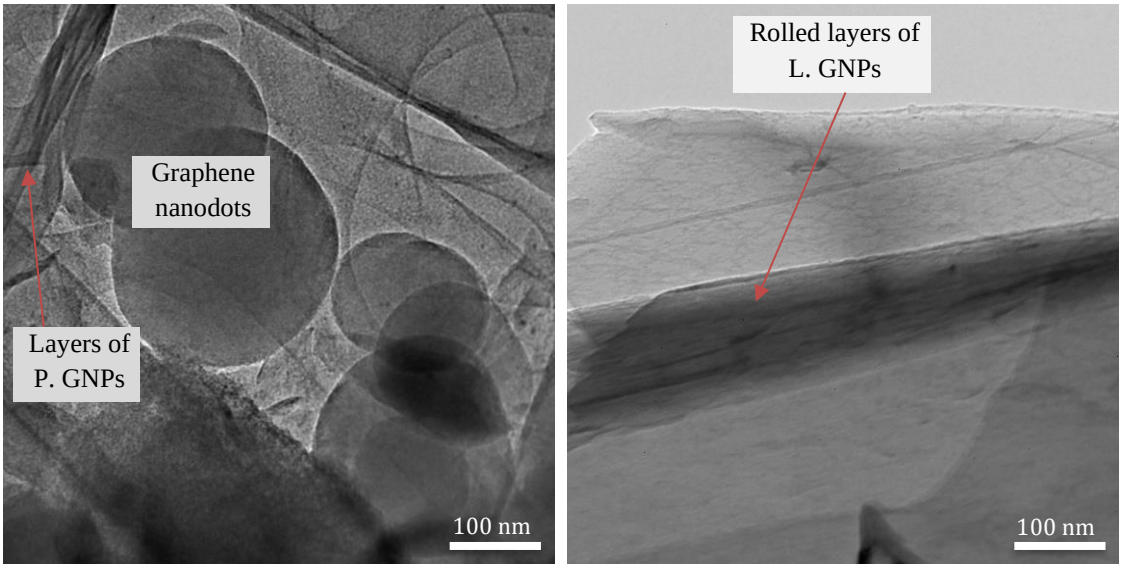

Figure 15: Transmission electron microscope (TEM) images showing the microstructure of powdered graphene that could possibly have presence of graphene nanodots in them. The image on the right shows layers of graphene sheets dispersed in liquid that could have been rolled up where edges are neatly visible. Both the images are taken at 40kx magnification.

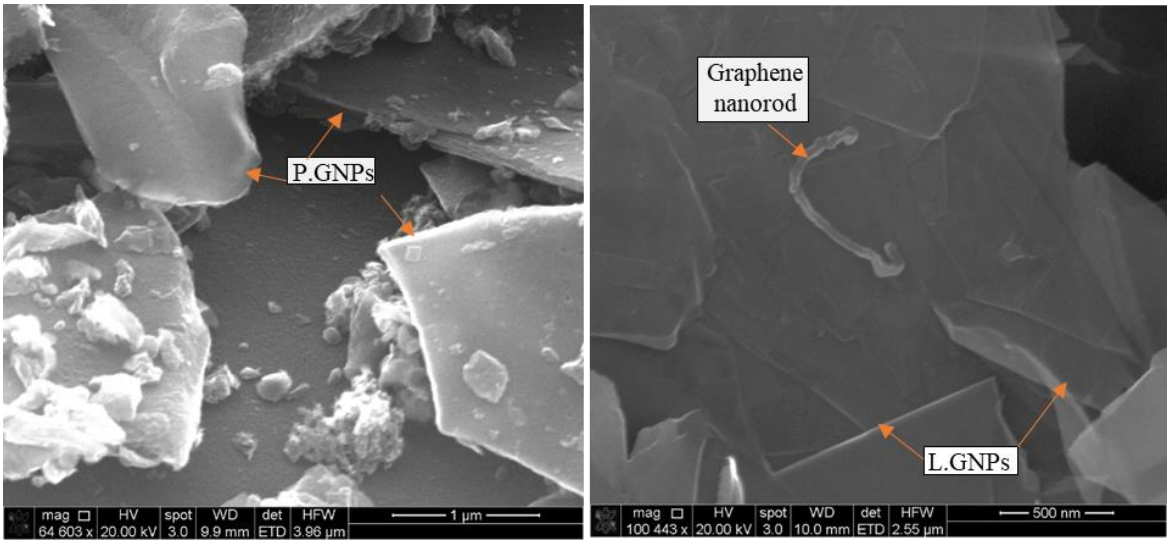

Figure 16: Secondary Electron (SE) images of powdered graphene on left and liquid GNP on right. The irregular sharp and rounded edges of platelets of graphene about 200 µm in size

and rounded shaped structures are observed. The few (~4-6) layers of nanoplatelets of liquid graphene with possible nanorod structures are seen on the right side image.

As atomic number increases the image gets brighter due to higher number of backscattered electrons being detected, as a result of higher volume of beam and sample interaction. The images contrast could be interpreted as alite (C_3S) and belite (C_2S) for dark grey, tricalcium aluminate (C_3A) for medium shade and tetracalcium aluminoferrite (C_4AF) the bright white.

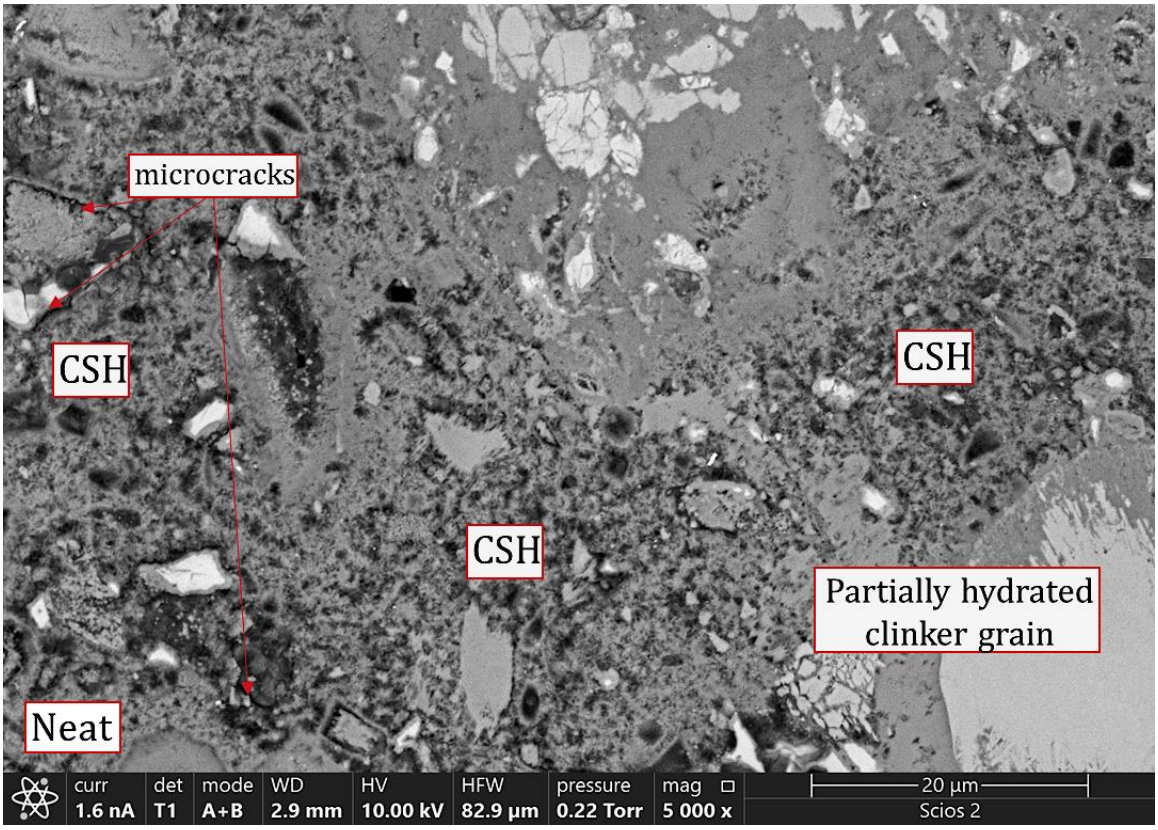

Figure 17: Backscattered Electron (BSE) image of neat sample hydrated for 28 days under thermal cyclic loading showing CSH gel and unhydrated clinker phases. On a global view, smaller size of unhydrated clinker grains and pores are observed when compared to 7 days of hydration. No GNP are present, and few micro cracks are observed which with time and force load could lead to fracturing of the sample.

0.1%LG samples are obtained by adding 11.62 ml of GNP to the same composition of all materials used to prepare cement slurry except water. The amount of water in solution of GNP is subtracted from the water to be added that is used to prepare neat samples as shown in table 1.

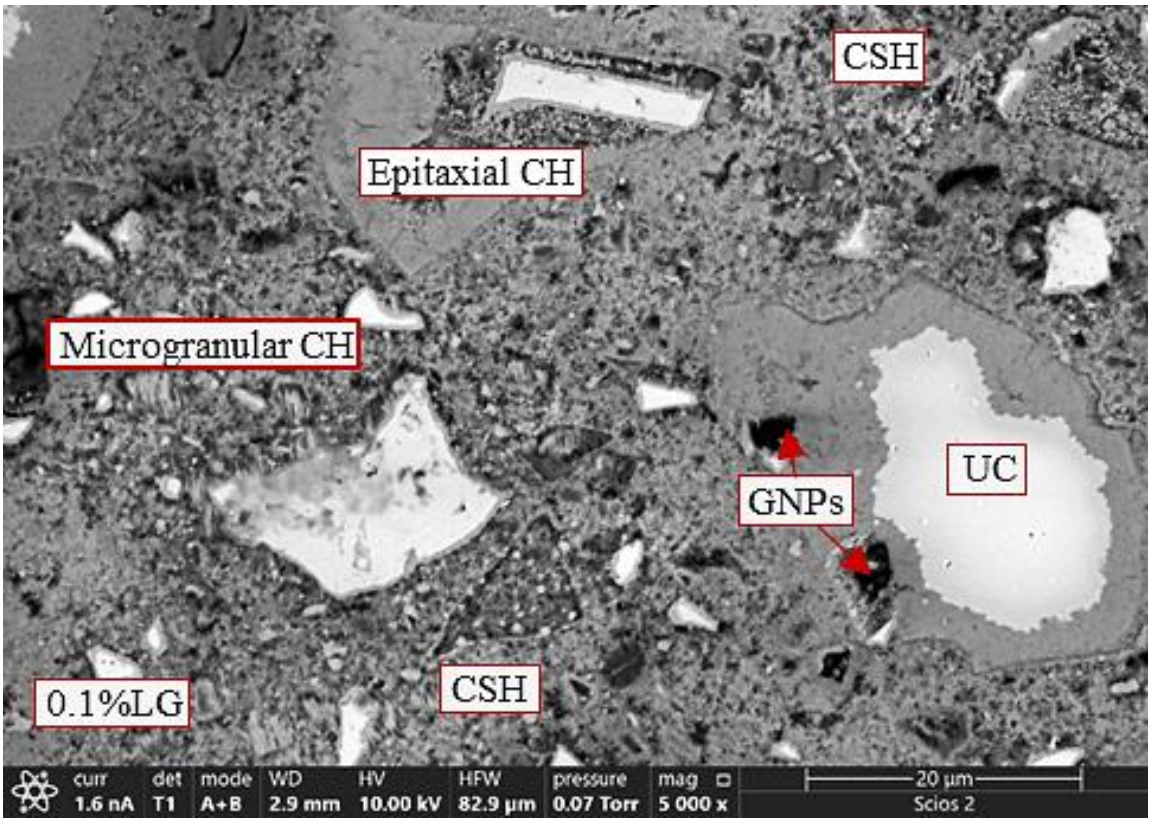

Figure 18: Backscattered Electron Image of 0.1% LG hydrated for 28 days (84 thermal cycles) at 5000x magnification. More CSH gel and microgranular CH structures are seen on samples hydrated for 84 thermal cycles when compared to 21 thermal cycles. GNP are observed on the outer CSH area of the partially hydrated grain on the right end of the image.

0.1%PG samples are obtained by adding 0.7 gms of GNPs to the same composition percentage that is used to prepare neat samples.

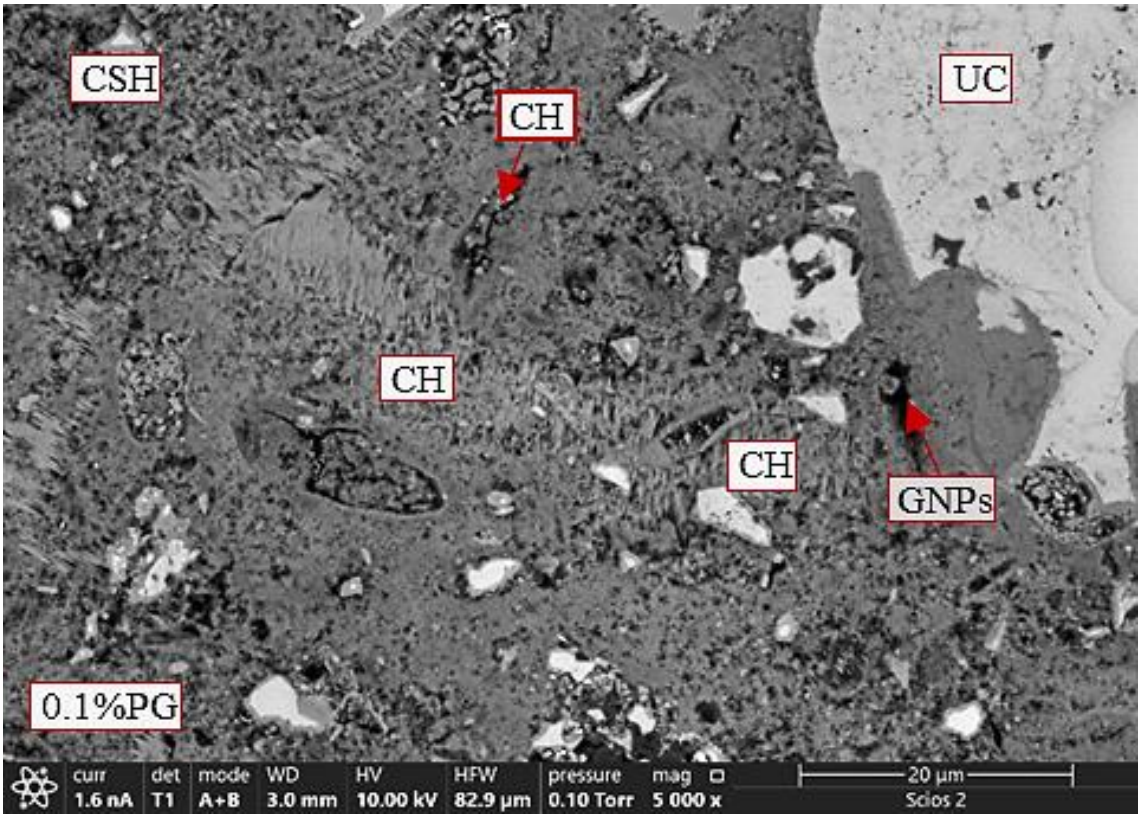

Figure 19: Backscattered Electron Images of 0.1% PG hydrated for 84 dynamic thermal cycles at 5000x magnification. The micrograph shows presence of the main cement hydration products: CSH matrix, CH platelets, that has mushroom like appearance. GNP embedded in micropores are seen close to the unhydrated clinker grain (UC).

4.1.4 Microchemistry

For chemical elemental analysis, energy dispersive X-ray spectroscopy (EDS) line profiles were obtained on polished cement sample surfaces. Profile lines were drawn intently focusing on the cement grains to obtain chemical compositions for variety of cement designs and verify the presence of GNP, as well as potential changes in cement hydration products in the presence of GNP. Furthermore these investigations would help distinguish any present differences in how powdered vs liquid GNP are distributed within partially (7 days) and fully hydrated (28 days) cement matrix.

The profile lines have from 50-150 point analysis, and were selected to capture similar features in different cement slurries, for example unhydrated cement clinker grain and hydration products in its vicinity. As we know, the unhydrated grain has a higher calcium content which decreases as we move out of the grain area due to hydrated matrix dominated by CSH phase. This was clearly observed for all the samples, Figures 17-26. For all the profiles obtained in this study, calcium, silica, carbon, aluminum, and iron seem to be consistent with the observed trend suggesting the elemental composition variation from the unhydrated clinker grains to outside the CSH phase is along the lines with the theory of hydration mechanism of alite (C_3S), belite (C_2S), tricalcium aluminate (C_3A), and tetracalcium aluminoferrite (C_4AF).

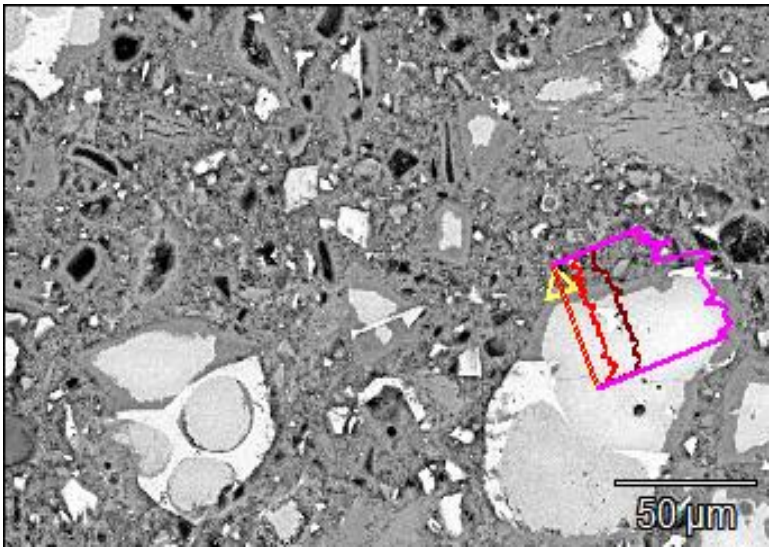

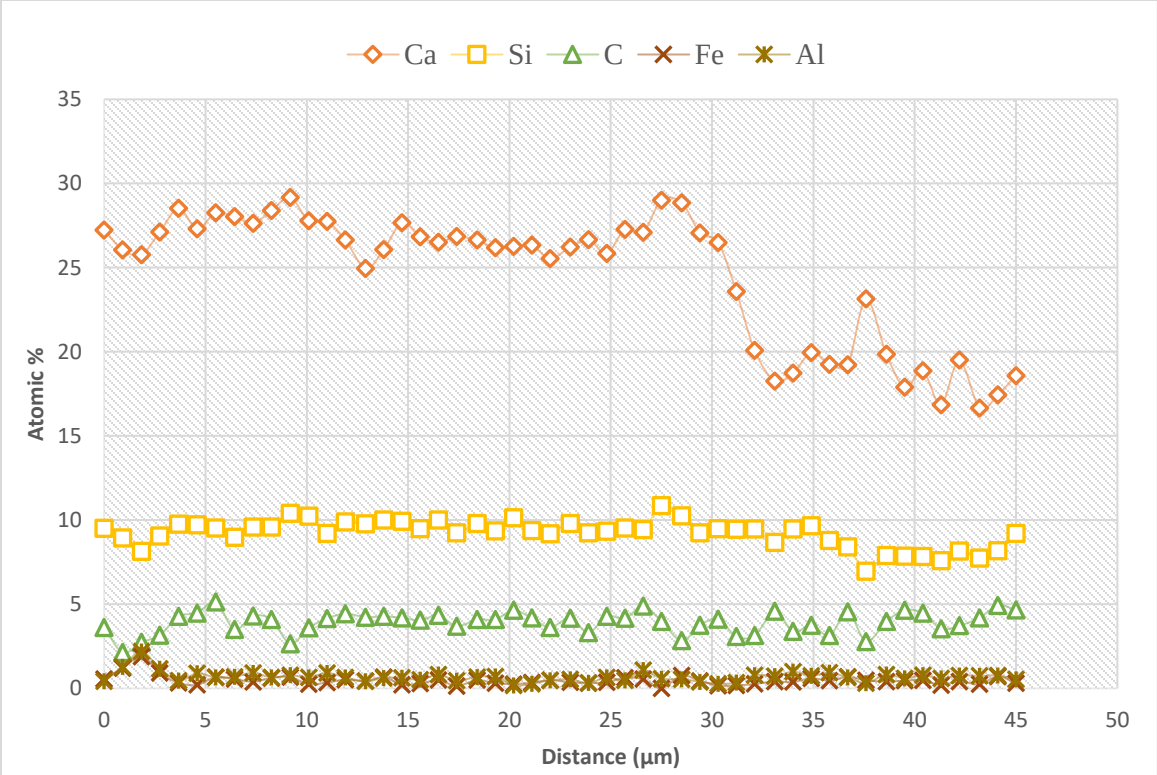

Figure 20: Energy dispersive X-ray spectroscopy (EDS) line profile image on a cement grain of a neat cement sample hydrated for 7 days (21 thermal cycles). The pink line indicates calcium, brown line silica and red line carbon. The lowering of the pink line outside of the grain is observed confirming the decrease in calcium when the line profile is extended out from the center of grain. The graph on the right side shows the atomic % of each element present on the sample where the line profile is measured.

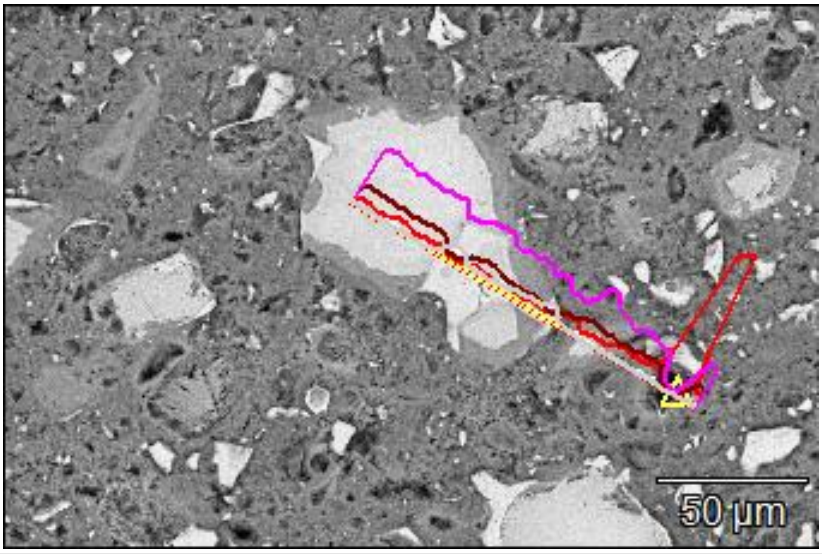

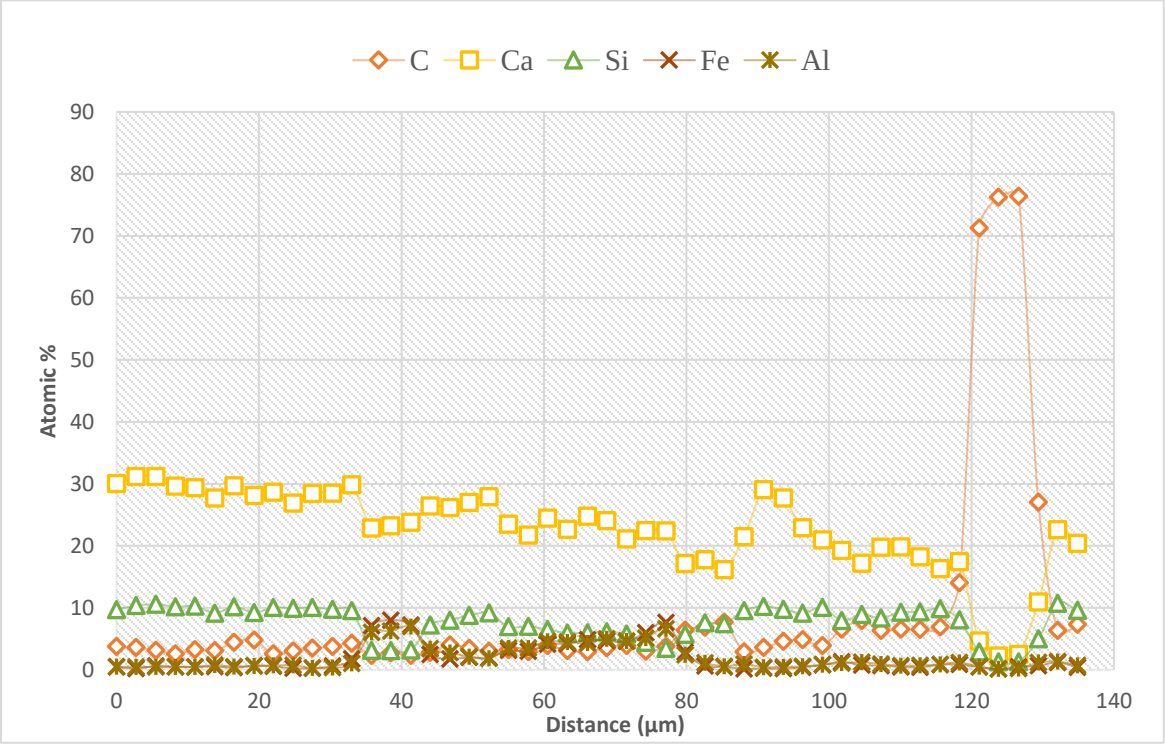

Figure 21: Energy dispersive X-ray spectroscopy (EDS) line profile on 0.1% LG cement sample hydrated for 7 days. The presence of graphene nanoplatelets (GNP) at the end of the line drawn on this image location is seen by the large increase in carbon content from 10 to 75 atomic%. The decrease in Ca/Si ratio for the stretch where GNP are present is also observed on the same image.

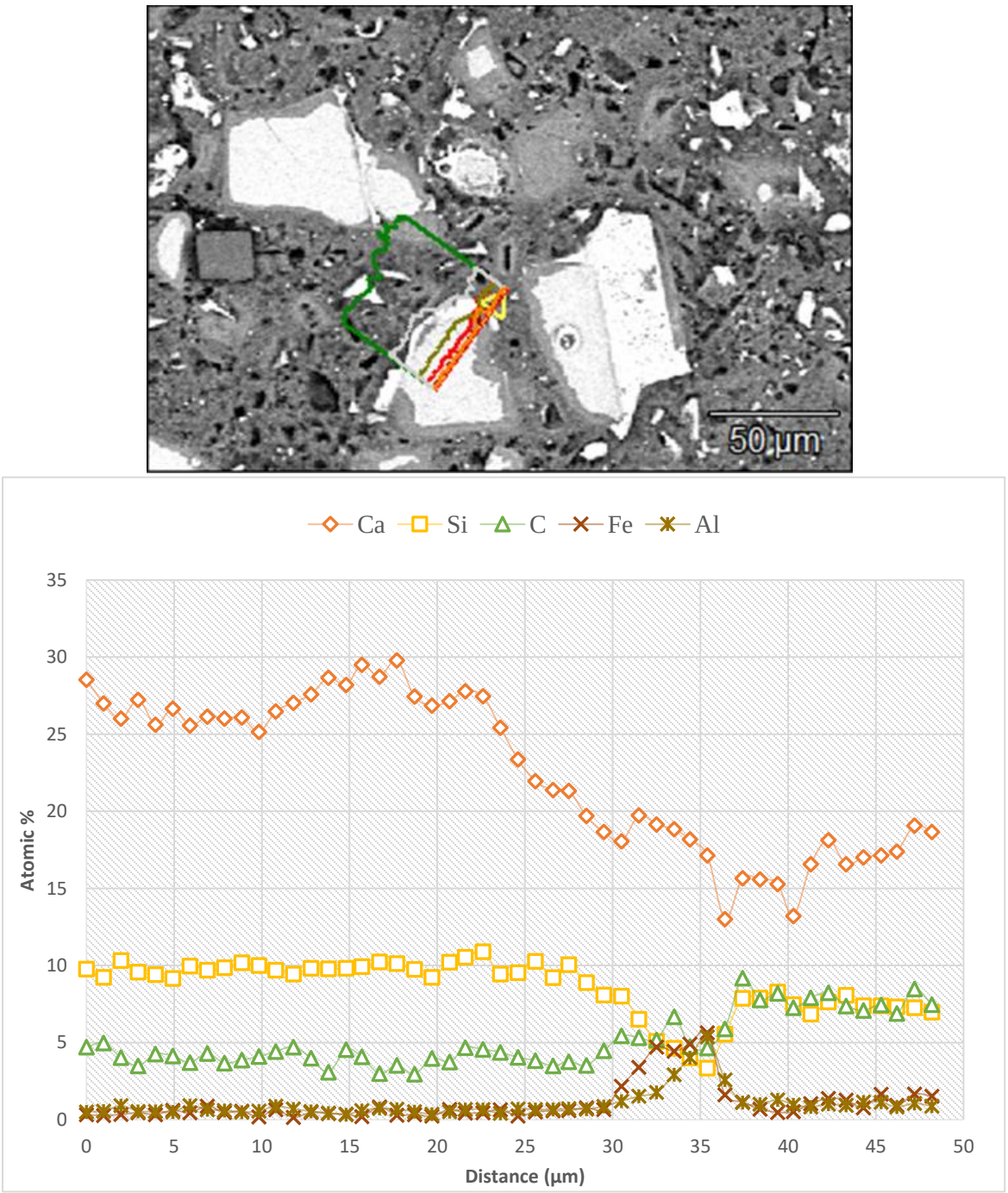

Figure 22: Energy dispersive X-ray spectroscopy (EDS) line profile on 0.1% PG cement sample hydrated for 21 thermal cycles with a high and low of 110 ºC and 20 ºC. The white line represents calcium, silica in light green, oxygen in dark green and carbon in red line. Here we observe the decreasing trend of calcium and silica while there is an increase in aluminum and iron suggesting presence of C_3A and C_4AF phases.

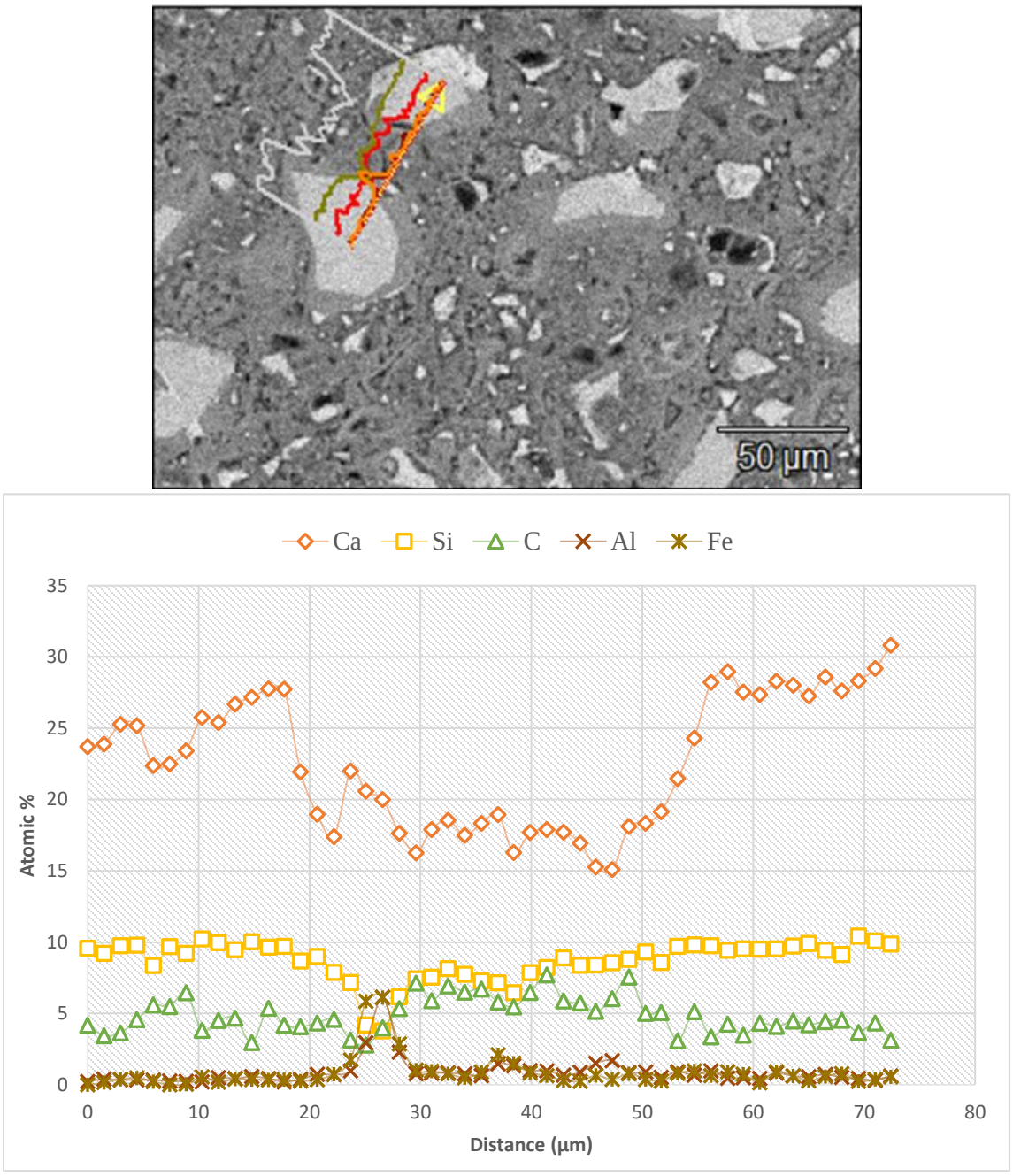

Figure 23: Energy dispersive X-ray spectroscopy (EDS) line profile on 0.008% LG cement sample hydrated for 7 days. In this image the line profile was chosen so that it starts from the center of a grain and ends at about the center of another grain where both the unhydrated grains are not connected. We observe there is a steep decrease and increase in the calcium curve, and increase in aluminum and iron curve consistently proving the elemental composition trend.

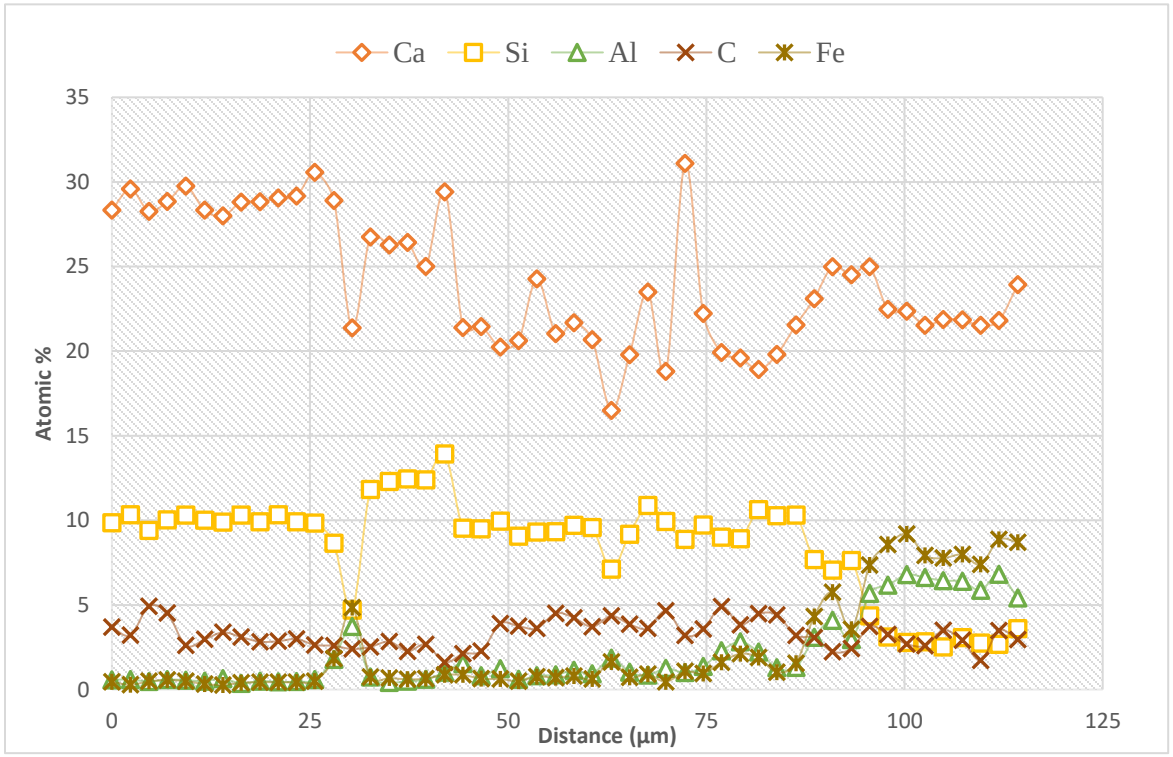

Figure 24: Energy dispersive X-ray spectroscopy (EDS) line profile on 0.008% PG cement sample hydrated for 21 thermal cycles. In this image, the line was selected to start in one grain and end in another that has brighter regions indicating presence of C_4AF or C_3A. The EDS analysis confirms it as we see in the graph on the right side showing the decreasing and increasing trend of calcium when there is an increasing and decreasing trend in aluminum and iron curves at the same points.

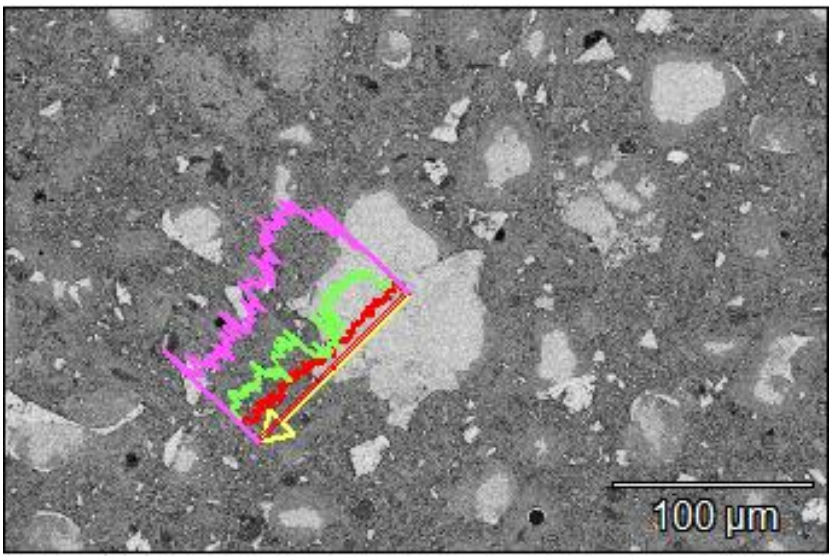

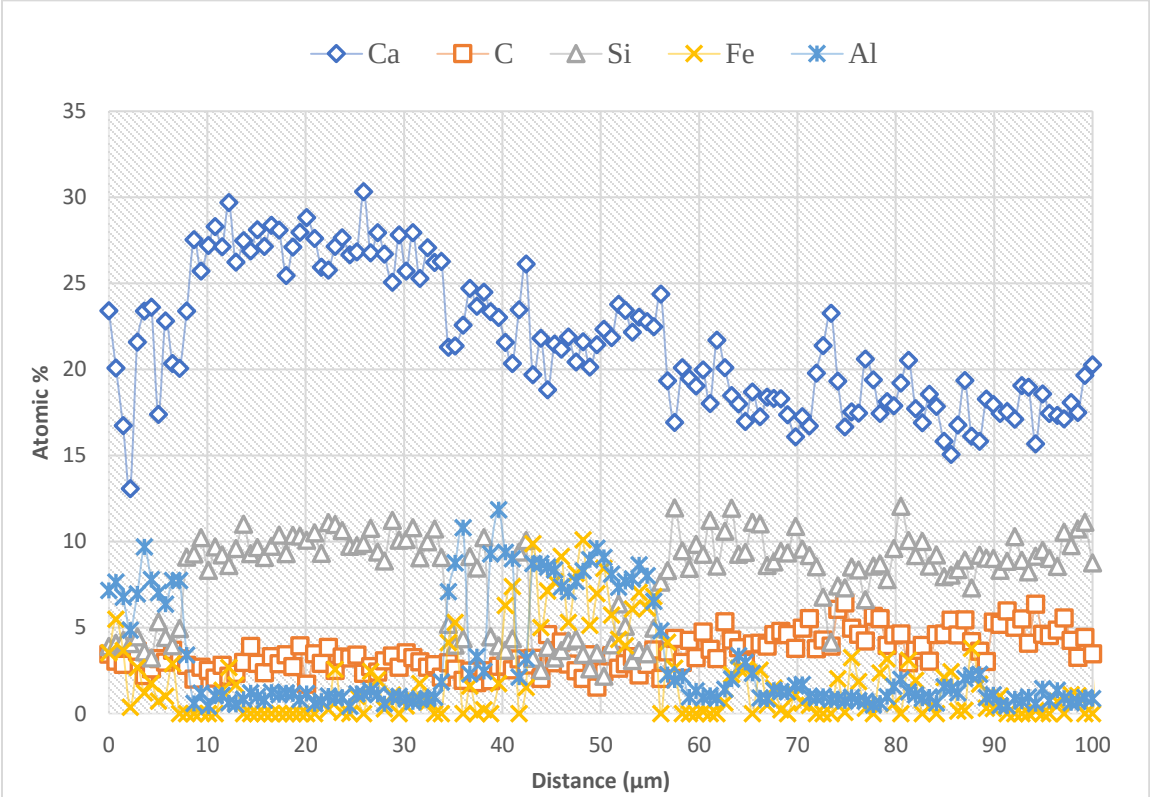

Figure 25: A 28 days hydrated 0% control GNP cement sample having undergone energy dispersive X-ray spectroscopy (EDS) line profile. The pink line represents calcium, green is silica and red one carbon. The line passes through the center of the unhydrated grain and goes out into the CSH phase. Less unhydrated areas were observed on 28 days sample in comparison to 7 days one.

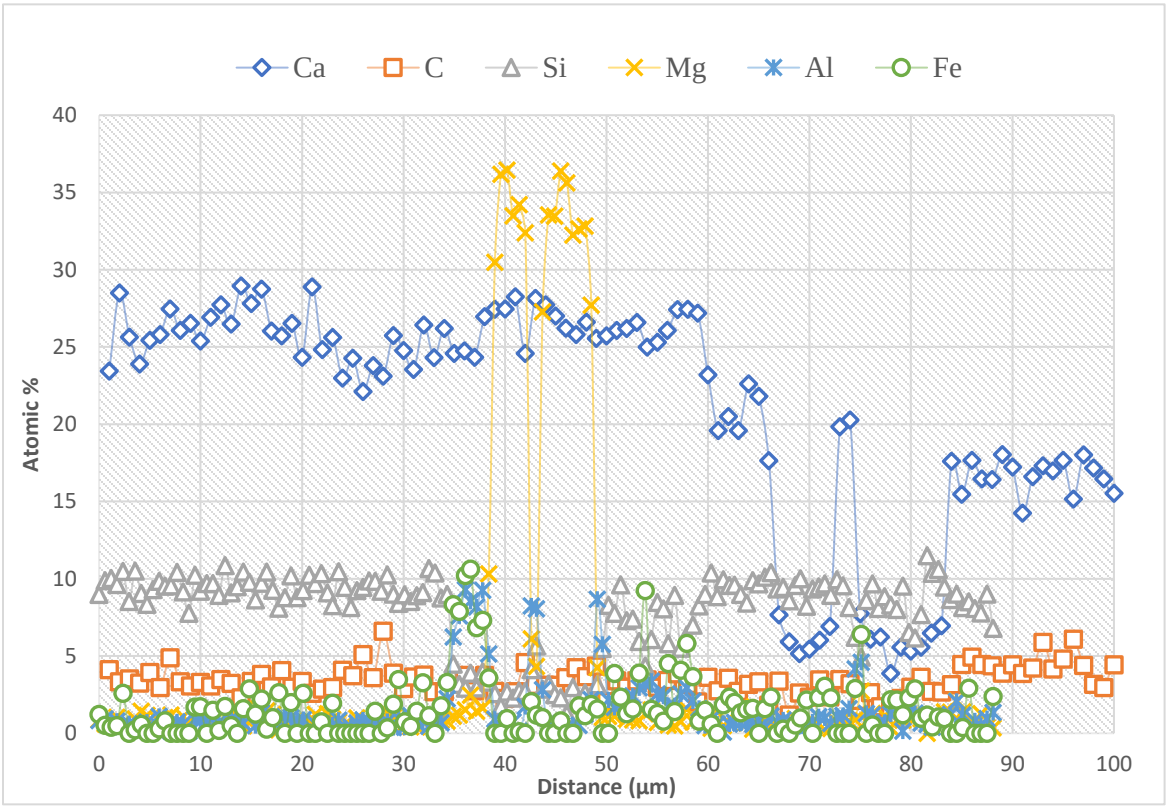

Figure 26: On 0.1% LG cement sample having undergone thermal cyclic loading for 28 days energy dispersive X-ray spectroscopy (EDS) line profile was performed. For this particular location the line starts from higher calcium and silica content and progresses into the outer CSH area decreasing in the elemental composition. Carbon as represented in red has no change stating that no GNP were detected on that line.

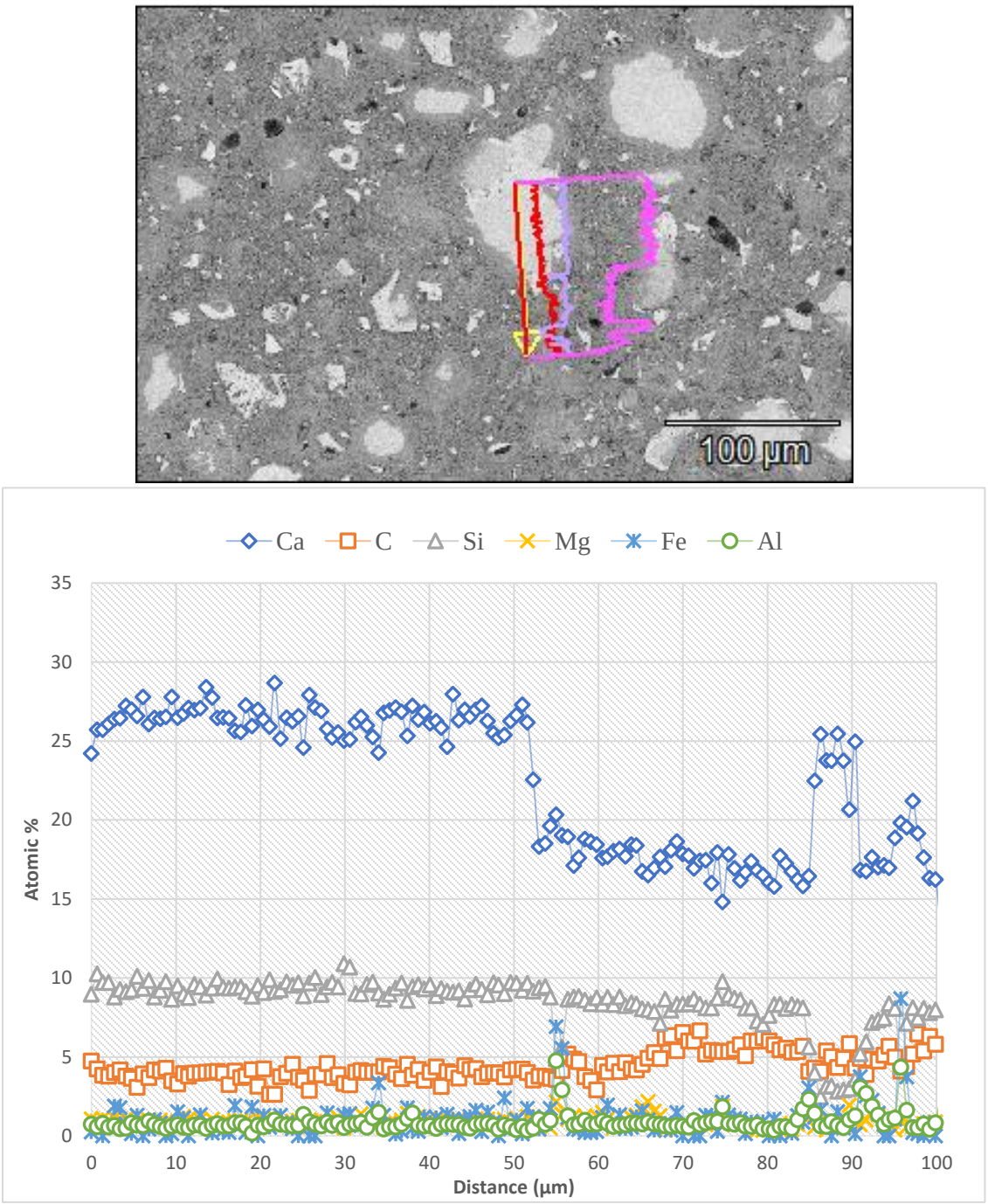

Figure 27: Energy dispersive X-ray spectroscopy (EDS) line profile on 0.1% PG cement sample hydrated for 84 thermal cycles between 20 ºC and 110 ºC. Here like other samples we see the decreasing trend of calcium and silica when moving out of the partially hydrated clinker grain. Close to the end of the line profile calcium increases and silica decreases at the same point that could possibly be CH.

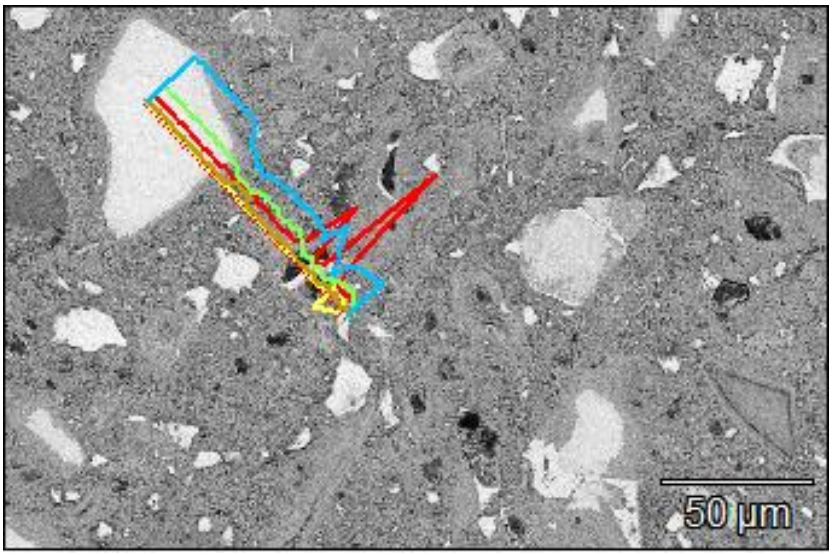

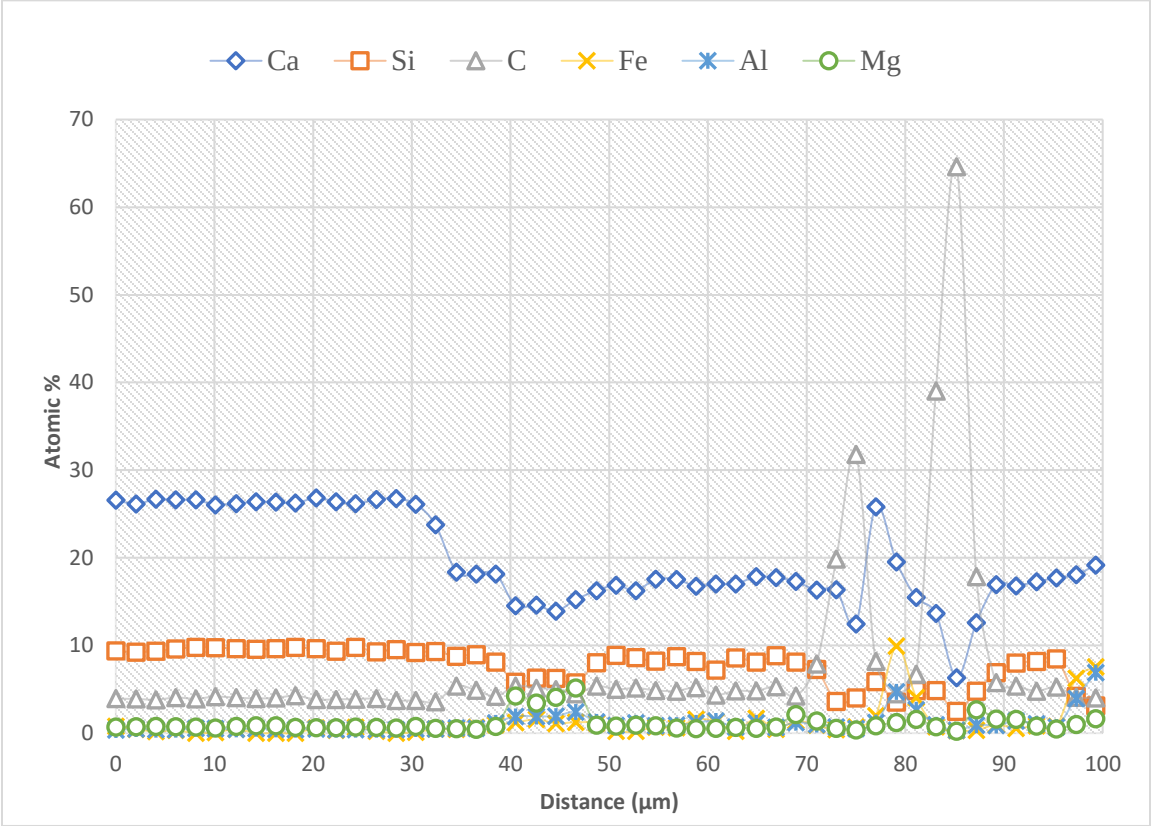

Figure 28: On the left is the energy dispersive X-ray spectroscopy (EDS) line profile on 0.008% LG cement sample hydrated for 84 dynamic thermal cycles with a high and low of 110 ºC and 20 ºC. On the right is the graph showing the atomic% of each element detected by the line profile on the core sample. As the red line moves out of the partially hydrated area, it shows a peak confirming the presence of GNP at that point.

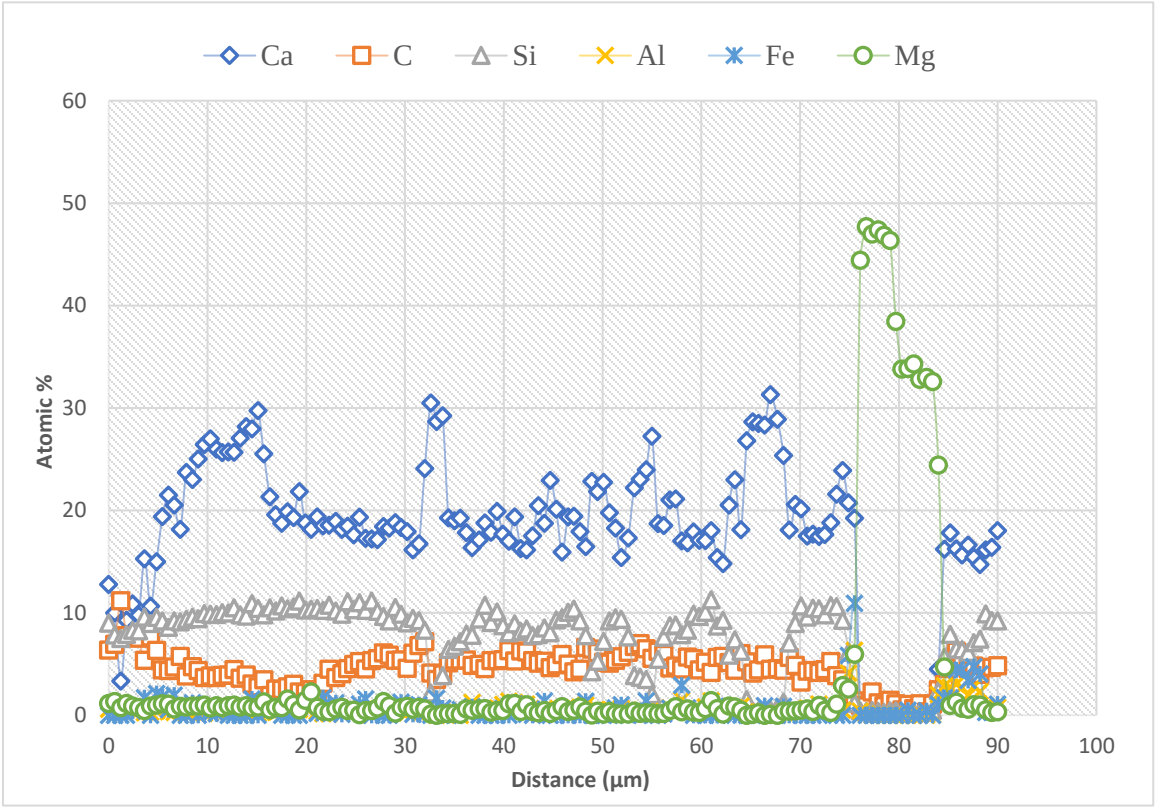

Figure 29: 0.008%PG cement sample of 0.7mm thickness after 28 days of hydration having undergone energy dispersive X-ray spectroscopy (EDS) line profile for elemental composition. Blue line represents calcium, green silica, and red carbon. On this sample, the calcium and silica compositions fluctuate as the line moves through CSH and CH phases outside the unhydrated grain.

4.1.4 Hardness and Elastic Modulus

Microindentation is used for measuring the micromechanical properties of materials primarily Hardness and Young's Modulus, thereby testing the capability of the material to withstand subsurface conditions by resisting fracturing. The cement cores that were hydrated for 7 days (21 thermal cycles) were tested by cutting 5mm discs that were polished prior to indentation. These set of samples have the highest elastic modulus value for 0.1% LG sample at 16.51 GPa and the lowest for neat sample at 9.09 GPa. On similar lines, the trend for hardness remains the same as highest for 0.58 GPa for 0.1% LG and lowest for neat at 0.25 GPa. However, interestingly, the trend reverses for samples hydrated for 28 days (84 dynamic thermal cycles). The elastic modulus value for 0.1%LG is 8.27 GPa and for neat it is 16.78 GPa; the hardness value for 0.1%LG is 0.26 GPa and for neat it is 0.36 GPa. The depth of each indent obtained is seen on the 3D graph with the fact that for each of the 28 days hydrated sample, the depth reduced for the same force load (5N), loading, and unloading rate (10 N/min) with a creep time of 30 seconds. Varying depths of indents could be explained based on the cement phase or composition present at that particular point as seen in Figures 27-31.

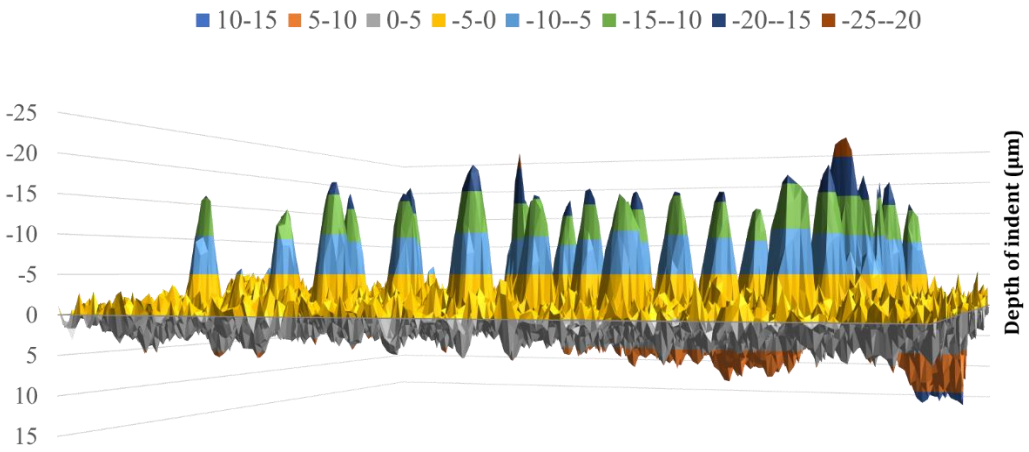

Figure 30: 4600×4600 µm map stitched for a 10×5 indented matrix on a hydrated neat (0% GNP control) sample having undergone 21 dynamic thermal cycles. The maximum depth of indents is 26 µm in the case of 7 days hydrated cement sample with an overall average of indent depth at 20 µm.

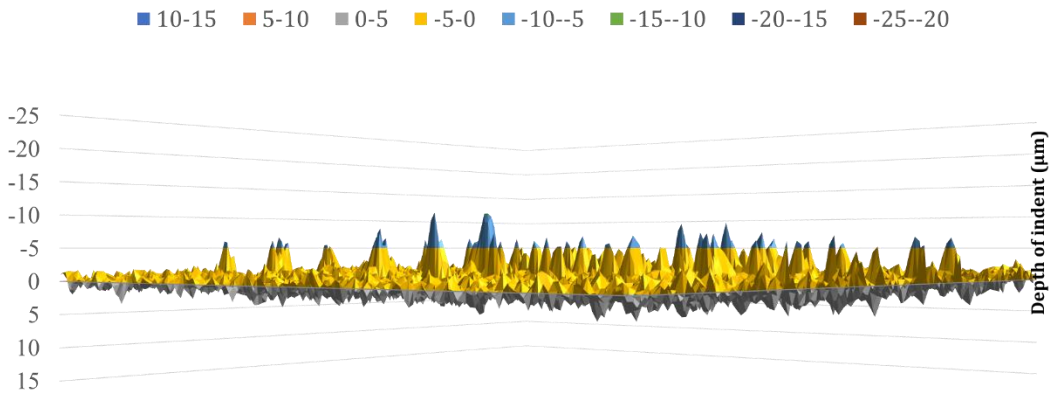

Figure 31: A 10×5 indented matrix map stitched on 4600×4600 µm area on a neat sample having undergone hydration for 84 dynamic thermal cycles between 20 ºC and 110 ºC. As we can see from the graphs the average depth of indents has decreased compared to the 7 days sample, but the elasticity value has increased. The maximum depth of indents is 12 µm.

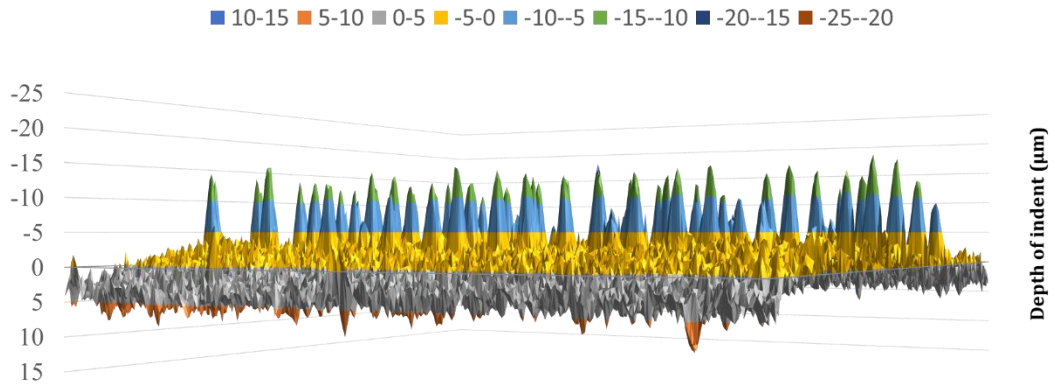

Figure 32: Surface profilometry of a 10×5 indented matrix on 0.1%LG cement sample hydrated for 7 days or 21 thermal cycles. It can be observed that the maximum value, which is around 18 µm, as well as the average depth of indents which is about 14 µm is lower as compared to the neat sample for the same period of hydration.

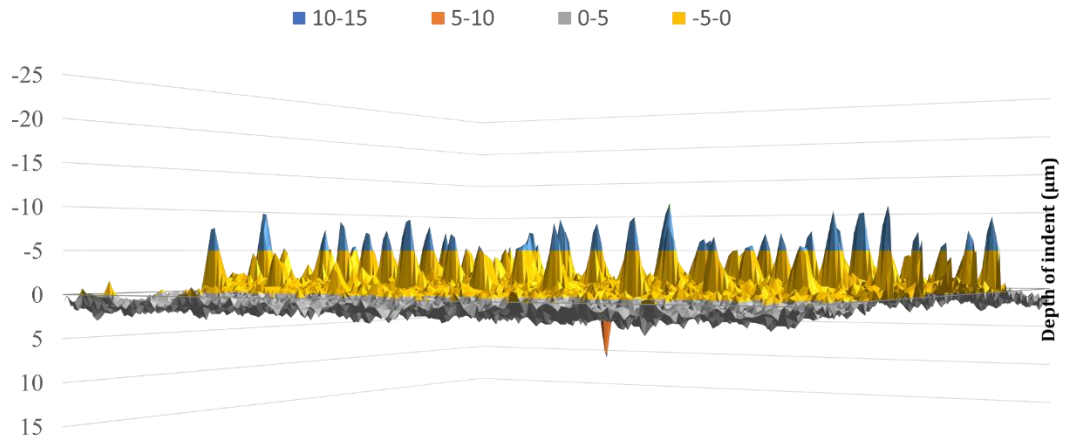

Figure 33: A 4600×4600 µm surface map on 0.1%LG hydrated for 28 days or 84 thermal cycles. Comparing the depth of indents for 7 and 28 days of hydration, a lower value is seen for 28 days for the same force load (5N) and creep time (30 secs). The maximum depth of indents is 11 µm with an average of about 8 µm.

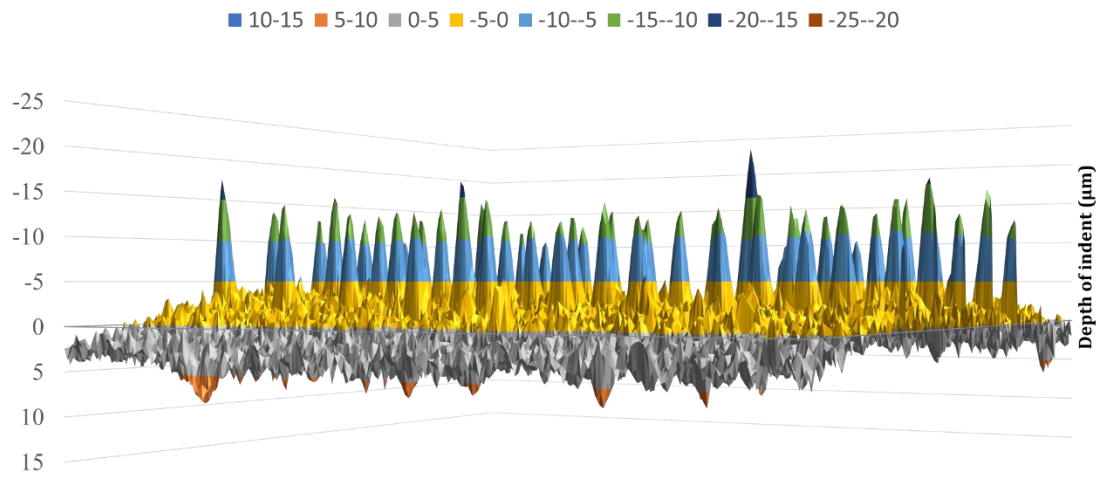

Figure 34: The average indent depth for 0.1%PG 7 days hydrated sample is 14 µm with the highest value at 23 µm. This cement sample as well is scanned on a 4600 × 4600 µm map stitched for a 10×5 indented matrix.

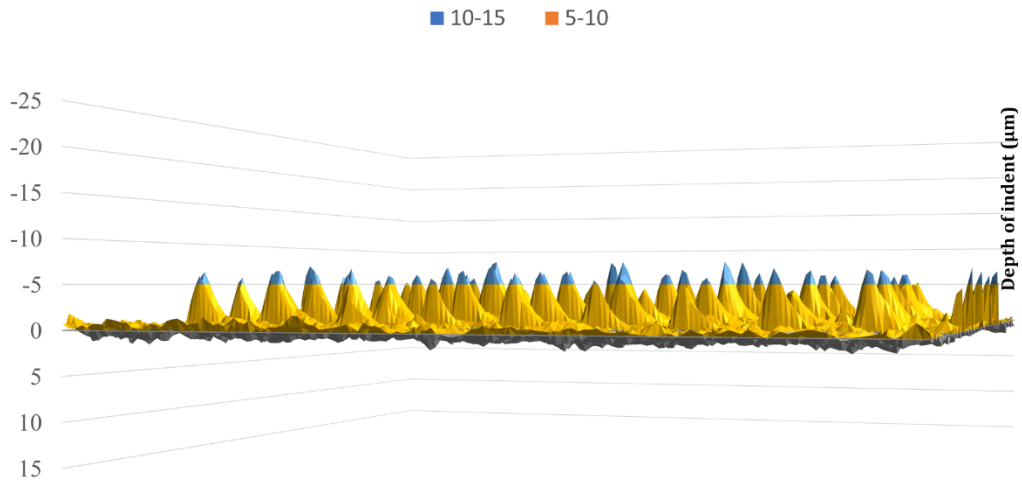

Figure 35: 0.1%PG cement sample having undergone hydration for 28 days under dynamic temperature conditions was polished, scanned for microstructural properties using SEM and later tested for elasticity and hardness using microindenter. The average depth value is 7 µm with a maximum at 9 µm.

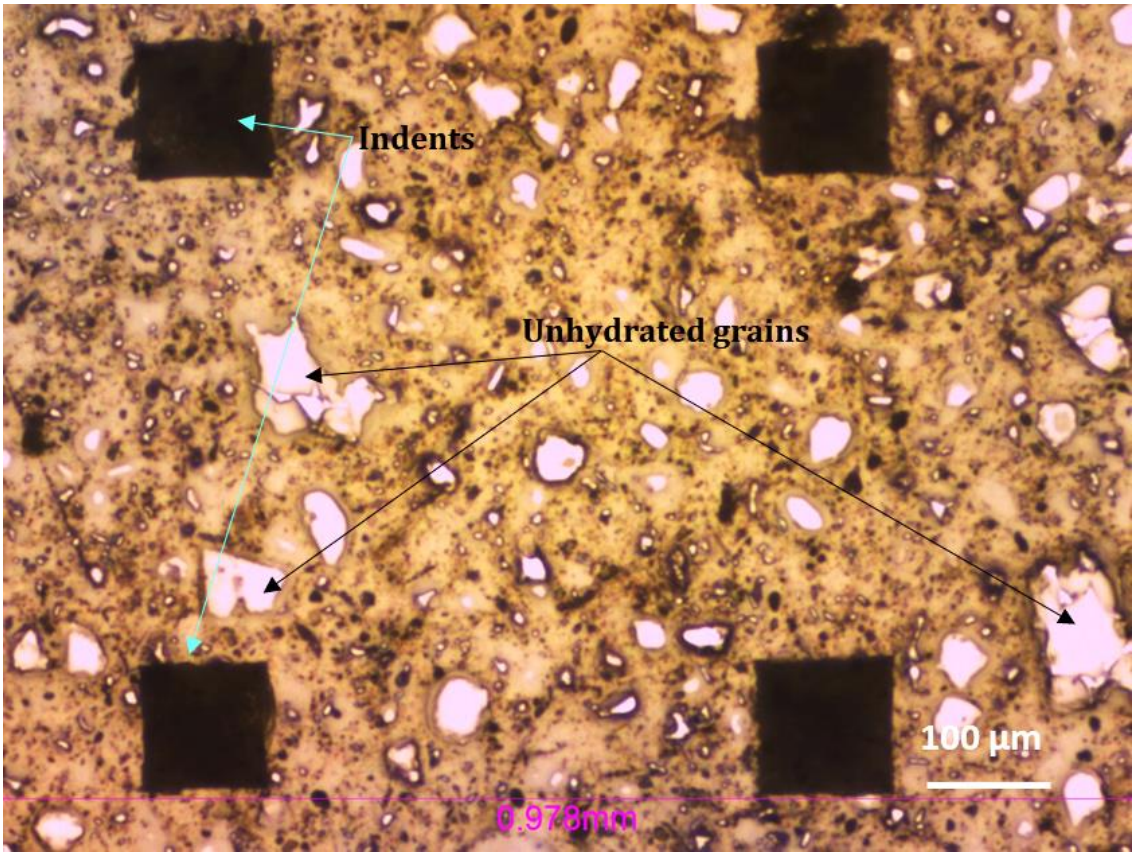

Figure 36: Microindented cement sample using a Vicker's diamond tip that made indents of average diameter between 110-140 µm. The spacing between each indent is 500 µm. A 10×5 matrix is made on the first and third quadrant on each cement sample to measure the elasticity and hardness.

From the results calculated after microindentation, 0.1% LG cement sample has lower values for hardness and elasticity over other samples at 28 days of hydration. Neat cement sample on the other hand has higher values which would imply brittle nature, which is well documented and known (Reddy et al., 2016). However, as seen there is a slight increase in elasticity and hardness values for 0.1%PG samples varying from the control and other mix designs.

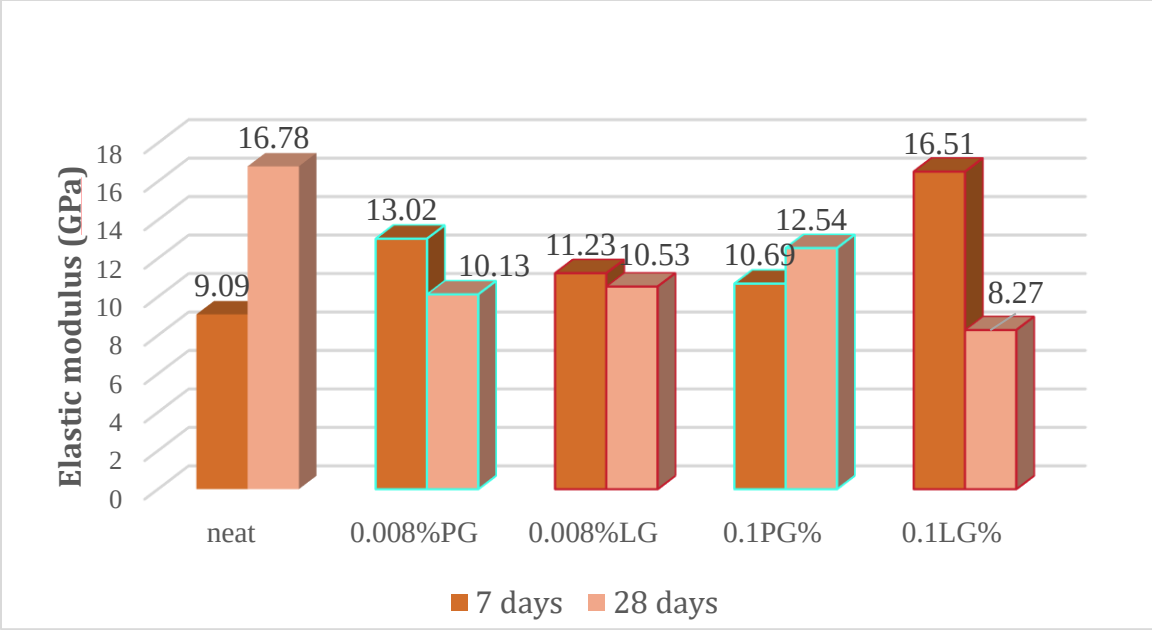

Figure 37: Bar graph showing the average elastic modulus values after microindentation using Vicker's diamond tip on neat and mix design cement samples hydrated for 7 and 28 days. A considerable decrease is observed in 0.1%LG sample.

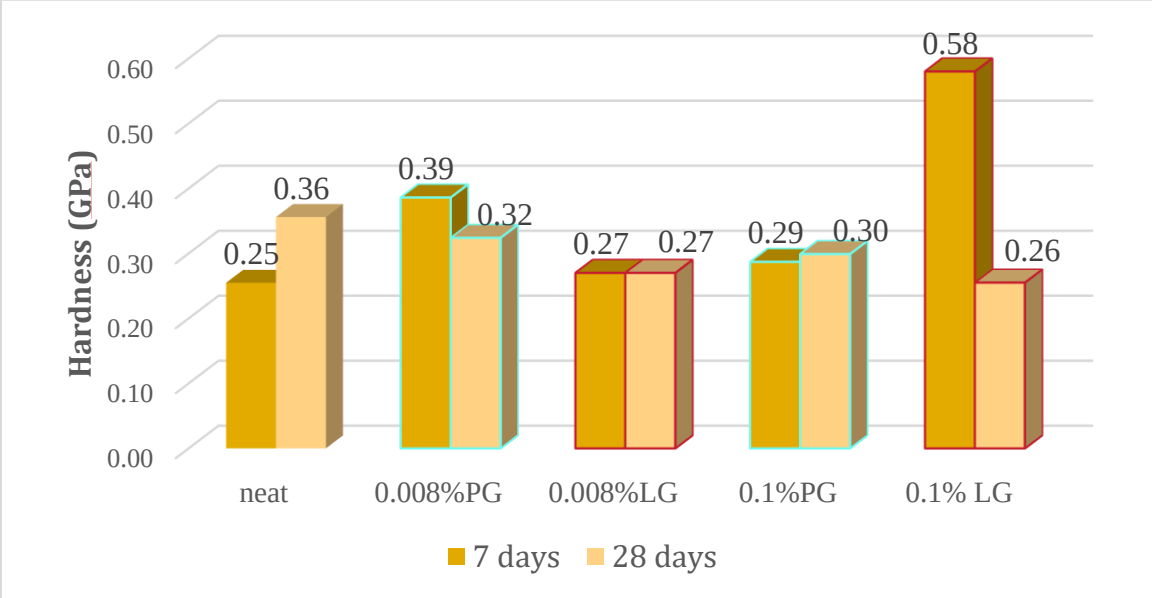

Figure 38: Bar graph displaying the comparison of average hardness values after microindentation on control and GNP mix design samples hydrated for 7 and 28 days. A notable decrease is seen in 0.1%LG sample on similar lines as elasticity.

CHAPTER V

DISCUSSION, KEY FINDINGS AND CONCLUSION, FUTURE WORK

5.1 DISCUSSION

Graphene, a 2D carbon material, is much thinner than human hair and exhibits unique thermal, mechanical, and electrical properties. A single sheet layer is exfoliated from graphite (Cui et al., 2011; Hernandez et al., 2008), a mineral with multi layered crystal structure. As seen below, a single sheet of graphene could be rolled into 0D, 1D forms, or stacked layers in 3D form thus exhibiting different properties. Less than 10 sheets of graphene stacked together are often termed as graphene nanoplatelets. In this study graphene nanoplatelets were used, with an average of 4~6 layers. Using GNP as a potential additive in wellbore cementing where temperature increases with depth has not been much researched upon due to its hydrophobic and unreactive nature. Although, graphene on a silicon wafer substrate, when heat treated at temperatures greater than 600^{o}C showed edge defects (Liu et al., 2019). Previous works focused on mechanical properties achieved by using low quantities (<1% bwoc) of powdered graphene nanoplatelets (GNP) mixed with cement have shown promising results (Massion et al., 2021; Zheng et al., 2017). GNP were found to occupy the pore spaces and strengthen the weak points present in the core samples when observed using SEM in this present work as well. The samples were cured under cyclic loading temperatures that ran between 20 ^{o}C and 110 ^{o}C for 7 days (21 thermal cycles) and 28 days (84 thermal cycles). Strength

retrogression, where cement undergoes phase changes after about 110 ^{o}C and decreases in mechanical strength would be an important factor to consider in analyzing the results. The fundamental explanation for the strengthening mechanism is yet unclear and the non-uniform dispersity of GNP in the cement still needs to be studied.

5.1.1 Impact of graphene nanoplatelets on the microstructure of cement

At 7 days (21 thermal cycles) of hydration, comparison of neat cement to mix designs containing different percentages of GNP, shows that cement slurries with GNP have higher porosity and permeability. The potential explanation is that the varying amounts of air entrainment when cement samples are cured at ambient pressure conditions would persist around hydrophobic GNP material more readily. At high pressure (about 2000 psi) the air voids would fully collapse as per observation in the field and in industrial laboratory testing (Dr. Iremonger, 2022). In contrast, the GNP containing cement slurries have a decrease in both, the porosity and permeability values when compared to neat sample after 28 days (84 thermal cycles). The potential explanation is that as cement hydration is almost completed at 28 days, the GNP can now only occupy the pore spaces, and in that capacity, they provide blocks in fluid flow and decrease in the effective porosity. Previous work (Massion et al., 2021; Massion et al., 2020) stated that GNP tend to occupy the pore spaces, and strengthen cement matrix, as shown in both, triaxial testing at reservoir temperature and pressure as well as in microindentation data. The same is observed in the microstructural characterization of GNP enhanced cement samples in this study. GNP fill the micropores and reduces the possibility of both initiation and propagation of microfractures as well as formation of more extensive fracture networking. Back Scattered Electron (BSE) micrographs provided a global view on the presence of unhydrated cement clinker grains. From the microsctructural analysis of the cement sample with and without GNPs, more CSH gel like or hazy structures were observed on 28 days hydrated samples.

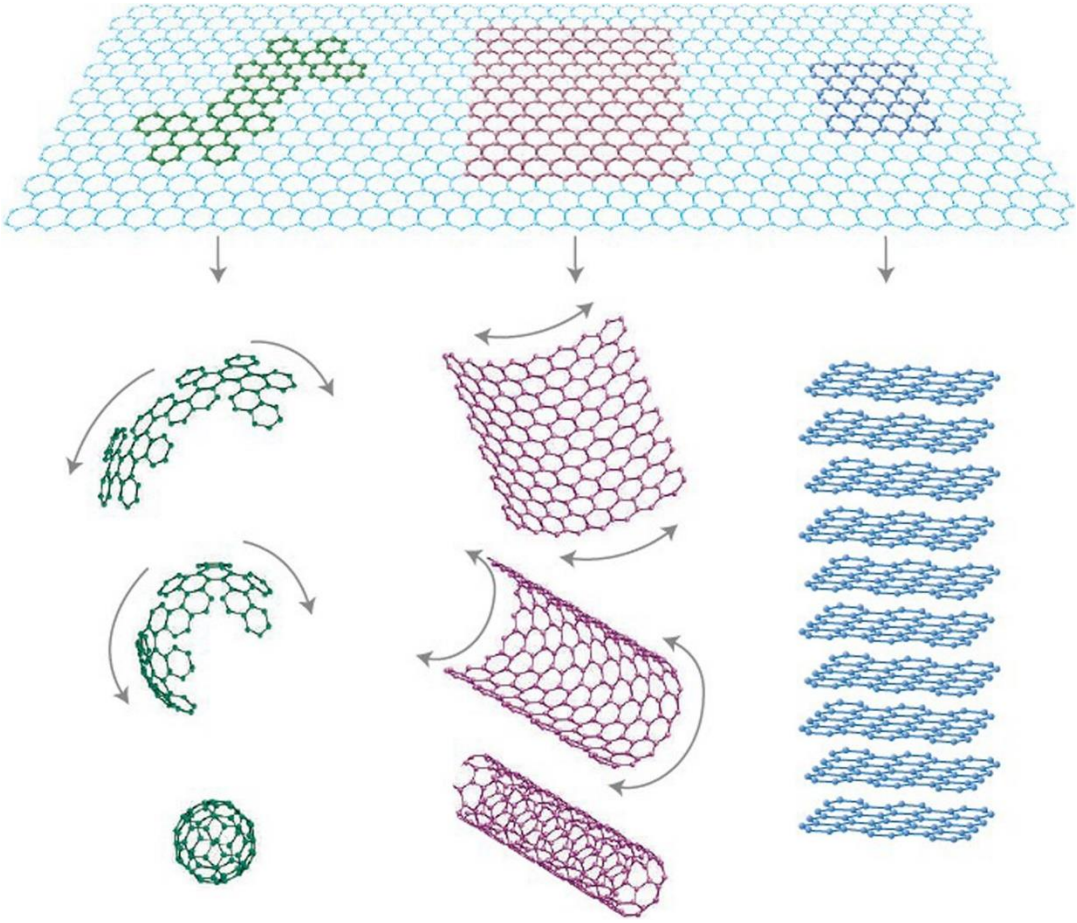

Figure 39: Single sheet 2D graphene nanoplatelet rolled into 0D Buckminster fullerene, 1D carbon nanotube and 3D layers of graphite. Image source (Zheng et al., 2017)

5.1.2 Impact of thermal cyclic loading on hydration of cement

For porosity, a maximum of 21.5% and a minimum of 5.5% decrease was clearly observed for 28 days (84 thermal cycles) compared to 7 days (21 thermal cycles) due to less free water content as cement completes hydration, and CSH and CH matrix form. Comparing the percentage change in average porosity between samples cured at static 90 ^{o}C and dynamic cycles 20^{o}C to 110^{o}C (84 thermal cycles), it stands at 15.7% for neat samples and -.014% for 0.008% powdered GNPs. There is not much difference in the values as we seen in Figure 40.

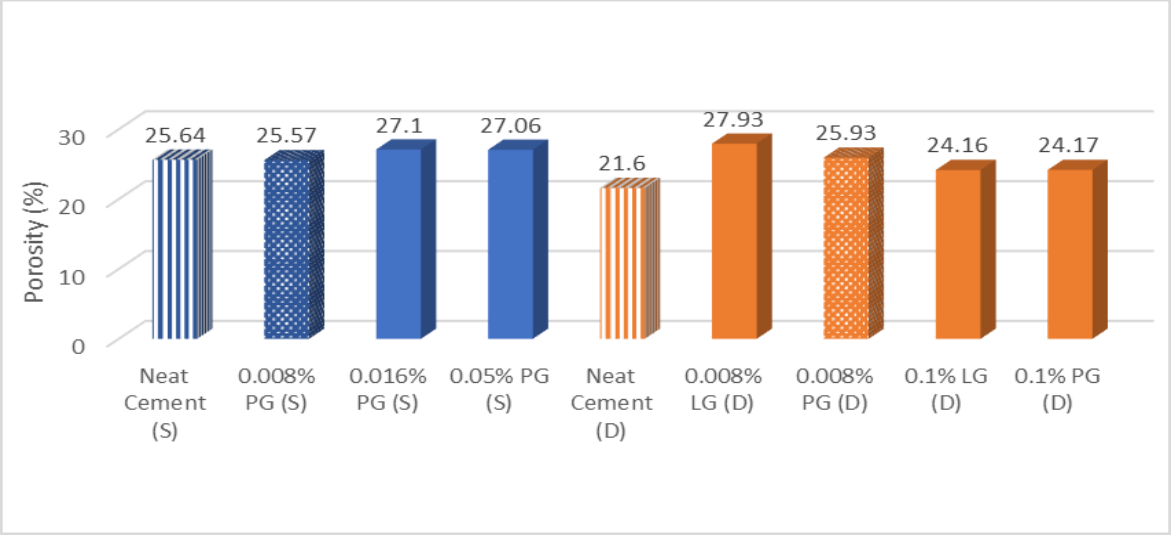

Figure 40: Bar graph with porosity values for cement samples cured at static 90°C in blue and dynamic cycles 20°C to 110°C in orange. All the samples were hydrated for 28 days in the environmental chamber at 95%RH.

For permeability, there is maximum decrease of 45.25 ± 0.02% and a minimum of 2.39 ± 0.07% when comparing between 7 days and 28 days of hydration. This decrease in permeability is due to the decrease in flow through volume, as seen in equation (8) used for calculating permeability. This change in volume could be explained due to the change in pore volume that is from the decreasing strength of the cement at temperatures about or higher than 110 °C (230 °F). For static 90 °C, dynamic cycles 20°C to 110°C (21 and 84 thermal cycles), helium gas Corelab™ Nano-KTM permeameter was used where gas flowed through dry samples. Comparing permeability values at static 90 °C (Massion et al., 2021), and dynamic cycles 20°C to 110°C (84 thermal cycles), neat sample has 31.31% and 0.008%PG has 38.01% higher permeability. The values for each design measured are seen in the graph in Figure 14.

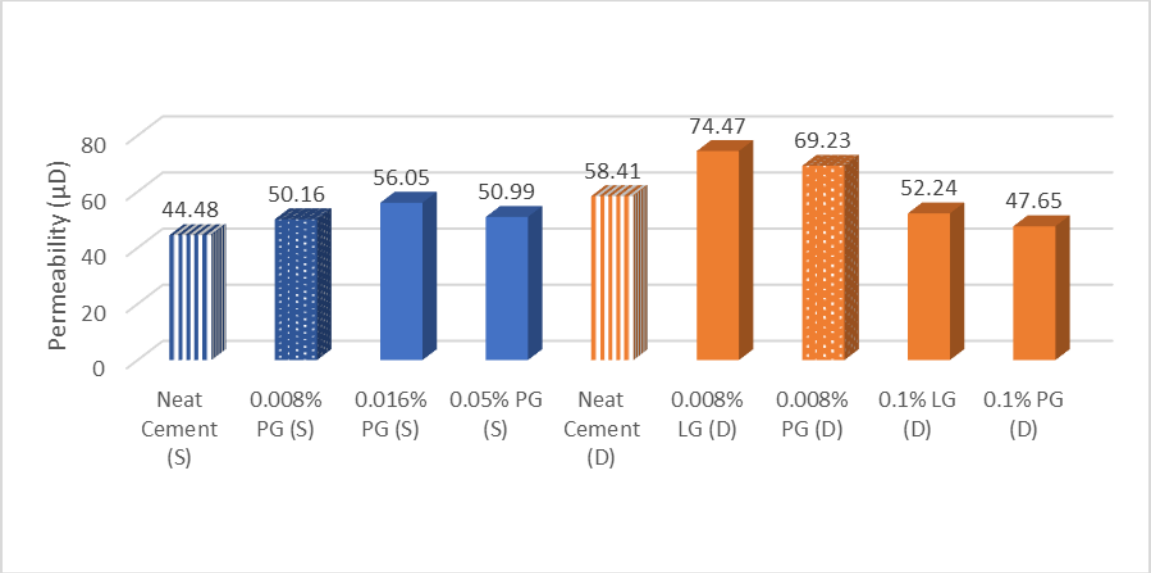

Figure 41: Average permeability values in µD for cement samples cured at static 90ºC (in blue) and dynamic cycles that ran between 20ºC and 110ºC (in orange). Neat cement and organic additives added cement cores were hydrated for 28 days in the ESPEC environmental chamber.

As an established certainty in cement chemistry, two morphological types of CSH exist namely as inner product (low density) and outer product (high density). CSH is the dominant hydration phase in Portland cement, at approximately 60% by volume and it is a main contributor towards elastic properties of cement matrix as well as its low permeability. The mechanical degradation of elasticity has been studied theoretically and experimentally by (Constantinides & Ulm, 2004). The decrease or loss in elastic stiffness is identified due to the increase in porosity and decalcification of CSH phase. In this study, elastic modulus and hardness values for each set of samples hydrated for 7 days (21 thermal cycles) and 28 days (84 thermal cycles) were obtained using microindentation. The data obatined for 0.1%PG sample for 7 days (21 thermal cycles) and 28 days (84 thermal cycles) sets is on similar lines.The elasticity and hardness values slightly increased for 28 days sample with lower values of porosity and permeability. This increase could also be due to the dynamic cycling of temperature until 110 ºC where the sample loses its

mechanical strength. On the other hand in the mix design sample 0.1%LG, elasticity and hardness decreased to almost half the value (8.27 GPa) from that of 7 days (16.51 GPa) making it ductile even with increase in temperature. This sample withstood the higher dynamic temperature preferring it over 0.1%PG, confirming that a well dispersed GNP within cement matrix is imperative for it be best.

To confirm the presence of GNP and the hydration of the cement phases, microstructure spot mode analysis was applied in imaging of the unhydrated grains of alite (C_3S), belite (C_2S), tricalcium aluminate (C_3A) tetracalcium aluminoferrite (C_4AF), and the impact of GNP on porosity and permeability. Microstructure showed unhydrated grains and drawing line profiles from the center of the grain higher values of calcium and silica, aluminum and iron as well were obtained validating the presence of C_3S, C_2S, C_3A, C_4AF phases. Most of the calcium and silica element lines on EDS analysis synchronized showing higher atomic% in the unhydrated grain region and reduced when in the outer CSH area as seen in Figures 20-29. On some spots, the lines had their own trend where calcium was increasing while silica was decreasing, that could potentially be a CH area only. On areas where GNP were present, only carbon line had a peak with the other elements at zero value, confirming the possible explanation of GNP occupying pore spaces. This spot mode analysis for EDS line profiles showed graphene might have influenced CSH in terms of compositional difference.

5.1.3 Impact of hydration time on the strength of cement

A reduction in porosity and permeability is observed on the cement cores cured for 28 days (84 thermal cycles) in comparison to 7 days (21 thermal cycles) which is connected to the growth of the CSH nuclei as seen in Figure 9. For the microstructure, higher volume of hazy like structures were seen on samples hydrated for 28 days (84 thermal cycles) from the Back Scattered Electron (BSE) micrographs. In microindentation, varying depths of indents on each sample could be

explained based on the cement phase or composition present at that particular point. It is observed that the depth of indents for each set of design decreased significantly for samples hydrated for 28 days (84 thermal cycles). Also, the values of elasticity and hardness decreased drastically for 0.1%LG sample hydrated for 28 days which proves its effectiveness and performance when mixed with OPC. This means that the material tends to be ductile thus increasing its mechanical elasticity; whereas on the other hand if the values increase it is becoming brittle in nature which could potentially lead to wellbore integrity failures due to fracturing. Thus, with the considerable decrease in elastic modulus and hardness values for 0.1%LG samples there is an increase in ductility which potentially prevents initiation and extension of microfractures during thermal cycling conditions. For the neat sample, there is an increase in the values which means that the material tends to become more brittle with increase in hydration days.

As part of the materials characterization study, the unhydrated clinker grains have higher elastic modulus and hardness value according to (Hughes & Trtik, 2004). That was explained due to the varying porosity values. As observed by (Massion, Lu, et al., 2022), the cement samples that underwent static temperature curing (90 ^{o}C) for 28 days and then triaxial testing showed brittleness in neat cement whereas GNPs based cement showed ductility and fracture toughness. As discussed above, similar results were observed in the current study, although using surface sensitive indentation technique rather than core sample triaxial tests clearly provides evidence that cement samples with GNP have improved ductility.

Table 6: Comparison of elasticity and hardness from samples cured at static 90 ^{o}C and dynamic thermal loading between 20 ^{o}C and 110 ^{o}C. All the samples in this study were indented using Vicker's diamond tip at a loading and unloading rate of 10 N/min with a load applied at 5 N and creep of 30 seconds.

Sample ID	Elasticity (GPa) Massion et al., 2021	Hardness (GPa) Massion et al., 2021	Elasticity (GPa) 7 days	Hardness (GPa) 7 days	Elasticity (GPa) 28 days	Hardness (GPa) 28 days
Neat	11.95	0.33	9.09	0.25	16.78	0.36
0.008%PG	8.74	0.27	13.02	0.39	10.13	0.32
0.008%LG	-	-	11.23	0.27	10.53	0.27
0.1%PG	-	-	10.69	0.29	12.54	0.30
0.1%LG	-	-	16.51	0.58	8.27	0.26
0.016%PG	13.22	0.27	-	-	-	-
0.05%PG	11.67	0.32	-	-	-	-

5.2 KEY FINDINGS AND CONCLUSIONS:

From the specific and detailed investigation as discussed above, it is concluded that GNP enhanced cement hydrated for 28 days (84 thermal cycles) can prevent deterioration of wellbore cement by resisting fracturing and be used for zonal isolation in producing and non-producing wells made of Portland cement-based slurries under geothermal conditions.

1. During early stages of wellbore construction when cement slurry is pumped into the annulus between the casing and the rock formation, neat cement sample would perform better than the GNP mix designs, as they have lowest values of porosity, permeability, elastic modulus, and hardness. It is suitable for resisting the attack of geofluids and would outperform the other cement samples.

2. In contrast, as hydration progresses under thermal cyclic loading conditions for 28 days, GNP mixed cement samples have shown improved durable properties such as the ability to withstand force loads and resist fracturing. This is very relevant to the realistic conditions that exist down the borehole where temperature changes thousands of times over the life of a well. The impact of GNP reinforced cement was clearly seen in micrographs, where some of the pore spaces have been occupied by GNP, reducing the possibility of the extension of the microcracks thus strengthening the wellbore cementing.

3. When powdered and liquid form of organic additives (GNP) were mixed with cement, but at different curing conditions, not much variation is seen in the petrophysical and micromechanical properties. However, the difference is seen in neat versus GNP cement samples for both static and dynamic cured temperature samples. GNP mixed cement samples have had higher ductility and fracture toughness. The microstructure data shows there are possible microcracks on neat sample that could further lead to fracturing of the sample compromising on wellbore integrity. On the other hand, the ductile nature of the GNP cement samples improved even under cyclic conditions when it reached about 110^{o}C where strength retrogression could have had its effect. Thus, GNP have shown better ability to withstand the harsh subsurface temperature conditions.

5.3 FUTURE WORK:

We see that GNP enhanced cement can potentially solve the problem of wellbore deterioration, the underlying mechanisms of the interaction of GNP with cement is yet unclear. This would be a good starting point for furthering this research on wellbore cement integrity. However, there are other areas of interest such as thermal and electrical properties, that would help better understanding of the role of GNP in wellbore cement. Below are few more parameters that could be studied upon,

- Another set of samples with increased hydration time (90 days).
- Higher temperatures for dynamic cyclic loading.
- Different load values and creep times for indentation.
- Different mix design compositions.
- Different nanoadditives from carbon family.

REFERENCES

Achee, T. C., Sun, W., Hope, J. T., Quitzau, S. G., Sweeney, C. B., Shah, S. A., Habib, T., & Green, M. J. (2018). High-yield scalable graphene nanosheet production from compressed graphite using electrochemical exfoliation. *Scientific Reports*, *8*(1), 1–8. https://doi.org/10.1038/s41598-018-32741-3

Agbasimalo, N., & Radonjic, M. (2014). Experimental Study of the Impact of Drilling Fluid Contamination on the Integrity of Cement–Formation Interface. *Journal of Energy Resources Technology*, *136*(4), 1–5. https://doi.org/10.1115/1.4027566

Aili, A., & Maruyama, I. (2020). Review of Several Experimental Methods for Characterization of Micro- and Nano-Scale Pores in Cement-Based Material. *International Journal of Concrete Structures and Materials*, *14*(1). https://doi.org/10.1186/s40069-020-00431-y

Applications, G. (2022). *Geothermal Applications*.

Bauer, S. J., Barrow, P., Pyatina, T., & Sugama, T. (2020). Thermal Expansion , Fluid Flow , and Thermal Shock of Cement and a Cement / Steel Interface at Elevated Pressure and Temperature. *PROCEEDINGS, 45th Workshop on Geothermal Reservoir Engineering*, 1–21.

Bello, K. (2014). *Use of Liquid Pressure-Pulse Decay Permeameter in Experimental Evaluation of Permeability in Wellbore Cement Under Geopressured*.

Bello, K. S., & Radonjic, M. (2014). Evaluation of wellbore cement integrity in contact with high temperature brine. *48th US Rock Mechanics / Geomechanics Symposium 2014*, *3*, 2142–2146.

Bergen, S. L., Zemberekci, L., & Nair, S. D. (2022). A review of conventional and alternative cementitious materials for geothermal wells. *Renewable and Sustainable Energy Reviews*, *161*(March), 112347. https://doi.org/10.1016/j.rser.2022.112347

Boden, D. R. (2022). *Geothermal 101- The heat beneath our feet*.

Cadix, A., & James, S. (2022). Cementing additives. In *Fluid Chemistry, Drilling and Completion*. INC. https://doi.org/10.1016/b978-0-12-822721-3.00008-3

California Energy Commission. (2019). California Geothermal Energy Statistics and Data. In *California Energy Commission*. https://ww2.energy.ca.gov/almanac/renewables_data/geothermal/index_cms.php

Cao, M. li, Zhang, H. xia, & Zhang, C. (2016). Effect of graphene on mechanical properties of cement mortars. *Journal of Central South University*, *23*(4), 919–925. https://doi.org/10.1007/s11771-016-3139-4

Cataldi, P., Athanassiou, A., & Bayer, I. S. (2018). Graphene nanoplatelets-based advanced materials and recent progress in sustainable applications. *Applied Sciences (Switzerland)*, *8*(9). https://doi.org/10.3390/app8091438

CHEMISTRY AND QUALITY CONTROL FORMULAS IN CHEMISTRY AND QUALITY CONTROL. (n.d.).

Chuah, S., Pan, Z., Sanjayan, J. G., Wang, C. M., & Duan, W. H. (2014). Nano reinforced cement and concrete composites and new perspective from graphene oxide. In *Construction and Building Materials* (Vol. 73, pp. 113–124). Elsevier Ltd. https://doi.org/10.1016/j.conbuildmat.2014.09.040

Chung, D. D. L. (2002). Review: Graphite. *Journal of Materials Science*, *37*(8), 1475–1489. https://doi.org/10.1023/A:1014915307738

Clean, D. (2022). *DOE Launches New Energy Earthshot to Slash the Cost of Geothermal*. 1–4.

Constantinides, G., & Ulm, F. J. (2004). The effect of two types of C-S-H on the elasticity of cement-based materials: Results from nanoindentation and micromechanical modeling. *Cement and Concrete Research*, *34*(1), 67–80. https://doi.org/10.1016/S0008-8846(03)00230-8

Costa, B. L. de S., Souza, G. G. de, Freitas, J. C. de O., Araujo, R. G. da S., & Santos, P. H. S. (2017). Silica content influence on cement compressive strength in wells subjected to steam injection. *Journal of Petroleum Science and Engineering*, *158*(June), 626–633. https://doi.org/10.1016/j.petrol.2017.09.006

Cui, X., Zhang, C., Hao, R., & Hou, Y. (2011). Liquid-phase exfoliation, functionalization and applications of graphene. *Nanoscale*, *3*(5), 2118–2126. https://doi.org/10.1039/c1nr10127g

DOE. (n.d.). *A History of Geothermal Energy in America | Department of Energy*. https://www.energy.gov/eere/geothermal/history-geothermal-energy-america%0Ahttp://energy.gov/eere/geothermal/history-geothermal-energy-america

Energy, Z. (2021). *Superhot Rock. October*.

Feng, G., Wang, X., Wang, M., & Kang, Y. (2020). Experimental investigation of thermal cycling effect on fracture characteristics of granite in a geothermal-energy reservoir. *Engineering Fracture Mechanics*, *235*(June), 107180. https://doi.org/10.1016/j.engfracmech.2020.107180

Finger, J., & Blankenship, D. (2010). Handbook of Best Practices for Geothermal Drilling. *Sandia Report (SAND2010-6048). …*, *December*, 84, Figure 2. http://artikel-software.com/file/geothermal drilling handbook.pdf

First well successfully drilled for geothermal heat project in Luttelsgeest, Netherlands _ ThinkGeoEnergy - Geothermal Energy News. (n.d.).

Geim, A. K., & Novoselov, K. S. (2007). The rise of graphene PROGRESS. *Nature Materials*, *6*(3), 183–191.

Guerrero, G. (1998). Cementing of geothermal wells. *Report 6 of Geothermal Training Programe*. http://www.os.is/gogn/unu-gtp-report/UNU-GTP-1998-06.pdf

Herbert, P., E.M, G., J.F, Y., D.A, D., & I, J. (n.d.). *Hydration of Portland Cement and Composition of cement phases*.

Hernandez, Y., Nicolosi, V., Lotya, M., Blighe, F. M., Sun, Z., De, S., McGovern, I. T., Holland, B., Byrne, M., Gun'ko, Y. K., Boland, J. J., Niraj, P., Duesberg, G., Krishnamurthy, S., Goodhue, R., Hutchison, J., Scardaci, V., Ferrari, A. C., & Coleman, J. N. (2008). High-yield production of graphene by liquid-phase exfoliation of graphite. *Nature Nanotechnology*, *3*(9), 563–568. https://doi.org/10.1038/nnano.2008.215

Hughes, J. J., & Trtik, P. (2004). Micro-mechanical properties of cement paste measured by depth-sensing nanoindentation: A preliminary correlation of physical properties with phase type. *Materials Characterization*, *53*(2–4), 223–231. https://doi.org/10.1016/j.matchar.2004.08.014

Ichim, A., & Teodoriu, H. C. (2017). Investigations on the surface well cement integrity induced by thermal cycles considering an improved overall transfer coefficient. *Journal of Petroleum Science and Engineering*, *154*(February), 479–487. https://doi.org/10.1016/j.petrol.2017.02.013

Iremonger, S., (2022). Discussions on wellbore cement mixed with graphene nanoplatelets from an industry's perspective

Jaganmohan, M. (2022). *Global geothermal energy capacity 2009-2021 Geothermal energy capacity worldwide from 2009 to 2021*. 2021–2022.

Jupudi, H., Massion, C., Johnson, B., & Radonjic, M. (n.d.). *Microstructural and Petrophysical Evaluation of Graphene Modified Portland Wellbore Cement Undergone Cyclic Temperature Loading*. 1485–1500.

Katalin Kopecskó, & Zaid Ali Abdulhussein Khaiqani. (2021). Graphene Oxide Application in Cement-Bound Materials—State of the Art. *Journal of Materials Science and Engineering B*, *11*(4), 144–155. https://doi.org/10.17265/2161-6221/2021.10-12.003

Katende, A., Lu, Y., Bunger, A., & Radonjic, M. (2020). Experimental quantification of the effect of oil based drilling fluid contamination on properties of wellbore cement. *Journal of Natural Gas Science and Engineering*, *79*(December 2019), 103328. https://doi.org/10.1016/j.jngse.2020.103328

Kutchko, B. G., Strazisar, B. R., Lowry, G. V., Dzombak, D. A., & Thaulow, N. (2008). Rate of CO2 attack on hydrated class H well cement under geologic sequestration conditions. *Environmental Science and Technology*, *42*(16), 6237–6242. https://doi.org/10.1021/es800049r

Lee, C., Wei, X., Kysar, J. W., & Hone, J. (2008). of Monolayer Graphene. *Science*, *321*(July), 385–388.

Li, D., Müller, M. B., Gilje, S., Kaner, R. B., & Wallace, G. G. (2008). Processable aqueous dispersions of graphene nanosheets. *Nature Nanotechnology*, *3*(2), 101–105. https://doi.org/10.1038/nnano.2007.451

Li, G. Y., Wang, P. M., & Zhao, X. (2005). Mechanical behavior and microstructure of cement composites incorporating surface-treated multi-walled carbon nanotubes. *Carbon*, *43*(6), 1239–1245. https://doi.org/10.1016/j.carbon.2004.12.017

Liska, M., Wilson, A., & Bensted, J. (2019). Special cements. In *Lea's Chemistry of Cement and Concrete* (5th ed.). Elsevier Ltd. https://doi.org/10.1016/B978-0-08-100773-0.00013-7

Liu, F., Wang, M., Chen, Y., & Gao, J. (2019). Thermal stability of graphene in inert atmosphere at high temperature. *Journal of Solid State Chemistry*, *276*(January), 100–103. https://doi.org/10.1016/j.jssc.2019.04.008

Mahmoud, A. A., & Elkatatny, S. (2019). The effect of silica content on the changes in the mechanical properties of class G cement at high temperature from slurry to set. *53rd U.S. Rock Mechanics/Geomechanics Symposium*, *June*.

Massion, C., Achang, M., Bour, D., & Radonjic, M. (2020). Graphene-enhanced wellbore cement: Improving cement performance in the construction of geothermal wellbores. *Transactions - Geothermal Resources Council*, *44*, 67–81.

Massion, C., Lu, Y., Bunger, A., Crandall, D., & Radonjic, M. (2021). Improvement of wellbore cement by addition of graphene nanoplatelets. *Transactions - Geothermal Resources Council*, *45*, 222–236.

Massion, C., Lu, Y., Crandall, D., Bunger, A., & Radonjic, M. (2022). Graphene nanoplatelets reinforced cement as a solution to leaky wellbores reinforcing weak points in hydrated Portland cement with graphene nanoparticles improves mechanical and chemical durability of wellbore cements. *Cement and Concrete Composites*, *133*(July), 104726. https://doi.org/10.1016/j.cemconcomp.2022.104726

Massion, C., Vissa, V. S. K., Lu, Y., Crandall, D., Bunger, A., & Radonjic, M. (2022). Geomimicry-Inspired Micro-Nano Concrete as Subsurface Hydraulic Barrier Materials: Learning from Shale Rocks as Best Geological Seals. In *Minerals, Metals and Materials Series: Vol. II* (Issue Volume II). Springer International Publishing. https://doi.org/10.1007/978-3-030-92559-8_13

Murali, M., Alaloul, W. S., Mohammed, B. S., Musarat, M. A., Salaheen, M. Al, Al-Sabaeei, A. M., & Isyaka, A. (2022). Utilizing graphene oxide in cementitious composites: A systematic review. *Case Studies in Construction Materials*, *17*(July), e01359. https://doi.org/10.1016/j.cscm.2022.e01359

Partoens, B., & Peeters, F. M. (2006). From graphene to graphite: Electronic structure around the K point. *Physical Review B - Condensed Matter and Materials Physics*, *74*(7), 1–11. https://doi.org/10.1103/PhysRevB.74.075404

Peigney, A., Laurent, C., Flahaut, E., Bacsa, R. R., & Rousset, A. (2001). CNTの比表面積の求め方.pdf. *Carbon*, *39*, 507.

Pyatina, T., & Sugama, T. (2020). Cements with supplementary cementitious materials for high-temperature geothermal wells. *Geothermics*, *86*(May), 101840. https://doi.org/10.1016/j.geothermics.2020.101840

Radonjic, M., & Oyibo, A. E. (2014). Comparative experimental evaluation of drilling fluid contamination on shear bond strength at wellbore cement interfaces. *World Journal of Engineering*, *11*(6), 597–604. https://doi.org/10.1260/1708-5284.11.6.597

Rahimi-Aghdam, S., Bažant, Z. P., & Abdolhosseini Qomi, M. J. (2017). Cement hydration from hours to centuries controlled by diffusion through barrier shells of C-S-H. *Journal of the*

Mechanics and Physics of Solids, *99*(November 2016), 211–224. https://doi.org/10.1016/j.jmps.2016.10.010

Rhee, I., Lee, J. S., Kim, Y. A., Kim, J. H., & Kim, J. H. (2016). Electrically conductive cement mortar: Incorporating rice husk-derived high-surface-area graphene. *Construction and Building Materials*, *125*, 632–642. https://doi.org/10.1016/j.conbuildmat.2016.08.089

Richter, A. (2022). ThinkGeoEnergy's Top 10 Geothermal Countries 2021 – installed power generation capacity (MWe). *ThinkGeoEnergy*, 27–28. https://www.thinkgeoenergy.com/thinkgeoenergys-top-10-geothermal-countries-2021-installed-power-generation-capacity-mwe/

Robins, J. C., Kolker, A., Flores-espino, F., Pettitt, W., Rising, G., Schmidt, B., Rising, G., Augustine, C., Blair, N., Cook, J., Cruce, J., Johnston, H., Kurtz, J., Levine, A., Porro, G., Rhodes, G., Rubin, R., Taverna, N., Turchi, C., & Warren, I. (2021). *2021 U.S. Geothermal Power Production and District Heating Market Report*. 64. https://www.nrel.gov/docs/fy21osti/78291.pdf

Routley, B. N. (2022). *Visualized : The World ' s Popula*. 1–21.

Stankovich, S., Dikin, D. A., Dommett, G. H. B., Kohlhaas, K. M., Zimney, E. J., Stach, E. A., Piner, R. D., Nguyen, S. B. T., & Ruoff, R. S. (2006). Graphene-based composite materials. *Nature*, *442*(7100), 282–286. https://doi.org/10.1038/nature04969

Systems, E. G. (2006). The Future of Geothermal Energy The Future of Geothermal Energy. In *Technology: Vol. Im* (Issue November). http://www.eere.energy.gov/geothermal/pdfs/structure_outcome.pdf

Taylor, H. F. W. (1997). Cement chemistry. *Cement Chemistry*. https://doi.org/10.1680/cc.25929

Teodoriu, C. (2013). Why and when does casing fail in geothermal wells. *Oil Gas European Magazine*, *39*(1), 38–40.

Terrones, M., Botello-Méndez, A. R., Campos-Delgado, J., López-Urías, F., Vega-Cantú, Y. I., Rodríguez-Macías, F. J., Elías, A. L., Muñoz-Sandoval, E., Cano-Márquez, A. G., Charlier, J. C., & Terrones, H. (2010). Graphene and graphite nanoribbons: Morphology, properties, synthesis, defects and applications. *Nano Today*, *5*(4), 351–372. https://doi.org/10.1016/j.nantod.2010.06.010

U.S. Energy Information Administration. (2022). Where geothermal energy is found. In *Eia*. https://www.eia.gov/energyexplained/geothermal/where-geothermal-energy-is-found.php

Yalcinkaya, T. K., Radonjic, M., Hughes, R. G., Willson, C. S., & Ham, K. (2011). The effect of CO2-saturated brine on the conductivity of wellbore-cement fractures. *SPE Drilling and Completion*, *26*(3), 332–340. https://doi.org/10.2118/139713-PA

Yoon, H., Kim, D., Park, M., Kim, J., Kim, J., Srituravanich, W., Shin, B., Jung, Y., & Jeon, S. (2018). Extraordinary Enhancement of UV Absorption in TiO2 Nanoparticles Enabled by Low-Oxidized Graphene Nanodots. *Journal of Physical Chemistry C*, *122*(22), 12114–12121. https://doi.org/10.1021/acs.jpcc.8b03329

Yu, M. F., Lourie, O., Dyer, M. J., Moloni, K., Kelly, T. F., & Ruoff, R. S. (2000). Strength and breaking mechanism of multiwalled carbon nanotubes under tensile load. *Science*,

287(5453), 637–640. https://doi.org/10.1126/science.287.5453.637

Zheng, Q., Han, B., Cui, X., Yu, X., & Ou, J. (2017). Graphene-engineered cementitious composites: Small makes a big impact. *Nanomaterials and Nanotechnology*, *7*, 1–18. https://doi.org/10.1177/1847980417742304

Zhu, Y., Murali, S., Cai, W., Li, X., Suk, J. W., Potts, J. R., & Ruoff, R. S. (2010). Graphene and graphene oxide: Synthesis, properties, and applications. *Advanced Materials*, *22*(35), 3906–3924. https://doi.org/10.1002/adma.201001068

APPENDICES

Appendix A: Scanning Electron Microscopy (SEM) Data

Appendix B: Energy dispersive X-ray spectroscopy (EDS) line profile Data

Appendix C: Microindentation and Surface Profilometry Data

Appendix D: Porosity and Permeability Data

APPENDIX A

Scanning Electron Microscopy (SEM) images for 7 days of hydrated samples at 5000x magnification

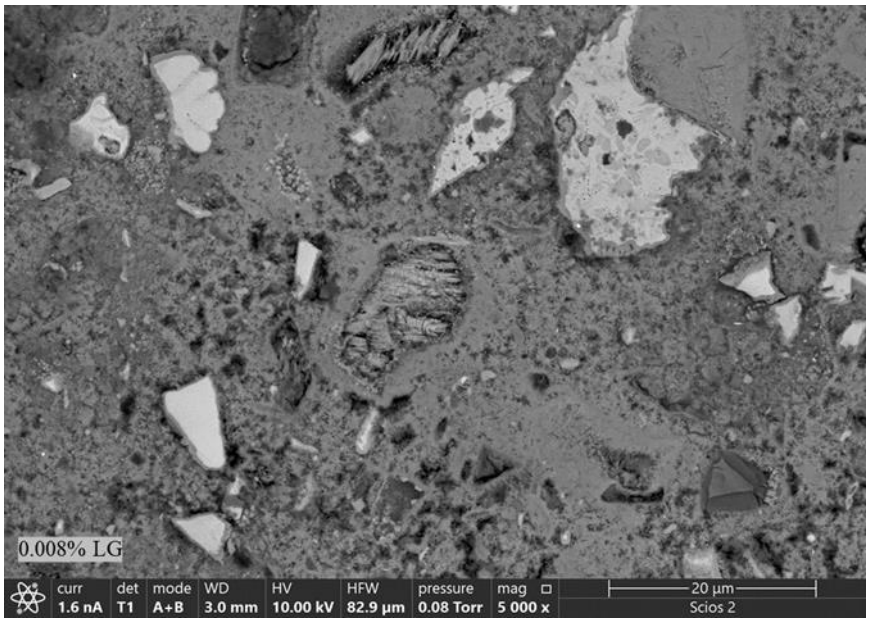

Backscatter Electron (BSE) micrograph on 0.008% LG cement sample hydrated for 7 days (21 thermal cycles)

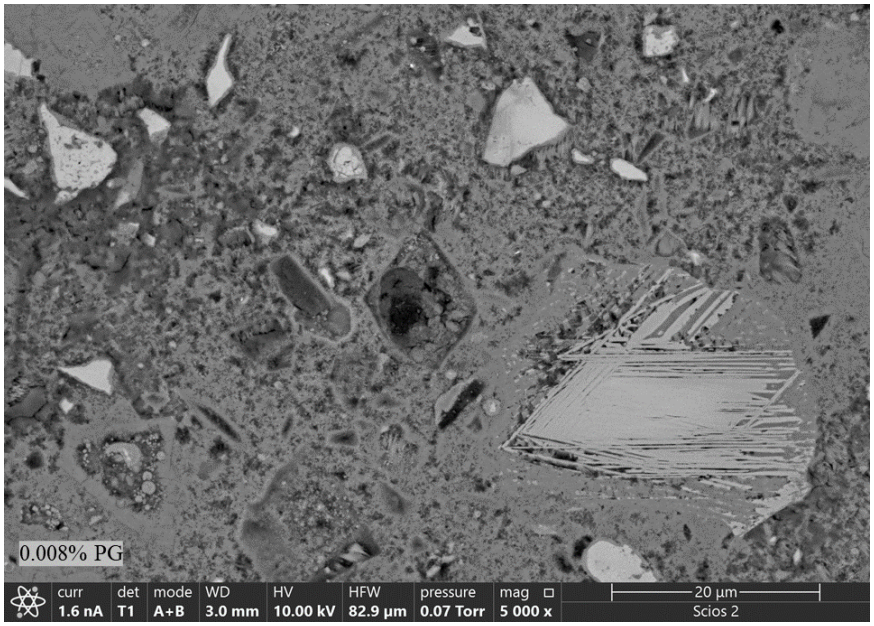

Backscatter Electron (BSE) micrograph on 0.008% PG cement sample hydrated for 7 days (21 thermal cycles)

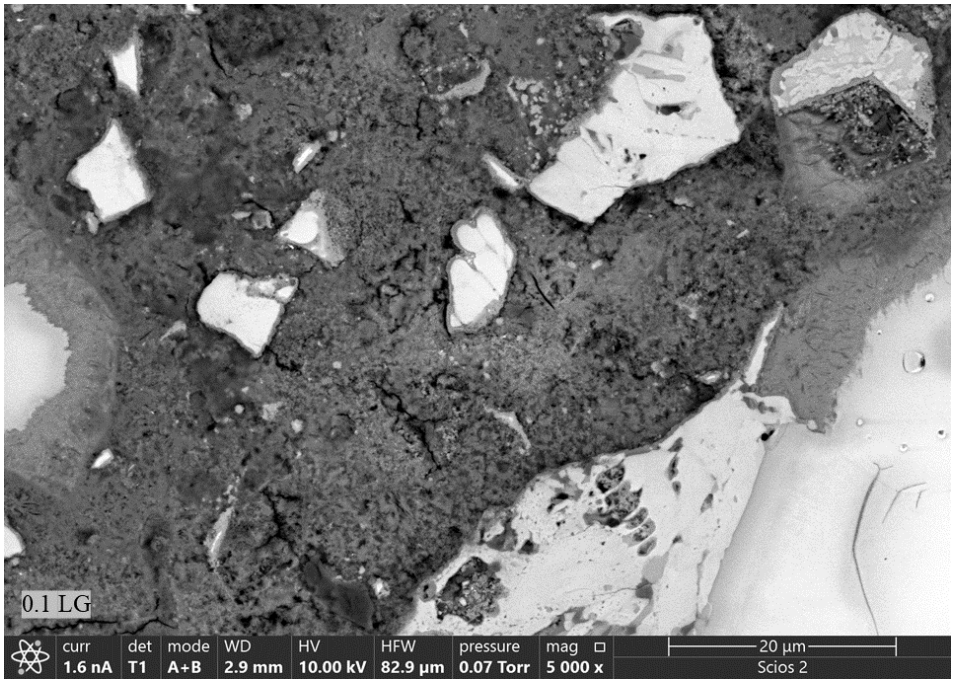

Backscatter Electron (BSE) micrograph on 0.1% LG cement sample hydrated for 7 days (21 thermal cycles)

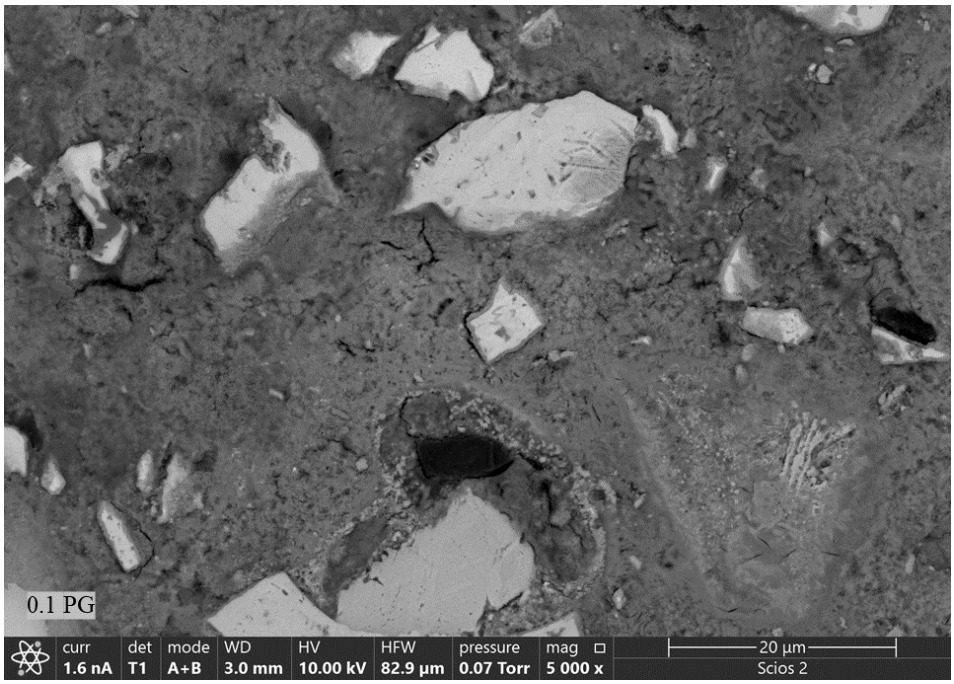

Backscatter Electron (BSE) micrograph on 0.1% PG cement sample hydrated for 7 days (21 thermal cycles)

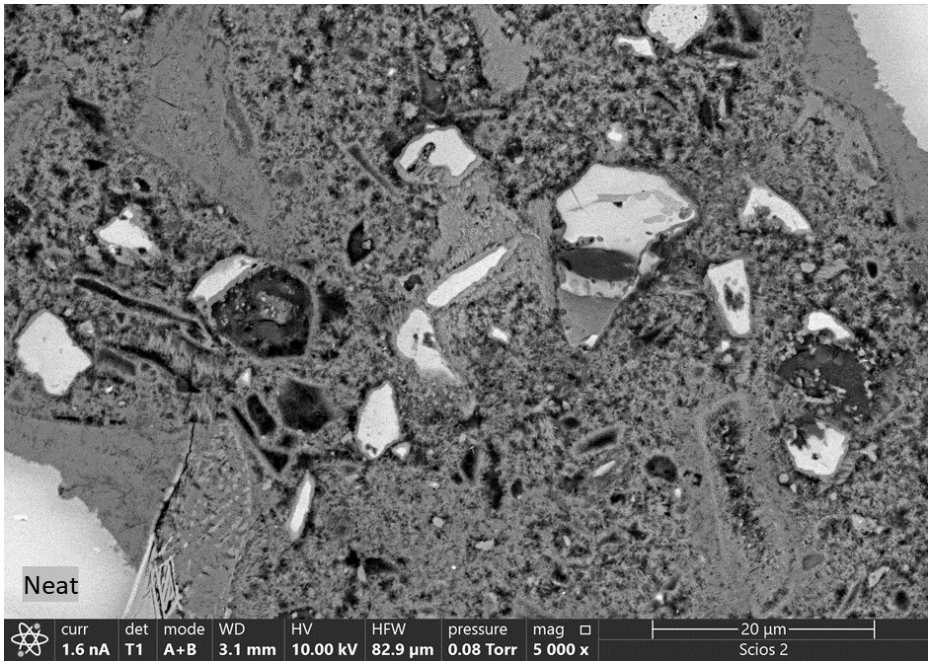

Backscatter Electron (BSE) micrograph on neat cement sample hydrated for 7 days (21 thermal cycles)

Scanning Electron Microscopy (SEM) images at 28 days of hydration for the remaining samples not listed in the results section at 5000x magnification.

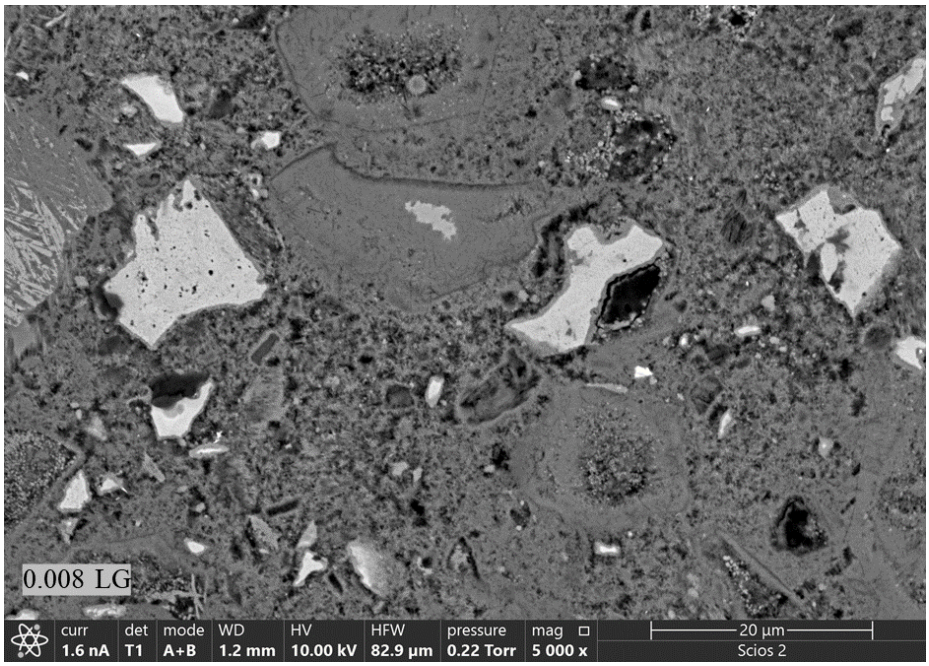

Backscatter Electron (BSE) micrograph on 0.008% LG cement sample hydrated for 28 days (84 thermal cycles)

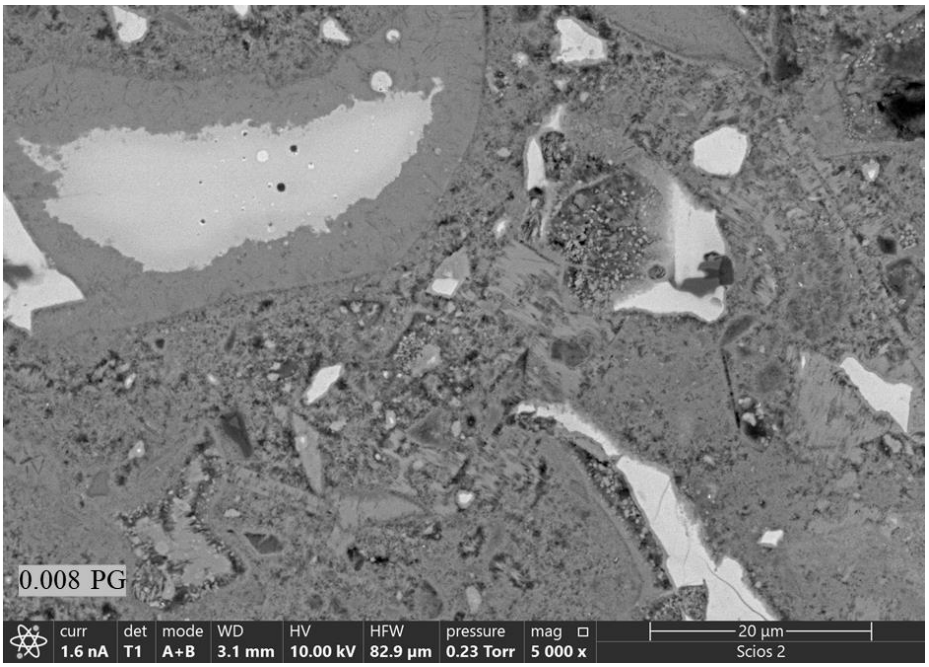

Backscatter Electron (BSE) micrograph on 0.008% PG cement sample hydrated for 28 days (21 thermal cycles)

APPENDIX B

01lg_loc1(1): Quant Atomic %																					
Point	C K	O K	Na K	Mg K	Al K	Si K	S K	Cl K	Ca K	Fe K	Total	Distance (| C K Err	O K Err	Na K Err	Mg K Err	Al K Err	Si K Err	S K Err	Cl K Err	Ca K Err	Fe K Err
1	4.537224	54.287	0.453453	1.22676	0.777439	9.65533	0.265639	0.007518	28.36616	0.423479	100	0	0.567153	3.147072	0.204054	0.165406	0.140501	0.333216	0.094871	0.097737	0.591251	0.186829
2	3.883656	55.62143	0.67321	1.162101	0.44657	9.818492	0.090599	0	27.82521	0.478732	100	1.77	0.47555	3.056123	0.217164	0.164061	0.139553	0.328849	0.084559	0	0.412327	0.171853
3	3.343754	55.75328	0.056715	1.096777	0.421321	9.64904	0.059229	0.081913	28.86284	0.67513	100	3.54	0.46657	2.779942	0.189051	0.176026	0.14044	0.319041	0.094767	0.088214	0.593493	0.184126
4	4.083728	57.13261	0.281723	0.951064	0.384146	9.370477	0.229597	0	26.92568	0.640975	100	5.31	0.437542	2.634756	0.181108	0.164851	0.128049	0.303673	0.086099	0	0.552224	0.160244
5	3.864967	54.17328	0.703452	0.833213	1.093929	9.255425	0.289892	0.342001	29.07739	0.366456	100	7.08	0.4934	3.186663	0.219829	0.166643	0.149597	0.333672	0.09453	0.09034	0.598673	0.189546
6	3.499776	54.28196	0.454021	2.294505	7.167461	3.861713	0.07197	0	22.69516	5.673432	100	8.86	0.524966	2.951502	0.252234	0.24639	0.263123	0.331274	0.09814	0	0.381669	0.523701
7	3.846989	54.34322	0	0.944185	2.188243	8.097297	0	0.097791	27.4533	3.02897	100	10.6	0.491105	3.152507	0	0.191788	0.179038	0.347633	0	0.084752	0.585464	0.290276
8	3.498879	57.10736	0.381281	0.836214	0.766754	9.409642	0.239371	0	27.30828	0.452218	100	12.4	0.466517	3.114947	0.211823	0.175335	0.146048	0.330838	0.092066	0	0.573278	0.195554
9	3.263691	53.71164	0.457318	0.809055	0.48639	10.74652	0.09785	0	29.45639	0.971145	100	14.2	0.477613	3.095772	0.217771	0.161811	0.137658	0.332686	0.091734	0	0.591303	0.16995
10	3.071154	54.98652	0.262871	0.861499	0.358655	9.812842	0.058908	0	29.90577	0.681788	100	15.9	0.484919	3.109357	0.215077	0.169475	0.135707	0.331679	0.091635	0	0.610757	0.180095
11	3.919931	52.55003	0.168469	1.156453	0.631759	10.36521	0.139099	0	30.44574	0.623304	100	17.7	0.500417	3.051292	0.216603	0.171326	0.145791	0.345507	0.099356	0	0.629164	0.194783
12	3.237186	54.10177	0.21963	1.240739	0.420242	10.31349	0.158851	0.036605	30.06119	0.210304	100	19.5	0.511135	3.212293	0.21963	0.171136	0.136823	0.344878	0.092663	0.095174	0.62461	0.170872
13	3.419466	52.91394	0.80223	0.966784	0.522539	10.16136	0.345766	0	30.4607	0.407215	100	21.3	0.417008	2.696252	0.206288	0.156392	0.135473	0.342793	0.097858	0	0.611227	0.170768
14	3.280315	55.97111	0.017065	0.819776	0.732667	10.49561	0	0	28.28947	0.393988	100	23	0.480046	2.745177	0.153587	0.161267	0.126634	0.246051	0	0	0.577336	0.160057
15	3.033316	57.37828	0.342954	0.672592	0.410293	9.568533	0.08446	0	28.13679	0.372779	100	24.8	0.466664	2.622126	0.228636	0.164716	0.139873	0.329408	0.078427	0	0.58071	0.173963
16	3.02481	55.60883	0	0.904753	0.389534	9.897204	0.163974	0.290674	29.07888	0.641346	100	26.6	0.420113	3.107552	0	0.186695	0.146075	0.33453	0.091826	0.085881	0.611959	0.16675
17	2.91239	57.09917	0.337275	0.728827	0.252626	9.450715	0.11386	0.099842	28.62059	0.38471	100	28.3	0.485398	2.719008	0.202365	0.171489	0.136029	0.337526	0.088558	0.08653	0.588434	0.192355
18	4.048208	55.99242	0.230517	0.949104	0.787013	9.210538	0.153738	0	27.83996	0.788501	100	30.1	0.47626	2.784154	0.207465	0.167489	0.142231	0.327521	0.086093	0	0.591895	0.175222
19	3.84259	55.25974	0	0.578301	0.507195	9.622337	0.099725	0	29.65563	0.434477	100	31.9	0.470521	2.942826	0	0.155154	0.143546	0.336221	0.087259	0	0.600459	0.178902
20	2.898799	56.82817	0.465883	0.703482	0.743622	10.24594	0.149195	0	27.56869	0.396215	100	33.7	0.483133	3.014757	0.199664	0.162342	0.137708	0.248387	0.093247	0	0.574633	0.173344
21	4.605794	59.51399	0.154686	0.538265	0.856076	9.709541	1.053119	0	23.0813	0.487233	100	35.4	0.552695	2.705181	0.176784	0.160025	0.139361	0.327855	0.114032	0	0.545286	0.17119
22	5.48004	60.39826	0.177458	0.798247	0.6044	10.64308	0.729316	0	20.61109	0.558113	100	37.2	0.597823	2.771901	0.202809	0.165674	0.143417	0.258746	0.112202	0	0.539356	0.190575
23	7.715396	63.38843	0.186812	0.54751	0.571459	8.562018	0.853216	0.095306	17.64782	0.432038	100	39	0.66369	2.405633	0.166055	0.146893	0.11792	0.307158	0.098212	0.076245	0.464776	0.156014
24	10.95179	64.44305	0.070804	0.431356	0.522457	7.52766	0.737435	0	15.02888	0.28657	100	40.7	0.631834	2.486229	0.159309	0.128241	0.112529	0.263536	0.091506	0	0.415295	0.137978
25	6.948625	59.73011	0.268091	0.406848	0.356809	8.589128	0.913566	0.109582	21.94378	0.733463	100	42.5	0.604228	3.178913	0.187664	0.152568	0.138119	0.24758	0.113252	0.093928	0.582802	0.194592
26	10.65347	64.46327	0.359703	0.168432	0.381904	6.963937	0.638855	0	16.22222	0.148219	100	44.3	0.68732	2.663771	0.179852	0.132339	0.116232	0.264894	0.088118	0	0.421356	0.148219
27	9.208584	69.33235	0.234181	0.322179	0.358146	6.442148	0.432023	0.06499	13.46474	0.140661	100	46.1	0.74355	2.358243	0.167272	0.124714	0.098314	0.23576	0.074327	0.054992	0.359407	0.121906
28	8.410515	61.97506	0.460755	0.295215	0.830332	9.590317	0.534908	0	17.5114	0.391498	100	47.8	0.659648	2.441794	0.188491	0.14119	0.129739	0.310318	0.096163	0	0.323186	0.14969
29	8.20811	62.42737	0.046516	0.451349	0.70948	9.702868	0.681192	0.026662	17.00247	0.743988	100	49.6	0.706074	2.755911	0.209323	0.15045	0.13821	0.319532	0.107225	0.086652	0.479628	0.170751
30	6.33549	64.10303	0.133203	0.990405	0.503919	8.822204	0.715227	0	17.73694	0.659586	100	51.4	0.583532	2.352405	0.199805	0.160606	0.137432	0.315079	0.103922	0	0.46819	0.155902
31	5.370831	67.63658	0.167339	0.434501	0.60408	8.21181	0.909968	0	16.06125	0.603637	100	53.1	0.572889	2.18489	0.167339	0.140919	0.117678	0.272619	0.095229	0	0.411375	0.145705
32	4.115019	61.24591	0	0.837514	0.98175	10.54747	1.077753	0	20.75923	0.43535	100	54.9	0.536742	2.719163	0	0.159527	0.135103	0.330811	0.180664	0	0.357089	0.169303
33	3.283391	60.86373	0.015251	0.724969	0.963462	10.28826	0.969038	0.030026	22.3087	0.553177	100	56.7	0.443701	2.865781	0.137258	0.164144	0.138961	0.331116	0.107671	0.078069	0.525323	0.159807
34	4.066824	57.30637	0.10128	1.025767	0.591551	9.700843	0.413655	0	26.24725	0.546455	100	58.4	0.47845	2.756509	0.182304	0.15986	0.136512	0.328195	0.09733	0	0.558023	0.170008
35	4.477246	57.9147	0.323414	0.994325	0.630642	10.2361	1.070299	0	23.72161	0.631661	100	60.2	0.583989	2.832784	0.199024	0.165721	0.155076	0.356568	0.118922	0	0.579518	0.205976
36	3.245263	64.58325	0.598041	1.885053	1.196841	8.23912	0.928906	0.067667	18.43709	0.81877	100	62	0.427008	2.633714	0.192227	0.171368	0.137043	0.301714	0.102542	0.073819	0.473088	0.187147
37	2.510111	62.44902	0.42605	0.92994	1.397571	7.95457	0.827882	0	20.86567	2.639188	100	63.8	0.448234	2.772578	0.200494	0.167694	0.155286	0.33144	0.1135	0	0.528989	0.442032
38	4.58544	55.40629	0.220111	3.416455	6.68352	2.342467	0.199042	0	19.39464	7.75204	100	65.5	0.491297	2.78639	0.244568	0.240807	0.238697	0.283658	0.093301	0	0.482552	0.568638
39	4.587617	51.7788	0.987841	27.25964	3.494984	1.924001	0.232796	0	7.645117	2.089206	100	67.3	0.625584	1.730079	0.254444	0.537955	0.227934	0.150728	0.073813	0	0.321961	0.344916
40	5.168142	55.54993	0.687797	12.42074	3.321102	3.913765	0.301554	0	15.58295	3.054019	100	69.1	0.593065	2.280375	0.248371	0.305524	0.19365	0.269071	0.079656	0	0.421812	0.428818
41	12.27863	48.94567	0	0.684019	1.269145	4.336192	0.724734	0	29.15869	2.602925	100	70.8	0.884061	3.326405	0	0.19238	0.185381	0.228855	0.141411	0	0.724439	0.327641
42	15.00651	52.66579	0.614195	0.646275	0.598183	3.170571	0.395834	0	26.42059	0.482054	100	72.6	0.721467	3.511053	0.195426	0.153065	0.126539	0.184223	0.100758	0	0.621954	0.210899
43	10.35814	57.08901	0.148187	0.400722	0.204162	3.236508	0.489126	0.010206	27.7926	0.271343	100	74.4	0.76727	3.594493	0.207462	0.171738	0.140362	0.271449	0.108695	0.122467	0.656589	0.207498
44	10.82975	55.17218	0.237744	0.64701	0.614268	4.148993	0.435454	0.020692	27.28596	0.607953	100	76.2	0.701207	3.546783	0.208026	0.157381	0.141754	0.198043	0.103328	0.082769	0.636531	0.202651
45	13.62593	65.06176	0	0.961522	2.603229	2.354993	0.184358	0.00396	12.62052	2.583727	100	77.9	0.615059	2.353298	0	0.143205	0.137737	0.207619	0.064311	0.051486	0.332744	0.31981
46	7.140963	56.72126	0.044716	0.574997	0.904203	3.560565	0.719415	0.103544	29.54779	0.68255	100	79.7	0.609594	3.572993	0.268294	0.178447	0.159565	0.300423	0.114452	0.094915	0.501451	0.238893
47	11.34781	62.51635	0.180059	0.438251	1.49891	3.932728	0.338282	0	18.80896	0.938649	100	81.5	0.630434	2.879832	0.202566	0.132803	0.125657	0.237188	0.08027	0	0.465696	0.197
48	11.83274	59.42124	0.057357	0.284058	1.40408	3.688823	0.530756	0	21.40456	1.376386	100	83.2	0.70433	3.096392	0.229429	0.15781	0.154862	0.279721	0.103562	0	0.537507	0.224986
49	14.28576	58.45313	0.10034	0.262624	1.491695	4.870781	0.646437	0	18.64849	1.240748	100	85	0.690133	2.910004	0.200679	0.152046	0.146424	0.187338	0.099904	0	0.47338	0.214745
50	14.33598	59.5572	0.362669	0.390638	1.024861	4.989679	0.613229	0	18.02463	0.701117	100	86.8	0.673051	2.584093	0.192001	0.148173	0.13485	0.265812	0.092563	0	0.465871	0.175279

Due to the large volume of data for EDS line profiles data on each of the cement samples used in this study, an example of one set of data on 7 days hydrated 0.1%LG cement sample on location 1 is provided above. For data on all the samples please contact for the excel file.

APPENDIX C

0.881093	0.89771	0.674326	0.900943	0.477559	0.624176	0.350792	0.667409	0.864025	0.350641	0.487258	0.273875	0.56049	1.14711	1.31372
1.21154	1.55816	1.02478	1.21139	0.988009	0.084626	-0.26876	0.337859	0.834475	0.951091	0.617707	1.02432	1.11094	0.387557	0.344173
0.701993	-0.24139	0.115226	0.151842	0.418458	0.625075	0.481692	0.738308	0.774924	0.621541	0.368157	0.414773	0.48139	0.268007	0.184623
1.51244	1.07906	0.795675	0.652291	0.438908	0.585525	0.82214	0.778757	0.295374	0.08199	-0.14139	0.295223	0.37184	0.388456	0.745073
1.07289	1.10951	0.906124	0.532741	0.289357	0.615974	0.602591	0.689207	0.335823	0.622439	0.079056	0.225673	0.622289	0.588905	0.695522
0.873341	0.949957	0.836574	0.94319	0.939806	1.00642	0.91304	0.919656	0.586273	0.572889	0.589506	0.756122	0.602738	0.399354	0.405972
0.59379	0.600407	0.237023	-0.05636	0.030256	0.396873	0.973489	1.04011	0.826722	0.913338	1.08995	1.52657	1.16319	0.659804	0.756421
1.13424	0.880856	0.777472	0.584089	0.580706	0.637322	0.993939	0.890555	0.777172	0.603788	0.550404	0.757021	0.683637	0.610254	0.51687
0.72469	0.291306	0.067922	0.094539	-0.21885	0.257772	0.154388	0.331004	0.587621	0.454237	-0.13915	-0.30253	-0.21591	0.270703	0.08732
0.265139	-0.33824	-0.77163	-0.85501	-0.5184	-0.04178	0.074838	-0.14855	0.26807	0.254687	0.461303	0.43792	0.544536	0.361153	0.267769
0.135589	-0.0178	-0.92118	-0.65456	-0.44795	-0.44133	0.085288	0.491903	0.50852	0.425137	-0.35825	0.03837	0.314986	0.961603	0.848219
0.196038	0.442655	0.779271	0.865887	0.772504	0.86912	0.785737	0.082353	0.40897	0.345586	0.842202	0.888819	0.755435	0.932052	0.988668
0.336488	0.323103	0.419721	0.376337	0.442953	0.67957	0.776186	0.862802	0.299419	-0.12396	-0.03735	-0.13073	-0.08412	-0.0575	-0.14088
0.996937	0.743553	0.86017	0.446786	0.833402	1.14002	0.406636	0.583252	0.509868	0.266485	-0.0969	0.329718	0.636335	0.722951	0.759568
0.347386	0.014003	-0.07938	0.207236	0.143852	0.630469	0.487085	0.273701	0.380318	0.516934	0.333551	0.250167	0.126784	0.3734	0.550017
0.607836	0.814452	0.861069	-0.70232	-2.4457	-3.34908	-3.30247	-2.37585	-1.63923	-1.49262	-1.176	-0.53938	0.127233	0.22385	0.540466
-0.29171	-0.0351	0.291518	-1.70187	-4.69525	-6.61863	-6.09202	-4.2754	-3.38878	-2.65217	-1.78555	-1.09893	-0.77232	-0.5957	-0.09908
-0.04127	0.025351	0.201967	-2.09142	-3.3148	-3.50818	-4.00157	-2.71495	-1.77833	-1.46172	-0.9151	-0.58849	-0.38187	0.044749	0.131365
0.509184	0.455801	0.572418	-0.76097	-2.49435	-4.05773	-4.13112	-2.8045	-1.74788	-0.91127	-0.89465	-0.48804	-0.06142	-0.4648	-0.35819
0.129634	0.176251	0.572866	0.879484	0.826099	0.442716	0.379333	0.085949	-0.03743	-0.08082	-0.1842	-0.64759	-0.59097	-0.08435	0.052264
0.630083	0.8767	0.973316	0.719932	0.396549	0.513165	0.539782	0.896399	0.563015	-0.15037	-0.24375	-0.15714	-0.46052	-0.5239	-0.10729
0.990532	1.25715	0.553766	0.510382	0.636999	0.243615	0.050232	0.436848	0.483464	0.220081	-0.2633	-0.45669	-0.02007	-0.32345	-0.07684
0.440983	0.677598	0.444215	-0.24917	-0.55255	-0.19594	-0.04932	0.047297	0.313914	-0.09947	-0.06285	-0.35624	-0.10962	0.106996	0.363613
0.501432	0.468048	0.204665	0.541281	0.817897	0.494514	0.701131	0.797747	0.464363	0.09098	0.137596	0.244213	0.210829	0.047446	-0.05594
0.421881	-0.1715	0.035114	0.011731	0.428347	0.624963	0.37158	0.198196	-0.03519	0.021429	-0.00195	0.274662	0.491278	0.697895	0.294512
0.31233	0.538947	0.505564	0.402181	0.718796	0.775413	0.44203	0.278646	0.015262	-0.03812	0.048495	-0.22489	-0.35827	-0.06166	-0.34504
0.39278	0.449396	0.116013	0.13263	0.419246	0.325862	0.582478	0.699095	0.795712	0.682328	0.488944	0.405561	0.272178	0.398794	0.27541
0.00323	0.279846	0.646463	0.833079	0.399696	0.276312	0.452929	0.449545	0.536161	0.502778	0.509394	0.376011	0.582627	0.519244	0.13586

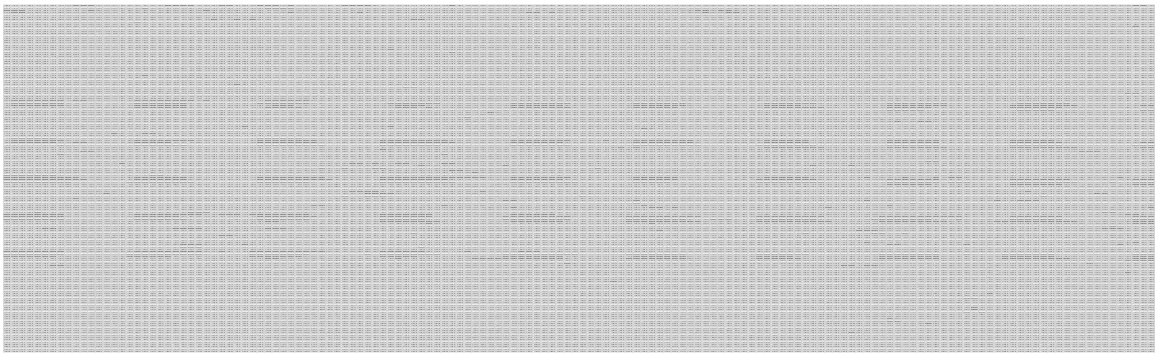

Due to the large volume of data for microindented surface profilometry on all the samples please contact for the excel file. An example of one set of data on 7 days hydrated neat sample is provided above. The first table shows a part of the data precisely for one indent and the second table is the entire data on one sample.

APPENDIX D

Sample:	NC71													
Diam,cm:	2.545													
Length,cm	5.388													
Baro mmH	760													
Visc, cp:	0.017569													
Time,sec	DT	Pres,inH2(	Flow_cc/s	P1,psi	Perm_md	Timestamp								
19	0	0.037	1.23E-05	2.025	0.001559	4/1/2022 3:58:07 PM	0.00199656216672769	0	0.0379346811678261	19				
39	20	0.067	1.07E-05	2.033	0.001346	4/1/2022 3:58:27 PM	0.00173067779113085	0	0.0674964338541031	39				
59	40	0.142	1.49E-05	2.04	0.00187	4/1/2022 3:58:47 PM	0.00241349378632287	0	0.142396133393049	59				
79	60	0.287	2.25E-05	2.048	0.002804	4/1/2022 3:59:07 PM	0.00363477805181395	0	0.287147466093302	79				
99	80	0.522	3.26E-05	2.056	0.004052	4/1/2022 3:59:27 PM	0.00527448880702558	0	0.522174391895533	99				
119	100	0.841	4.37E-05	2.063	0.005413	4/1/2022 3:59:47 PM	0.00707100372479743	0	0.841449443250895	119				
139	120	1.279	5.69E-05	2.071	0.00702	4/1/2022 4:00:07 PM	0.00920772555170299	0	1.27987385168672	139				
159	140	1.797	6.99E-05	2.079	0.008583	4/1/2022 4:00:27 PM	0.0113041821000336	0	1.79736495390534	159				
179	160	2.39	8.25E-05	2.088	0.010092	4/1/2022 4:00:47 PM	0.0133528456549738	0	2.3901593722403	179				
199	180	3.044	9.46E-05	2.098	0.011505	4/1/2022 4:01:07 PM	0.0153004392494808	0	3.04478741064668	199				
219	200	3.761	0.000106	2.107	0.012856	4/1/2022 4:01:27 PM	0.0171763211250577	0	3.76161432638764	219				
239	220	4.489	0.000116	2.115	0.014002	4/1/2022 4:01:47 PM	0.0187825478426333	0	4.48902893438935	239				
261	242	1.336	0.000486	2.101	0.059006	4/1/2022 4:02:09 PM	0.0785933702307589	0.0188429375644773	1.3360872939229	17				
281	262	2.574	0.00043	2.11	0.051993	4/1/2022 4:02:29 PM	0.0695679463647507	0.0188429375644773	2.57401401549578	37				
301	282	3.671	0.000398	2.119	0.047919	4/1/2022 4:02:49 PM	0.0644098218334349	0.0188429375644773	3.67135984450579	57				
323	304	0.192	0.000595	1.953	0.078064	4/1/2022 4:03:11 PM	0.0961979795247316	0.0620460878700426	0.192395959049463	2				
343	324	1.88	0.000528	1.96	0.069095	4/1/2022 4:03:31 PM	0.0854702600362626	0.0620460878700426	1.88034572079778	22				
363	344	3.227	0.000475	1.959	0.062143	4/1/2022 4:03:51 PM	0.076829053550249	0.0620460878700426	3.22682024911046	42				
383	364	4.445	0.000443	1.959	0.057994	4/1/2022 4:04:11 PM	0.0716997234210853	0.0620460878700426	4.44538285210729	62				
404	385	1.561	0.000603	1.96	0.078868	4/1/2022 4:04:32 PM	0.0975598951335996	0.0715412831613942	1.56095832213759	16				
424	405	3.035	0.000521	1.96	0.068154	4/1/2022 4:04:52 PM	0.084305761485464	0.0715412831613942	3.03500741347671	36				
444	425	4.352	0.00048	1.961	0.062799	4/1/2022 4:05:12 PM	0.0777238894120923	0.0715412831613942	4.35253780707717	56				
466	447	1.496	0.000617	1.961	0.080594	4/1/2022 4:05:34 PM	0.0997483332951864	0.0769023440020569	1.4962249994278	15				
486	467	2.994	0.000529	1.961	0.069132	4/1/2022 4:05:54 PM	0.085562150818961	0.0769023440020569	2.99467527866364	35				
506	487	4.327	0.000486	1.961	0.063577	4/1/2022 4:06:14 PM	0.078687258200212	0.0769023440020569	4.32779920101166	55				
529	510	1.497	0.000617	1.961	0.080659	4/1/2022 4:06:37 PM	0.0998288450141748	0.0778295068905271	1.49743267521262	15				
549	530	3.052	0.000539	1.961	0.070469	4/1/2022 4:06:57 PM	0.0872172993208681	0.0778295068905271	3.05260547623038	35				
569	550	4.38	0.000492	1.958	0.064448	4/1/2022 4:07:17 PM	0.079635855758732	0.0778295068905271	4.37997206673026	55				
591	572	1.597	0.000617	1.956	0.080852	4/1/2022 4:07:39 PM	0.0997971736360341	0.0791398113626137	1.59675477817655	16				
611	592	3.125	0.000536	1.953	0.070437	4/1/2022 4:07:59 PM	0.086799955719875	0.0791398113626137	3.1247984059155	36				
631	612	4.458	0.000492	1.951	0.064675	4/1/2022 4:08:19 PM	0.0796118397930903	0.0791398113626137	4.45826302841306	56				

Due to the large volume of data for permeability on all the samples please contact for the excel file. An example of one set of data for 10 minutes on 7 days hydrated neat sample is provided above. There is data for at least 7 to 48 hours on each sample. Three sets of cores were tested for permeability on each mix design.

Tables 1: Summarized data for porosity values comparing previous works related to wellbore cementing with thermal cyclic loading and static temperature to that of the current work done.

1a: (K. S. Bello & Radonjic, 2014) measured porosity using a Helium-porosimeter.

Sample identification for average Porosity (%)	(K. S. Bello & Radonjic, 2014) after 100 thermal cycles between 40 ^{o}C and 90 ^{o}C each cycle running for 12 hours
Neat Cement	57.41
Steel Fiber	54.36
Silica Sand	56.56
Calcined Clay	55.63
Glass Fiber	56.97

1b: (Massion et al., 2021) measured porosity at 90 ^{o}C using Helium gas-porosimeter.

Sample identification for average Porosity (%)	(Massion et al., 2021) at static 90 ^{o}C
Neat Cement	25.64
0.008% PG	25.57
0.016% PG	27.10
0.05% PG	27.06

1c: Porosity values on the currently worked samples undergone thermal cycling.

Sample identification for average Porosity (%)	**Current work** after 21 thermal cycles between 20 ^{o}C and 110 ^{o}C running each cycle for 8 hours	**Current work** after 84 thermal cycles between 20 ^{o}C and 110 ^{o}C running each cycle for 8 hours
Neat Cement	27.5	21.6
0.008% LG	29.55	27.93
0.008% PG	29.63	25.93
0.1% LG	28.76	24.16
0.1% PG	29.78	24.17

Tables 2: Summarized data for permeability values comparing current work of examining wellbore cementing with graphene and previous works that have used graphene and other materials as mentioned below.

2a: (K. S. Bello & Radonjic, 2014) measured permeability using liquid pulse pressure decay permeameter; fluid used is water.

Sample identification for average Permeability (µD)	(K. S. Bello & Radonjic, 2014) after 100 thermal cycles between 40 °C and 90 °C each cycle running for 12 hours
Neat Cement	0.31
Steel Fiber	0.26
Silica Sand	0.39
Calcined Clay	0.29
Glass Fiber	0.05

2b:(Massion et al., 2021) measured permeabilty using helium gas permeameter.

Sample identification for average Permeability (µD)	(Massion et al., 2021) at static 90 °C
Neat Cement	44.48
0.008% PG	50.16
0.016% PG	56.05
0.05% PG	50.99

2c: Permeability values measured using helium gas permeameter for the current samples.

Sample identification for average Permeability (µD)	**Current work** after 21 thermal cycles between 20 °C and 110 °C running each cycle for 8 hours	**Current work** after 84 thermal cycles between 20 °C and 110 °C running each cycle for 8 hours
Neat Cement	82.87	58.41
0.008% LG	89.10	74.47
0.008% PG	87.11	69.23
0.1% LG	91.58	52.24
0.1% PG	94.28	47.65

VITA

HAVILA JUPUDI

Candidate for the Degree of

Master of Science

Thesis: MICROSTRUCTURAL AND MICROMECHANICAL EVALUATION OF GRAPHENE NANOPLATELETS EMBEDDED IN WELLBORE CEMENT UNDERGONE THERMAL CYCLIC LOADING FOR GEOTHERMAL WELLBORE APPLICATIONS

Major Field: Chemical and Petroleum Engineering

Education:

Completed the requirements for the Master of Science in Petroleum Engineering at Oklahoma State University, Stillwater, Oklahoma in December 2022.

Completed the requirements for the Master of Technology in Chemical Engineering at Andhra University College of Engineering (A), Visakhapatnam, Andhra Pradesh, India in January 2014.

Completed the requirements for the Bachelor of Technology in Chemical Engineering at Andhra University College of Engineering (A), Visakhapatnam, Andhra Pradesh, India in May 2011.

First Author Publications and Presentations:

- Published and presented at Geothermal Rising Conference, GRC Transactions, Vol. 46, 2022, (GRC) August 28-31, in Reno, Nevada, (2022).
- Presented virtually at Division of Energy & Fuels, ACS Fall 2022, Chicago, IL & Hybrid, August 21-25, 2022.
- Paper accepted to be presented at the TMS, San Diego, CA, Spring 2023.
- Abstract accepted to be presented at the AIChE Annual Meeting, Phoenix, AZ, Nov 13-18, 2022.
- Abstract accepted and poster prepared to be presented at AGU Fall Meeting 2022, December 12-16, Chicago, IL.